University of Alberta

Dielectric Phases, Solitary Waves, and Information Capacity in Microtubules

By

Beáta Trpišová ©

A dissertation

presented to the Faculty of Graduate Studies and Research

in partial fulfilment of the requirements for the degree

of

Doctor of Philosophy

in

Theoretical Physics

Department of Physics

Edmonton, Alberta

Fall 1996

National Library
of Canada

Acquisitions and
Bibliographic Services Branch

395 Wellington Street
Ottawa, Ontario
K1A 0N4

Bibliothèque nationale
du Canada

Direction des acquisitions et
des services bibliographiques

395, rue Wellington
Ottawa (Ontario)
K1A 0N4

Your file *Votre référence*

Our file *Notre référence*

The author has granted an irrevocable non-exclusive licence allowing the National Library of Canada to reproduce, loan, distribute or sell copies of his/her thesis by any means and in any form or format, making this thesis available to interested persons.

L'auteur a accordé une licence irrévocable et non exclusive permettant à la Bibliothèque nationale du Canada de reproduire, prêter, distribuer ou vendre des copies de sa thèse de quelque manière et sous quelque forme que ce soit pour mettre des exemplaires de cette thèse à la disposition des personnes intéressées.

The author retains ownership of the copyright in his/her thesis. Neither the thesis nor substantial extracts from it may be printed or otherwise reproduced without his/her permission.

L'auteur conserve la propriété du droit d'auteur qui protège sa thèse. Ni la thèse ni des extraits substantiels de celle-ci ne doivent être imprimés ou autrement reproduits sans son autorisation.

ISBN 0-612-18120-0

Canada

UNIVERSITY OF ALBERTA
RELEASE FORM

NAME OF AUTHOR:	Beáta Trpišová
TITLE OF THESIS:	Dielectric Phases, Solitary Waves, and Information Capacity in Microtubules
DEGREE:	Doctor of Philosophy
YEAR THE DEGREE GRANTED:	1996

Permission is hereby granted to the University of Alberta library to reproduce single copies of this thesis and to lend such copies for private, scholarly or scientific research purposes only.

The author reserves other publication rights, and neither the thesis or extensive extracts from it may be printed or otherwise reproduced without the author's written permission.

Beáta Trpišová

Beáta Trpišová
Department of Physics
University of Alberta
Edmonton, Alberta
T6G 2J1

Date: July 30, 1996

UNIVERSITY OF ALBERTA

FACULTY OF GRADUATE STUDIES AND RESEARCH

The undersigned certify that they have read, and recommend to the Faculty of Graduate Studies and Research for acceptance, a thesis entitled "Dielectric Phases, Solitary Waves, and Information Capacity in Microtubules " submitted by Beáta Trpišová in partial fulfilment of the requirements for the degree of Doctor of Philosophy in Theoretical Physics

Professor J. Tuszyński, Supervisor

Professor M. Razavy, Chairman

Professor A. Scott, External Examiner

Professor M. Klobukowski

Professor M. Pasdar

Professor D. Schmitt

Date: May 13, 1996

Garland Publishing Inc.
717 Fifth Avenue
New York NY 10022-8101
Telephone (212) 751-7447
Fax (212) 308-9399

March 14, 1996

Beata Trpisova
University of Alberta
Department of Physics
412 Avadh Bhatia Physics Laboratory
Edmonton, Alberta
Canada T6G 2J1

Dear Beata Trpisova,

Thank you for your recent correspondence. We are able to grant you permission to reproduce figures from the third edition of Alberts, et al, Molecular Biology of the Cell in your upcoming Ph.D. thesis. The figures include the drawing of an animal cell in a panel on page 18, figure 16-3 on page 790, figure 16-37a on page 814, figure 17-2 on page 864, and panel 18-1 on page 916-917.

Permission is granted for this one-time use only, and is free of charge. Proper credit must be given to the authors and to Garland Publishing. Include in your citation the title, date, figure and page numbers that apply. Garland does not acknowledge any previously published source for this material.

Thank you for pursuing your request. Please contact me with any further queries.

Sincerely,

Michael R. Galligan
Editorial Assistant

University of Alberta
Edmonton
Canada T6G 2J1

Department of Physics
Faculty of Science
412 Avadh Bhatia Physics Laboratory
Telephone: General Office (403) 492-5286 Chairman (403) 492-4127
E-mail: MHEN@PHYS.UALBEKTA.CA Fax: (403) 492-0714

Garland Publishing, Inc.
717 Fifth Avenue
New York, NY 10022

March 1, 1996

Dear Madam/Sir,

In this letter I want to ask for a permission to use some parts of the book published by your company in my Ph.D. thesis. The book was written by B. Alberts, D. Bray, J. Lewis, M. Raff, K. Roberts and J. Watson, the title is Molecular Biology of the Cell, 3rd edition. The parts I would like to photocopy or copy mechanically are:

Page 18 : picture of the animal cell ✓
Page 790 : Figure 16-3 ✓
Page 864 : Figure 17-2 ✓
Page 916-917 : the drawn parts ✓
Page 814 : Figure 16-37 (A) ✓

I hope I can have the permission since the above listed material is necessary to illustrate some parts of the thesis.

Thank you for your time and consideration.

Yours Sincerely

Beáta Trpišová

Beata TRPISOVA
University of Alberta
Department of Physics
412 Avadh Bhatia Physics Laboratory
Edmonton, Alberta
T6G 2J1, CANADA
Tel: (403) 492-5519
E-mail: beata@phys.ualberta.ca

Division of Physical Biochemistry
National Institute for Medical Research
The Ridgeway
Mill Hill
London NW7 1AA
Phone : 0181-959-3666 ext 2088

18th April 1996

Beata Trpisova
Department of Physics
Faculty of Science
University of Alberta
Edmonton
Canada T6G 2J1

To whom it may concern

I hereby give permission for Beata Trpisova to use Figures 2, 5 and 9 (and any other figures she wishes) from "Dynamic Instability of Microtubules: Monte Carlo Simulations and Application to Different Lattice Types" by Stephen R. Martin, Maria J. Schilstra, and Peter M. Bayley (published in Biophysical Journal **65** (1993) 578-596).

Yours faithfully,

Stephen Martin

(Dr Stephen R. Martin, for all the authors)

Aug. 2, 1995

I hereby grant permission to Miss Beata Tripsova to use Fig. 5c of P.R.A 44 (1991) 1366, which I co-authored, in her Ph.D thesis

(T.A. Tsigutkin)

Date: Tue, 30 Jul 96 16:41:56 -0600
From: beata (Beata Trpisova)
To: MANDELKOW@mpasmb.desy.de
Subject: copyrights
Cc: Beata

Dr. Mandelkow,
I am Jack Tuszynski's former graduate student. I just finished my thesis and thanks for giving me copyrights to the pictures from your papers. But I still need one copyright permission since the queen of Canada is very strict on this. This picture is from the paper written by your wife Mrs. Mandelkow and Karin Kirchner. Would you be able to forward this message to her? The paper is:

Tubulin domains responsible for assembly of dimers and protofilaments, EMBO Journal, Volume 4, p. 2397-2402, Figure 7

Thank you very much. Yours sincerely
Beata Trpisova

Date: Wed, 31 Jul 1996 16:26:13 +0100
From: Mandelkow <MANDELKOW@mpasmb.desy.de>
Subject: Re: copyrights
To: beata@phys.ualberta.ca
X-Vms-To: IN%"beata@phys.ualberta.ca"
X-Vms-Cc: MANDELKOW
Mime-Version: 1.0
Content-Transfer-Encoding: 7BIT

Dear Beata,
you can use whatever picures you need, both from my papers and Eva's.
But please note that the copyright is with the publisher, not with us.

Regards,
E. Mandelkow

Date: Tue, 30 Apr 1996 21:09:08 +0300
From: Flytzanhs Nikolaos <flytzani@cc.uch.gr>
To: beata@phys.ualberta.ca
Subject: paper

Dear Beata

Feel free to use the figure. If I can be of any assistance let me know.
Best regards
Nikos flytzanis

From: remsnet@u-bourgogne.fr (Michel Remoissenet)
Subject: Re: http://www.u-bourgogne.fr/cgi-bin/ph2www.pl
To: beata@phys.ualberta.ca (Beata Trpisova)
Date: Thu, 11 Apr 1996 08:15:01 +0200 (DST)
In-Reply-To: <9604110204.AA05377@mach.phys.ualberta.ca> from "Beata Trpisova" at Apr 10, 96 08:04:43 pm
X-Mailer: ELM [version 2.4 PL24]
Mime-Version: 1.0
Content-Type: text/plain; charset=US-ASCII
Content-Transfer-Encoding: 7BIT
Content-Length: 120

Dear Mrs Beata Trpisova,

No problem, you can use Figure 1 of our paper as you like.

Yours sincerely,

M. Remoissenet.

Date: Tue, 06 Feb 1996 20:58:27 +0100
From: Mandelkow <MANDELKOW@mpasmb.desy.de>
Subject: Re: contact
To: jtus@phys.ualberta.ca
X-Vms-To: IN%"jtus@phys.ualberta.ca"
X-Vms-Cc: MANDELKOW
Mime-Version: 1.0
Content-Transfer-Encoding: 7BIT

Dear Jack,
there is no problem for your student to use whatever pictures she needs. Regarding your stay in Europe, the second part of August looks better than the spring date, although things still keep shifting around. Let me know when you would expect to pass through Hamburg.

On the science side, we have lately concentrated on how microtubule dynamics is affected by tau constructs and their phosphorylation by cell cycle kinases and other kinases that we think may play a role in Alzheimers disease. I think it is interesting to note how different the responses of on rates, off rates, catastrophe or rescue respond to the state of the MAP. I am sure the cell uses this for regulation. One paper has recently come out in the December issue of Mol. Cell Biol. (Trinczek et al.).

Best regards, Eckhard

Hi Beata
These are the emails
I got from Hamouth
and Mandelkow about
permissions to use their
figures in your thesis
J.T.

Date: Thu, 28 Mar 1996 18:49:19 +0100
From: Mandelkow <MANDELKOW@mpasmb.desy.de>
Subject: RE: contact
In-Reply-To: Your message dated "Mon, 25 Mar 1996 11:44:20 -0700"
<9603251844.AA03986@landau.phys.ualberta.ca>
To: jtus@phys.ualberta.ca
Cc: Mandelkow <MANDELKOW@mpgars.desy.de>
Mime-Version: 1.0
Content-Type: TEXT/PLAIN
Content-Transfer-Encoding: 7BIT

Dear Jack,
use whatever you need.
Regards, Eckhard

Date: Mon, 12 Feb 1996 15:01:26 -0700 (MST)
From: SRH@ccit.arizona.edu
Subject: Re: request
To: jtus@phys.ualberta.ca
X-Envelope-To: jtus@phys.ualberta.ca
X-Vms-To: IN%"jtus@phys.ualberta.ca"
Mime-Version: 1.0
Content-Transfer-Encoding: 7BIT

Hi Jack
Of course Beata can use them. Do you need an official letter? if so just let me know, and cc to cle@ccit.arizona.ed - thats Carol Ebbeke my new assistamnt and she'll make sure I do it.
Did you get anything out of the video?
Hope all's well.
Stuart
From: IN%"jtus@phys.ualberta.ca" 12-FEB-1996 13:20
To: IN%"SRH@CCIT.ARIZONA.EDU"
CC:
Subj: RE: request

Return-path: <jtus@landau.phys.ualberta.ca>
Received: from relay.phys.ualberta.ca (relay.phys.ualberta.ca)
by CCIT.ARIZONA.EDU (PMDF V5.0-5 #2381)
id <01I14LAN7ONK91VVJ3@CCIT.ARIZONA.EDU> for SRH@CCIT.ARIZONA.EDU; Mon,
12 Feb 1996 13:19:55 -0700 (MST)
Received: from landau.phys.ualberta.ca ([129.128.7.140])
by relay.Phys.UAlberta.CA with SMTP id <58153-1>; Mon,
12 Feb 1996 13:18:52 -0700
Received: by landau.phys.ualberta.ca (NX5.67c/NeXT-2.0) id AA09948; Mon,
12 Feb 1996 13:20:46 -0700
Received: by NeXT.Mailer (1.87.1)
Received: by NeXT Mailer (1.87.1)
Date: Mon, 12 Feb 1996 13:20:46 -0700
From: jtus@phys.ualberta.ca (Jack Tuszynski)
Subject: Re: request
To: SRH@CCIT.ARIZONA.EDU
Message-id: <9602122020.AA09948@landau.phys.ualberta.ca>
X-Envelope-to: SRH
Content-transfer-encoding: 7BIT

Dear Stuart,
How are things in the New Year with you? I guess you must be very busy with the upcoming conference.
The reason I'm writing to you at this time is to ask your permission so that Beata could use a few of the diagrams you published in her thesis. The diagrams she was interested in are:
Figs. 3,4,5 from Physica D42 (1990) 428-449 with Rasmussen et al.
Your permission is needed because of the copyright and would cut through a lot of bureaucratic crap. Thanks in advance.
All the very best,
Jack

Date: Mon, 25 Mar 1996 13:17:35 -0700 (MST)
From: SRH@ccit.arizona.edu
Subject: Re: request
To: jtus@phys.ualberta.ca
X-Envelope-To: jtus@phys.ualberta.ca
X-Vms-To: IN%"jtus@phys.ualberta.ca"
Mime-Version: 1.0
Content-Transfer-Encoding: 7BIT

Hi Jack
Of course she can use them. Do you need a special letter?
Yes, things are crazy. Ezio is arriving the 1st. I think he is coming up to you
the 3rd thru 6th?
Have you seen this stuff about MT "shimmering" and vibrations of flagellar
assemblies up to 600 Hz?
later
Stuart
From: IN%"jtus@phys.ualberta.ca" 25-MAR-1996 11:38
To: IN%"SRH@CCIT.ARIZONA.EDU"
CC:
Subj: RE: request

Return-path: <jtus@landau.phys.ualberta.ca>
Received: from relay.phys.ualberta.ca (relay.phys.ualberta.ca)
by CCIT.ARIZONA.EDU (PMDF V5.0-5 #2381)
id <01I2R5YTMGKG984SO1@CCIT.ARIZONA.EDU> for SRH@CCIT.ARIZONA.EDU; Mon,
25 Mar 1996 11:38:02 -0700 (MST)
Received: from landau.phys.ualberta.ca ([129.128.7.140])
by relay.Phys.UAlberta.CA with SMTP id <58223-2>; Mon,
25 Mar 1996 11:36:02 -0700
Received: by landau.phys.ualberta.ca (NX5.67c/NeXT-2.0) id AA03980; Mon,
25 Mar 1996 11:40:05 -0700
Received: by NeXT.Mailer (1.87.1)
Received: by NeXT Mailer (1.87.1)
Date: Mon, 25 Mar 1996 11:40:05 -0700
From: jtus@phys.ualberta.ca (Jack Tuszynski)
Subject: Re: request
To: SRH@CCIT.ARIZONA.EDU
Message-id: <9603251840.AA03980@landau.phys.ualberta.ca>
X-Envelope-to: SRH
Content-transfer-encoding: 7BIT

Dear Stuart,
I'm writing again to you to ask your permission so that Beata could use in her thesis a few of the diagrams you published.
The diagrams she was interested in are:
Figs. 5.13, 5.14 and 5.15 from Ultimate Computing.
Your permission is needed because of the copyright and would cut through a lot of bureaucratic crap. Thanks in advance.

I presume you are getting into a high gear with the upcoming conference. I wish you much success. Please let me know how it went.

All the very best,
Jack

Abstract

Microtubules (MTs) are cylindrical protein structures which participate in a variety of cellular activities. Research on the biological aspects of MT behaviour has been growing especially over the last decade, and it has revealed many interesting features of MTs. However, the mechanisms which underlie the numerous functions of the MTs in the cell are mostly unknown. The main objective of this work is to show that such mechanisms may be linked to the dielectric properties of MTs.

The dielectric properties of MTs arise from the dipolar character of the tubulin molecules that are the building subunits of MTs. Based on this feature, MTs can be viewed as ferroelectric crystals. Ferroelectric crystals consist of atoms or molecules which carry permanent dipole moments. They are known to undergo a phase transition from a low temperature ferroelectric phase in which all dipoles are ordered in a preferred direction, to a high temperature paraelectric phase characterized by random orientation of dipoles. If such dielectric phases exist in MTs they may serve different purposes in the biological MT activities. This feature of MTs is the subject of investigation in the second chapter of this thesis.

It has been suggested by other researchers that quanta of energy may propagate along MTs which are in the ferroelectric phase in the form of solitary waves of tubulin dipole states. The energy may be supplied by the hydrolysis of guanosine 5' triphosphate (GTP) that follows the addition of one molecule of tubulin to a MT end. In the third chapter of this thesis, the above concept was used to study the collision of these solitary waves with a local defect in a MT which can be an attached protein or a discontinuity in the arrangement of the tubulin molecules.

In the last chapter, the hypothesis is studied whether different configurations of the dipole states of the tubulin molecules could be a way of storing information in MTs.

Acknowledgements

I want to thank my supervisor Dr. Jack Tuszyński for supervision and support. I also want to thank Bahman Darian, Terrence Kolber, Jon Johansson, Andrei Maximov and Robert Teshima for the time they spend with my research problems. I appreciated very much the help from Lynn Chandler. Thanks to the space physics center for letting me produce the colour plots of some of my results. Thanks to the friends I found at this department and to my colleagues, graduate students, for friendship and help. I am grateful for being given the opportunity to be a graduate student at this university and in Canada.

Contents

Introduction 1

References 6

1 Structure and Properties of Microtubules 8

1.1 Eucaryotic Cell and Cytoskeleton 8

1.2 Cytoskeletal Components 9

1.2.1 Actin Filaments 9

1.2.2 Intermediate Filaments 10

1.2.3 Microtubules 11

1.3 Structure of Microtubules 11

1.4 Microtubule Assembly and Disassembly 14

1.4.1 Dynamic Instability 14

1.4.2 Cell Division 15

1.4.3 GTP Hydrolysis in Microtubule Assembly/Disassembly 20

1.4.4 Tubulin Conformational States and Microtubule Assembly/Disassembly 22

1.4.5 Microtubule Oscillations 25

1.5 Microtubule Associated Proteins 30

1.5.1 MAPs 30

1.5.2 Motor Proteins 32

1.5.3 Cilia and Flagella 35

1.6 Structure of Proteins and Structure of Tubulin 37

References **41**

2 Dielectric Phases in Microtubules **44**

2.1 Some Features of Phase Transitions 44

2.2 Phase Transitions in Lattices 47

2.3 Calculation of Polarization and Susceptibility of the Microtubule Lattice 49

2.4 Two Models of the Dipole States of the Tubulin Dimer 52

2.5 Model with Nontilted States 54

2.5.1 A Lattice 60

2.5.2 B Lattice 70

2.6 Model with Tilted States 70

2.6.1 A Lattice 73

2.6.2 B Lattice 80

References **84**

3 Energy Transfer in Microtubules **86**

3.1 Solitary Waves in Biological Systems 86

3.2 Davydov's Model of Propagation of Solitons along an α-Helix 88

3.3 Kink-Like Solitary Waves in Microtubules 91

3.4 Model with Strong Coupling between Polarization and Displacement . 93

3.4.1 Equation of Motion 93

3.4.2 Electric Fields in Microtubules 95

3.4.3 Analytical Solution 99

3.4.4 Numerical Solution 103

3.4.5 Numerical Solution in the Presence of an Impurity 105

3.5 Two Other Models of Propagation of Kinks in Ferroelectric Systems . 111

3.5.1 Coupled Polarization and Displacement 111

3.5.2 Coupled Polarization and Stress 116

References **126**

4 Information in Microtubules **128**

4.1 Models of Communication in Biological Systems 128

4.2 Calculation of Information Capacity in Microtubules 131

4.2.1 Continuous Probability Distribution 132

4.2.2 Discrete Probability Distribution 136

References **142**

Conclusions **143**

Appendix A **148**

References **152**

Appendix B **153**

List of Figures

1.1 Animal eucaryotic cell. 8

1.2 An actin filament. 9

1.3 An intermediate filament. 10

1.4 A and B lattices in a MT with 13 protofilaments and their planar projections. α monomers are shaded black, β monomers are light. The arrow indicates a seam. 12

1.5 Two possible arrangements of the ends of a MT protofilament. On the left, the protofilament ends at the plus end with the β-tubulin. On the right, the exposed monomer at the plus end is the α-tubulin. The exchangeable guanosine 5' triphosphate (GTP) binds to the β-tubulin at the plus end of the protofilament. On the β-tubulin inside the protofilament GTP hydrolyses and the product of the hydrolysis is guanosine 5' diphosphate (GDP). γ-tubulin is located near the minus end. 13

1.6 The observed time change of the net length of a single MT. 15

1.7 A schematic illustration of the array of MTs radiating from the centrosome. The MTs are attached to the centrosome at the minus end, the end growing out of the centrosome is the more active plus end. . . 16

1.8 Prophase, prometaphase, metaphase. 17

1.9 Anaphase, telophase, cytokinesis. 18

1.10 Guanosine 5′ triphosphate. 21

1.11 The growing MT end is capped with the GTP tubulin (solid circles). After GTP hydrolyses the tubulin binds GDP (open circles). When the protofilaments are not capped with tubulin GTP they start to uncoil and the MT disassembles. The disassembled GDP tubulin molecules associate themselves into rings and double rings. 23

1.12 Numerically calculated length changes as a function of time for the MT lattices (a) A with 13 protofilaments, (b) A with 14 protofilaments, (c) B with 13 protofilaments. 25

1.13 Numerically calculated length changes of a MT with the A lattice with 13 protofilaments as a function of time. The pool of free GTP tubulin contains (a) tubulin GTP only (b) 20% of GMPPNP, (c) 10% of tubulin GDP. 26

1.14 The oscillation cycle of an assembly of MTs. 28

1.15 Regular oscillations of the MT assembly. c_{pol} is the concentration of the tubulin GTP in the MT polymer, c_{tot} is the total concentration of tubulin, the solid line is the calculated MT dynamics and the dotted line represents *in vitro* observations. 29

1.16 The rate of growth of the assembly of MTs with the A lattice which consists of 13 protofilaments as a function of the tubulin GTP concentration. 30

1.17 MAP attachment patterns observed by electron microscopy. 33

1.18 A schematic drawing of kinesin and cytoplasmic dynein. The direction of movement along MTs is indicated by arrows. 34

1.19 A schematic cross-section through a flagellum (a) and the MT doublet (b). 36

1.20 An amino acid molecule. 37

1.21 Formation of a dipeptide. 38

1.22 The domain structure of α- and β-tubulin. Nonexchangeable GTP (GTP_n) is bound to the α monomer. Exchangeable GTP (GTP_e) binds to the β monomer. 39

2.1 Spontaneous polarization (a) and electric susceptibility (b) for a first and second order phase transition. 45

2.2 The free energy of a ferroelectric crystal as a function of spontaneous polarization for a first (a) and second order (b) phase transition. . . . 46

2.3 The geometrical configuration of the A and B lattice for a MT with 13 protofilaments. The hexagonal lattices can be transformed into triangular lattices in which the hexagonal arrangement of sites in the MT lattices is taken into account by shifting the rows at the boundaries by a number of rows n. 51

2.4 The α and the β state of the tubulin dimer. In the β state the tubulin dimer is shifted with respect to the vertical axis by about 29°. 53

2.5 The hexagonal nearest neighbour cluster for the model with nontilted and tilted states. The corresponding up and down states are at the same sites in the cluster. 54

2.6 The interaction constants in the three directions that characterize the MT lattice. 55

2.7 The geometrical configuration of the A lattice and inside the B lattice. 56

2.8 Relative permittivity of free water as a function of frequency at 20°. . 57

2.9 A system of three frustrated spins. 58

2.10 Dielectric transition in a MT with the A lattice. The size of the lattice is 13x100 and $\bar{Q} = 12 \times 10^{-56}\,\mathrm{C^2m^2}$. The spontaneous polarization per site decreases from $P = 1$ at low temperatures to almost zero at high temperatures. The transition temperature is indicated by the peak of the electric susceptibility, $T_c = 300\,\mathrm{K}$. 61

2.11 Spontaneous polarization per site in a MT with the lattice 13x3000A for $\bar{Q} = 12 \times 10^{-56}\,\mathrm{C^2m^2}$. The excursions of polarization are almost removed due to the large size of the lattice. 62

2.12 Transition in the MT lattice 13x100A when $\bar{Q}$ is $10 \times 10^{-56}\,\mathrm{C^2m^2}$, $12 \times 10^{-56}\,\mathrm{C^2m^2}$ and $14 \times 10^{-56}\,\mathrm{C^2m^2}$. As $\bar{Q}$ increases the transition moves towards higher temperatures. The values of $\bar{Q}$ are given in $10^{-56}\,\mathrm{C^2m^2}$. 63

2.13 Polarization per site in the MT lattice 13x100A when the external electric fields are $0\,\mathrm{Vm}^{-1}$, $10^3\,\mathrm{Vm}^{-1}$, $10^4\,\mathrm{Vm}^{-1}$, $10^5\,\mathrm{Vm}^{-1}$, $10^6\,\mathrm{Vm}^{-1}$. $\bar{Q} = 12 \times 10^{-56}\,\mathrm{C}^2\mathrm{m}^2$ for all curves. As the external electric field increases, the ordering of dipoles in the lattice in the direction along the field increases as well. 65

2.14 Polarization per site in the MT lattice 13x100A when the external electric fields are $-10^4\,\mathrm{Vm}^{-1}$ and $-10^6\,\mathrm{Vm}^{-1}$ and $\bar{Q} = 12 \times 10^{-56}\,\mathrm{C}^2\mathrm{m}^2$ for both curves. 66

2.15 Three MAP patterns in a MT with the A lattice and 13 protofilaments. The ratios of the number of sites at which MAPs are attached to the total number of sites in the lattice are 1/11, 1/22, 1/48. 68

2.16 The effect of MAPs attached to the MT A lattice in the three regular patterns shown in Figure 2.15. The lattices consist of 13 columns and 99, 110 and 96 rows for the corresponding ratios 1/11, 1/22 and 1/48. $\bar{Q} = 12 \times 10^{-56}\,\mathrm{C}^2\mathrm{m}^2$ for all curves. The values of the spin variable at the MAP attachment sites are +1 and 0. 69

2.17 Spontaneous polarization per site for the values of the stagger of the MT lattice 3.1 nm (A lattice), 2.9 nm, 2.3 nm, 1.5 nm, 0.9 nm (B lattice). The size of the lattice is 13x100 and $\bar{Q} = 12 \times 10^{-56}\,\mathrm{C}^2\mathrm{m}^2$ for all curves. 71

2.18 Polarization per site in a MT with 13x100A lattice for $\bar{Q} = 12 \times 10^{-56}\,\mathrm{C}^2\mathrm{m}^2$ and $\theta = 29^\circ_+$. The two curves correspond to the tilted and nontilted starting configuration of dipoles, respectively. 74

2.19 A dipole in the MT A lattice and its nearest neighbours in the tilted and nontilted configuration, respectively. The energy of the central dipole due to the interation with its nearest neighbours is calculated for $\bar{Q} = 12 \times 10^{-56}\,\mathrm{C}^2\mathrm{m}^2$ and $\theta = 29^\circ_+$. 75

2.20 Polarization per site in the MT lattice 13x100A for $\theta_{tilt} = 5^\circ_\pm$ and $29^\circ_\pm$ and $\bar{Q} = 12 \times 10^{-56}\,\mathrm{C}^2\mathrm{m}^2$. 76

2.21 Dielectric transition in the MT lattice 13x100A in which $\theta_{tilt} = 29^{\circ}_{+}$, $\bar{Q} = 5 \times 10^{-56}\,\mathrm{C^2m^2}$ and the external electric field is present. The values of the external electric fields are $-10^{6}\,\mathrm{Vm^{-1}}$, $-10^{5}\,\mathrm{Vm^{-1}}$, $-10^{4}\,\mathrm{Vm^{-1}}$, $+10^{4}\,\mathrm{Vm^{-1}}$, $+10^{5}\,\mathrm{Vm^{-1}}$, and $+10^{6}\,\mathrm{Vm^{-1}}$. 77

2.22 Dielectric transition in the MT A lattice to which MAPs are attached according to the patterns shown in Figure 2.15. The corresponding lattice sizes are 13x99, 13x110, and 13x96. $\theta_{tilt} = 29^{\circ}_{+}$ and $\bar{Q} = 2 \times 10^{-56}\,\mathrm{C^2m^2}$ for all curves. The value of the dipole variable at a MAP attachment site is -1 or 0. 79

2.23 Spontaneous polarization per site in the MT lattice 13x100B in which $\theta_{tilt} = 29^{\circ}_{+}$ and $\bar{Q} = 5 \times 10^{-56}\,\mathrm{C^2m^2}$. For comparison, the corresponding curve for the A lattice is also shown. 80

2.24 Dielectric transition in the MT lattice 13x100B for the values of $\bar{Q}$: $5 \times 10^{-56}\,\mathrm{C^2m^2}$, $25 \times 10^{-56}\,\mathrm{C^2m^2}$ and $55 \times 10^{-56}\,\mathrm{C^2m^2}$. The $\bar{Q}$'s are shown in units $10^{-56}\,\mathrm{C^2m^2}$ and $\theta_{tilt} = 29^{\circ}_{+}$. 81

3.1 Possible types of solitary waves: (a) pulse, (b) kink, (c) breather, (d) symmetric envelope solitary wave, (e) asymmetric envelope solitary wave, (f) symmetric dark solitary wave. Asymmetric dark solitary wave and nonlinear periodic wave are not shown. 87

3.2 The α-helix conformation of a protein molecule. 89

3.3 The local potential energy at a site n in a MT protofilament when the MT is in the ferroelectric phase. (a) $V(u_n)$, (b) $V(u_n) + V_E$. . . . 94

3.4 The cross-section of a MT with 13 protofilaments. The 13-th protofilament is subjected to the electric field of the surrounding 12 protofilaments. 97

3.5 The electric field generated by 12 protofilaments on the axis of the 13-th protofilament of a MT whose protofilaments consist of (a) 125 and (b) 1000 dimers. 98

3.6 A domain wall between two subchains of a MT protofilament in which the tubulin dimers are in two different states. 101

3.7 A kink wave moving on a section of a MT which is 125 dimers long. The time interval between two successive waves is $\Delta t = 3.38 \times 10^{-7}$s. Figure (a) shows the time evolution of a kink wave exposed to a decreasing electric field of the MT. Figure (b) shows the kink moving in a constant electric field of value equal to that at the beginning of the kink motion in figure (a). The electric field is in units of $2.62 \times 10^{6}\,\mathrm{Vm}^{-1}$ and the displacement $u(x)$ is in units of 1.58×10^{-11} m. 104

3.8 A kink wave moving on the background of an increasing electric field along a MT which is 125 dimers long. The time interval between two successive waves is $\Delta t = 3.38 \times 10^{-7}$s. As the electric field increases the kink moves faster. The dashed line shows how far the kink would travel if the electric field was constant and equal to the value at the starting point. The units of the plots are the same as in Figure 3.7. . 105

3.9 Local potential energy (a) and the corresponding local force (b) produced by local defects placed at each 10-th dimer along a MT protofilament. 107

3.10 A kink wave traveling along the section of a MT protofilament in which the electric field decreases (a) and increases (b) and a defect represented by a localized potential energy is placed at a point $x_0 = -3.7 \times 10^{-7}$ m (a) and at a point $x_0 = 4.3 \times 10^{-7}$ m (b). The amplitude of the local potential energy is 1.00×10^{-22} J and the length of the MT protofilaments is 125 dimers. The solid line shows how far the kink would travel if there was no defect. The electric field is plotted in units $2.62 \times 10^{6}\,\mathrm{Vm}^{-1}$, the local force is in units 2.71×10^{-13} N and the kink wave is in units 1.58×10^{-11} m. 109

3.11 When the defect on the MT produces a sufficiently large potential barrier, the kink wave is stopped. In this case the amplitude of the potential energy due to the defect is 1.00×10^{-21} J and it is located at $x_d = -3.7 \times 10^{-7}$ m in the MT which is 125 dimers long. The units for all the curves are the same as in Figure 3.10. 110

3.12 The electric force $q_{eff}E(x)$ for a MT which is 125 dimers long and the local forces $-dV(x)/dx$ that correspond to the amplitudes of the localized potential energy $V_0 = 1.00 \times 10^{-22}$ J and $V_0 = 1.00 \times 10^{-21}$ J. The local forces are plotted with the opposite sign to see the difference between the electric force and the local forces at the point of their minimum $x_{min} = -3.72 \times 10^{-7}$ m. 111

3.13 Numerical solution of the coupled system of equations (3.35) and (3.36) for parameters $\gamma_e = 0.1$, $v = 1$, $M = 1$, $v_0 = 3$, $\alpha_2 = \alpha_4 = A_2 = A_4 = 1$ and $D = 2$. 114

3.14 Numerical solution of the coupled system of equations (3.35) and (3.36) when a local force $-dV(x)/dx$ is added to the right hand side of equation (3.35). The parameters in the equations are the same as for the solution drawn in Figure 3.13. The parameters of the local force are $\beta = 0.5$, $x_d = 15$ and (a) $V_0 = 0.2$, (b) $V_0 = 0.4$. The solution for u is plotted in regular time intervals and the solution for P is plotted only at the end of the simulation. In Figure 3.14b the dotted line shows u before it is reflected and the solid line is the solution for u after it is reflected from the local potential energy barrier. 115

3.15 Numerical solution of (3.41), (3.44) and (3.52) at times $t = 0$, $t = 10$ and $t = 20$ when the amplitude of the density fluctuation is $\rho_r = 0.5$. 119

3.16 Numerical solution of (3.41), (3.44) and (3.52) at times $t = 50$, $t = 150$ and $t = 300$ when the amplitude of the density fluctuation is $\rho_r = 0.5$. 120

3.17 Numerical solution of (3.41), (3.44) and (3.52) at times $t = 0$ and $t = 350$ when the amplitude of the density fluctuation is $\rho_r = 1$. . . . 121

3.18 Numerical solution of (3.41), (3.44) and (3.52) at times $t = 0$, $t = 10$ and $t = 20$ when the amplitude of the density fluctuations is $\rho_r = 0.5$. 123

3.19 Numerical solution of (3.41), (3.44) and (3.52) at times $t = 30$, $t = 50$ and $t = 350$ when the amplitude of the density fluctuations is $\rho_r = 0.5$. 124

4.1 Number of clusters and information capacity of a MT with the A lattice for both tilted and nontilted model. The MT consists of 13 columns and 100 rows. 135

4.2 Number of clusters and information capacity of a MT with the A lattice for both tilted and nontilted model. The size of the MT is 13 columns and 3000 rows. 137

4.3 Information capacity of a MT with the A lattice that consists of 13 columns and 3000 rows. The calculation was performed using the tilted model. The critical temperature is $T_c = 311\,\mathrm{K}$. 139

4.4 The configuration of dipoles on a section of a MT with the A lattice of size 13x3000 at $T = 311\,\mathrm{K}$ and $T = 400\,\mathrm{K}$. The empty sites represent the dipoles in the down states, the sites with a star represent the up states. The configuration was obtained for the nontilted model. . . . 140

A.1 Relative polarization in a MT with the A lattice and size 13x3000 for $\bar{Q} = 12 \times 10^{-56}\,\mathrm{C^2m^2}$ (dotted line), and the curve calculated by finding the roots of equation (A.8) (solid line). 149

B.1 Nearest neighbours to a site (i,j) in a hexagonal lattice. 154

B.2 An example of an input and corresponding output for the program CLUSTER. The A lattice that consists of 13 columns and 20 rows contains 4 clusters of -1's and one cluster of +1's. After the lattice is examined by the program CLUSTER, -1's are replaced with 0's and +1's are replaced with 5's. 156

Introduction

Microtubules (MTs) are hollow tubes that are found in all eucaryotic cells [1, 2]. They are composed of molecules of tubulin which are dimers formed of two monomers termed α- and β-tubulin. The tubulin dimers in a MT are arranged into protofilaments. Most MTs have 13 or 14 protofilaments [3]. Their diameter is approximately 25×10^{-9} m and the length of an intermediate MT is about 10^{-6}m. In the axons of neurons they can be as long as several centimeters.

In the cell MTs are typically attached with one end to the centrosome and the other end is free. They emanate from the centrosome in all directions. The free end of each MT is continuously assembling and disassembling molecules of tubulin from pool of free tubulin in the cytoplasm. This phenomenon is known as dynamic instability. The dynamic instability of MTs is a major mechanism in cell division and polarization [1,4,5].

In cell division processes, MTs radiate from the two spindle poles located at the opposite extremities of the dividing cell. They probe the cellular space at random by continuously growing and shrinking in all directions so that eventually a MT attaches to a place (called a kinetochore) that is located on each of the two chromatids of a chromosome. After all chromatids are attached to MTs, they are pulled apart by the disassembling MTs towards the opposite poles of the cell. In this way the DNA material is divided into two equal portions, one for each of two daughter cells.

Most animal cells are polarized. Polarization of the cell is achieved when a majority of MTs attached to the centrosome extend in a preferred direction. At this time the growth of MTs is rather stabilized which results in fewer and longer MTs since the total amount of tubulin in the cell is fixed. This means that there is a biochemical or biophysical event or a cascade of events that cause the MTs to change their mode of behaviour from rapid growing and shrinking characterized by a large number of short MTs to stabilized growth in a preferred direction characterized by longer and fewer MTs.

Dynamic instability is also the basis for the regular oscillations which have been observed *in vitro* in assemblies of MTs [6]. During this process the population of MTs switches in regular time intervals between the phase when almost all tubulin is bound in MTs and the phase when no MTs exist and all tubulin is free. According to experiments such regular oscillations don't seem to exist in the cell [7]. However,

the mechanisms of this mode of behaviour of MTs *in vitro* may be relevant to the pathways through which the dynamic instability of MTs takes place in the cell.

One of the essential processes associated with the dynamic instability of MTs is the hydrolysis of guanosine 5' triphosphate (GTP) bound to the β monomer of each tubulin dimer. GTP bound on the β-tubulin hydrolyses every time a tubulin dimer attaches to the growing MT end. In the hydrolysis 8.7 kcal/mol of energy is released [8]. Experiments indicate that most of this energy is consumed in changing the conformational state of the tubulin molecule and only a fraction is freed [9]. Different conformational states of the tubulins on which the GTP has hydrolysed can be a source of mechanical strain which may be a factor in MT disassembly. However, it is not known how the free portion of the energy released in the GTP hydrolysis is utilized in the MTs.

In some cellular activities MTs are stable. MTs are usually stabilized by binding microtubule associated proteins (MAPs). MAPs bound to MTs can form bridges which interconnect MTs into a compact network. Such connections may be channels through which MTs communicate among themselves.

Stable MTs inside the cell function as tracks along which organelles are transported to the proper position. In axons, transport of neuronal vesicles towards the synapse takes place along MTs as well. The transport along MTs is mediated by proteins called motor proteins which attach to MTs at regular sites [10]. Motor proteins have also been detected on the surface of MTs which form the cores of the projections from the cell surface called cilia and flagella. The coordinated beat-like motions of these structures are used to move fluids or other particles around the cell or the whole cell. Experiments suggest that these motions result from the cooperative behaviour of the motor proteins attached to MTs.

In this work, physical mechanisms are suggested that could explain some aspects of the MT behaviour outlined above.

Chapter 1 describes in more detail the structure of MTs, dynamic instability of a single MT, the role of MTs in the cell division processes, GTP hydrolysis and its connection to the conformational states of the tubulin molecule, the cycle of chemical reactions that lead to the regular oscillations of populations of MTs, the specific roles of different associated proteins and motor proteins and their isoforms in the MT activities, and the structure of tubulin.

In Chapter 2, different dielectric phases which may exist in MTs are studied. Such phases could be linked to different regimes of MT behaviour which are associ-

ated with different biological functions of MTs.

The dielectric properties of MTs are based on the dielectric character of the tubulin molecule. At the present time it is accepted that each tubulin molecule carries a permanent dipole moment which can be in at least two distinct orientational states [11]. Due to this, a MT can be viewed as an assembly of dipoles. Inorganic crystals which are composed of atoms or molecules that carry permanent dipole moments are called ferroelectric crystals. They are known to undergo a phase transition from a low temperature phase in which all dipoles are aligned in one direction to a high temperature phase that is characterized by random orientation of dipoles. The ordered phase is termed the ferroelectric phase and the phase in which the dipoles are oriented at random is termed the paraelectric phase [12].

One of the objectives of this thesis was to find whether MTs can exhibit a phase transition similar to that observed in ferroelectric crystals. To study the possibility of a transition from a low temperature ferroelectric phase to a high temperature paraelectric phase, the average configuration of dipoles in a MT at each temperature has to be found. In this work this was achieved using the Monte Carlo procedure by means of which the states with the highest weight of the assembly of dipoles in a MT were selected at each temperature [13]. These states were then used to find the degree of alignment of dipoles (polarization) as a function of temperature.

The configuration of dipoles in a MT depends on the following characteristics: the magnitude and orientation of the dipole moments; the relative permittivity of the medium surrounding the MT; and the geometrical arrangment of the tubulin molecules in the MT. A combination of these parameters determines the dielectric phase in a MT at body temperature. This implies that if there are mechanisms that govern the values of the parameters above, they determine the dielectric phase in a MT at biological temperatures and consequently a specific mode of behaviour of the MT.

Experiments indicate that the dipole state of tubulin is coupled to its elastic (conformational) state. In other words, a change of the dipole state of the tubulin molecule causes its deformation. It has been shown by other authors [14], that these properties may lead to propagation of quanta of energy along MTs in the form of solitary waves.

In Chapter 3, three different models are discussed which are represented by partial differential equations. The equations have been derived under the assumption that the elastic and dielectric degrees of freedom of the tubulin molecules are coupled

nonlinearly. A special class of solutions of these equations are travelling solitary waves called kinks which represent a domain wall between two states of a physical system [15,16].

In this work it is suggested that along MTs may propagate kink-like waves that represent domain walls between two subchains of tubulin dimers in each of which the tubulin molecules are in states with different orientation of dipoles and, consequently, in different elastic states. The kink arises when all dipoles in the MT are initially ordered in the same direction, that means when the MT is in the ferroelectric phase, and a sufficient amount of energy is supplied which can switch the dipole state of one of the tubulin dimers. Due to the interaction between the dipoles on the tubulin molecules this will induce switching of the dipole state of one of the neighbouring dimers and so on. The energy needed to initiate the kink can be, for example, the free portion of the energy of the GTP hydrolysis. It is speculated here that such kink-like excitations could be viewed as bits of information that propagate along MTs and signal other events, for example, the detachment of a tubulin molecule from the disassembling MT end or attachment of a MAP.

The concept explained above has been used to study numerically the effect of a collision of a travelling kink wave with a local impurity in the MT such as an attached MAP or a structural discontinuity. The sites of attached MAPs may be places where the signals in the form of travelling kink-like waves can be transferred to other parts of the cytoskeleton. When the travelling energy collides with a structural discontinuity in the MT it may contribute to the overall destruction of the MT.

The dielectric properties of MTs outlined above raise the question about the existence of electric fields in MTs. The presence of electromagnetic fields on the surface of MTs has been demonstrated in several experiments. For example, it has been found that MTs align themselves along the field lines of the electric and magnetic fields applied externally [17]. The intrinsic electromagnetic fields of MTs may be a way through which MTs interact with each other. The interaction between the electromagnetic fields of MTs and the external fields may be a mechanism by means of which the cells controls the behaviour of MTs. For example, in metaphase of mitosis the pattern formed by aligned MTs is very much reminiscent of the electric field lines which characterize the electric field produced by two point charges of opposite signs located at the opposite poles of the mitotic spindle.

In order to perform the numerous functions in the cell, MTs process and transfer information in the form of biochemical and biophysical processes. In Chapter 4, it

is suggested that the information in a MT can be encoded and processed by means of patterns of tubulin dipole states. Since the density of the tubulin subunits is $10^{17}\,\mathrm{cm}^{-3}$, which is very close to the theoretical limit of charge separation [18], this could provide MTs with large information storage capabilities. Through coupling of the tubulin dipole states to the conformational states, the information could be coupled to the mechanical and chemical events.

Within the framework of this thesis the information capacity of a MT is estimated on the basis of the average configuration of dipoles in a MT at a temperature T. This configuration was determined using the Monte Carlo procedure. The MT is divided into domains that differ in their orientation of dipoles and the information capacity is assumed to depend on the size and on the number of these domains. Because in the ferroelectric phase all dipoles are oriented in one direction, the information capacity in this phase is zero. As the temperature approaches the critical temperature, domains of dipoles with different orientation start to form [12]. Based on this the information capacity in a MT is expected to increase in the transition region between the ferroelectric and paraelectric phases.

The results of the calculations that were performed on the basis of the assumptions and suggestions outlined above are summarized in Conclusions. In Appendix A are derived estimates of the coefficients of the Landau free energy expansion that describes a dielectric phase transition in a MT. These estimates were obtained by fitting the polarization curves calculated in Chapter 2 and they may be useful in solving the coupled systems of partial differential equations in Chapter 3. In Appendix B is described a Fortran program by means of which the number and size of domains in a two-dimensional hexagonal lattice with different kinds of constituent particles can be found. This program is the original work of the author.

References

[1] B. Alberts, D. Bray, J. Lewis, M. Raff, K. Roberts, and J. D. Watson, *Molecular Biology of the Cell*, 3-rd edition (Garland Publishing, New York and London, 1994)

[2] P. Dustin, *Microtubules* (Springer, Berlin, 1984)

[3] S. R. Martin, M. J. Schilstra, and P. M. Bayley, Dynamic Instability of Microtubules: Monte Carlo Simulation and Application to Different Types of Microtubule Lattice, *Biophysical Journal* **65**, p. 578-596 (1993)

[4] T. J. Mitchison and M. W. Kirschner, Microtubule assembly nucleated by isolated centrosomes, *Nature* **312**, p. 232-237 (1984); Dynamic instability of microtubule growth, *Nature* **312**, p. 237-242 (1984)

[5] M. Kirschner and T. Mitchison, Beyond Self-Assembly: From Microtubules to Morphogenesis, *Cell* **45**, p. 329-342 (1986)

[6] A. Marx, E. Mandelkow, A model of microtubule oscillations, *European Biophysics Journal* **22**, p. 405-421 (1994)

[7] E.-M. Mandelkow, E. Mandelkow, and R. A. Milligan, Microtubule dynamics and microtubule caps: A time-resolved cryo-electron microscopy study, *Journal of Cell Biology* **114**, p. 977-991 (1991)

[8] B. Mickey and Jonathon Howard, Rigidity of Microtubules Is Increased by Stabilizing Agents, *Journal of Cell Biology* **139**, p. 909-917 (1995)

[9] M. Caplow, R. L. Ruhlen, and J. Shanks, The Free Energy for Hydrolysis of a Microtubule-Bound Nucleotide Triphosphate Is Near Zero: All of the Free Energy for Hydrolysis Is Stored in the Microtubule Lattice, *Journal of Cell Biology* **127**, p. 779-788 (1994)

[10] *Microtubules*, editors J. S. Hyams and C. W. Lloyd (Wiley-Liss, 1994)

[11] S. Rasmussen, H. Karampurwala, R. Vaidyanath, K. S. Jensen and S. Hameroff, Computational Connectionism within Neurons: A Model of Cytoskeletal Automata Subserving Neural Networks, *Physica D* **42**, p. 428-449 (1990)

[12] H. E. Stanley, *Phase Transitions and Critical Phenomena* (Clarendon Press, Oxford, 1971)

[13] K. Binder, D. W. Heermann, *Monte Carlo Simulation in Statistical Physics* (Springer-Verlag, Berlin, Heidelberg, 1988)

[14] M. V. Satarić, R. B. Žakula, J. A. Tuszyński, A model of the energy transfer mechanism in microtubules involving domain-wall-type solitons, *Physical Review E* **48**, p. 589-597 (1993)

[15] J. M. Dixon, J. A. Tuszyński and M. Otwinowski, Special analytical solutions of the damped-anharmonic-oscillator equation, *Physical Review A* **44**, p. 3484-3491 (1991)

[16] A. Gordon, Propagation of solitary stress waves at first-order ferroelectric phase transitions, *Physics Letters A* **154**, p. 79-80 (1991)

[17] P. M. Vassilev, R. T. Dronzine, M. P. Vassileva, and G. A. Georgiev, Parallel Arrays of Microtubules Formed in Electric and Magnetic Fields, *Bioscience Reports* **2**, p. 1025-1029 (1982)

[18] F. Gutmann, Some aspects of charge transfer in biological systems, in *Modern Bioelectrochemistry*, p. 177-197, editors F. Gutmann and H. Keyzer (Plenum Press, New York, 1986)

1 Structure and Properties of Microtubules

1.1 Eucaryotic Cell and Cytoskeleton[1]

Eucaryotic cells form the tissues of higher animals and plants. Each eucaryotic cell consists of cell nucleus and cytoplasm that is comprised of organelles and the **cytoskeleton** (Figure 1.1). The water solution of molecules and ions that fills the rest of the space between these structures is called cytosol. The contents of the cell are enclosed by the cell membrane.

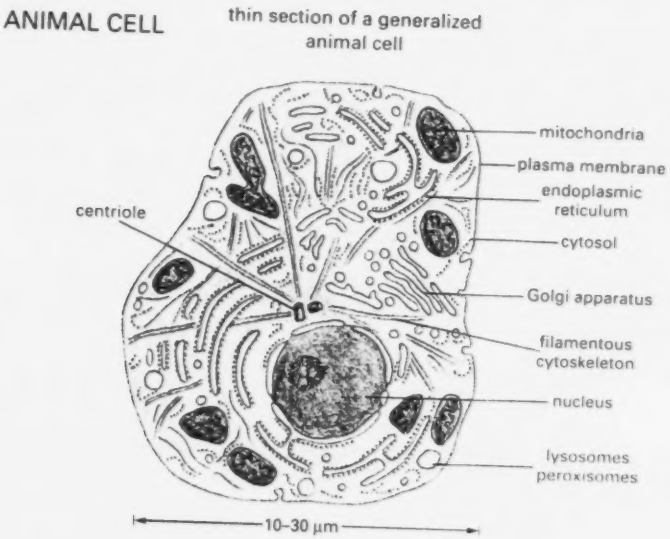

Figure 1.1: Animal eucaryotic cell. (From Reference [1].)

The cell nucleus plays a specific role in cell division. It contains most of the cell's DNA which is enclosed by the nuclear membrane. Near the cell nucleus is the centrosome that consists of two cylindrical centrioles positioned at right angles with respect to each other. At the beginning of cell division each centriole divides in two resulting in two new centrosomes that become two poles of the mitotic spindle which is the major tool of cell division.

[1]Based on Reference [1].

Organelles are "organs" of the cell and they occupy nearly half of the cell volume. Each organelle is a membrane bound structure and has a specific function in the cell. The organelles of the animal eucaryotic cell are listed in Figure 1.1.

The cytoskeleton is a compact network of proteins. The major components of this network are actin filaments, intermediate filaments and tubular polymers called **microtubules**. Filaments and microtubules are interconnected by means of a special class of proteins called associated proteins. The cytoskeleton provides mechanical support to the cell. It is a highly dynamic structure that can quickly reorganize itself according to the changing requirements of the cell.

1.2 Cytoskeletal Components[2]

1.2.1 Actin Filaments

Actin filaments are fibres with diameter 5-9 nm that are formed by two stranded helical protein polymers (Figure 1.2). The main building block of the actin filaments are actin monomers. Unlike microtubules, actin filaments rarely occur isolated but they are cross-linked into networks or bundles. This suggests that a bundle of actin filaments could be viewed as a structure functionally equivalent to one microtubule.

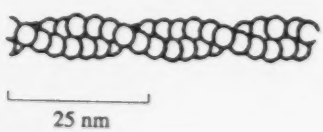

Figure 1.2: An actin filament.

Actin filaments are located mostly beneath the plasma membrane where they form a gel-like network called the cell cortex. The cell cortex functions with various forms of the associated motor protein **myosin** to control the movements of the cell surface. It can push the cytoplasm outwards to form thin projections called microspikes or sheet-like projections called lamellipodia. In the last phase of cell

[2]Most of this section is based on Reference [1].

division the network of actin filaments forms a contractile ring that draws the plasma membrane inside to divide the cell in two. In some cases the actin filaments in the cell cortex move the whole cell. The cell cortex and microtubules often act together to polarize the cell.

Actin filaments are dynamic structures. *In vitro* they exhibit a special kind of behaviour called **treadmilling** when at one end of the filament actin monomers are added and at the other end they are released. Since the rates of addition and dissociation are the same, the net length of the actin filament is constant. Treadmilling can play a role in the dynamic changes of the actin filament network.

1.2.2 Intermediate Filaments.

Intermediate filaments are rather stable tubes with diameter 8-10 nm that consist of highly elongated protein molecules (Figure 1.3). They are found in most animal cells. Usually they are interconnected into a network that surrounds the nucleus and extends out to the plasma membrane. These cytoskeletal fibres are also found on the inner side of the nuclear membrane where they form a structure called nuclear lamina. Nuclear lamina rapidly disassembles at the beginning of cell division and assembles again after the division.

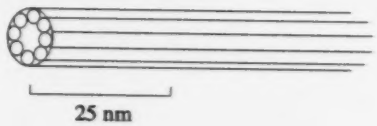

Figure 1.3: An intermediate filament.

Since intermediate filaments are quite rigid, they are mainly present in cells that have to sustain mechanical stresses. These are epithelial cells and muscle cells. Intermediate filaments have been also detected in neurons along axons and many other types of cells.

In different types of cells intermediate filaments are formed of different proteins. For example, in epithelial cells the intermediate filaments are composed of keratins, in nerve cells they consist of neurofilament proteins. Nuclear lamina is composed of special class of intermediate filament proteins called nuclear lamins.

1.2.3 Microtubules

Microtubules (MTs) are the largest tube-like cytoskeletal components. They assemble from the molecules of tubulin which is a globular protein present in cytosol. MTs participate in many important cytoskeletal activities. They are the major tools of chromosome separation during anaphase of cell division. MTs are tracks along which organelles and other structures are transported to a proper position in the cell. In neurons, neuronal vesicles are transported along MTs towards the synapse. MTs also form the cores of the protrusions from the cell surface called cilia and flagella whose beat-like motions enable the cell to move.

Some aspects of MT behaviour and MT functions in the cell are the subject of this thesis. The most important facts known about these cytoskeletal structures are summarized in the following sections of this chapter.

1.3 Structure of Microtubules

MTs are hollow cylinders with an outer diameter of about 25 nm and an inner diameter of about 15 nm. The MT subunit tubulin is a dimer that consists of two monomers, α- and β-tubulin, each of which has a molecular weight 50-55 kilodaltons [2]. The length of a tubulin dimer is 8 nm and the width is about 5 nm.

The tubulin subunits within a MT arrange themselves into protofilaments. An overwhelming majority of MTs have 13 or 14 protofilaments, but generally the number of protofilaments can range from 10 to 17 [3]. Changes in the number of protofilaments along MTs have been observed, but they are not very frequent.

Each protofilament in a MT is shifted with respect to the neighbouring one which results in a helical arrangement of the tubulin dimers within the MT. Until recently it was assumed that the MT lattice of tubulin dimers was helically symmetric. Such MTs have an odd number of protofilaments which are shifted with respect to each other by 3.1 nm. The MT lattice in which the longitudinal shift between two neighbouring protofilaments, or stagger, is 3.1 nm, is termed the A lattice (Figure 1.4a). However, experimental evidence strongly suggests that the cytoplasmic MTs have a lattice with stagger 0.9 nm. This type of MT lattice is termed the B lattice (Figure 1.4b) [4–6]. In the B lattice the end of the previous row doesn't match with the beginning of the next row which results in a structural discontinuity called a

"seam". MTs with the A lattice and an even number of protofilaments have a seam as well.

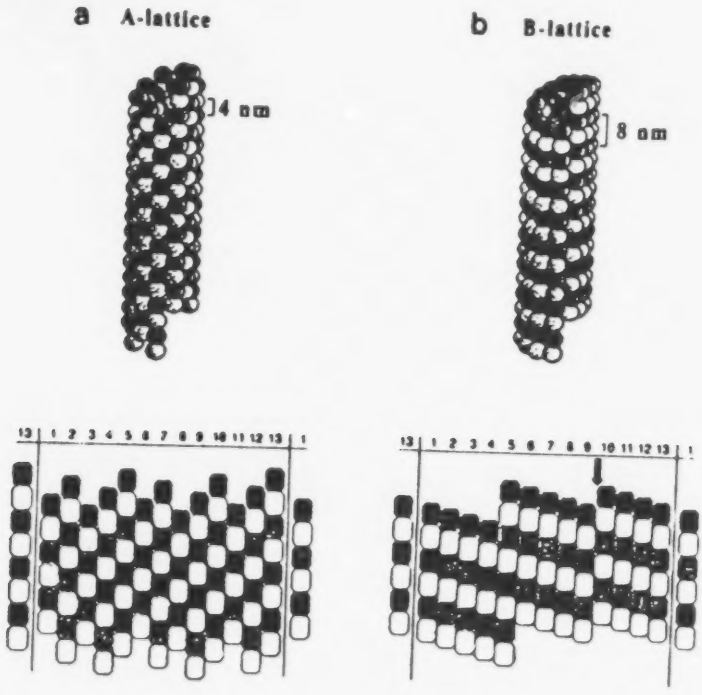

Figure 1.4: A and B lattices in a MT with 13 protofilaments and their planar projections. α monomers are shaded black, β monomers are light. The arrow indicates a seam. The tubules are from Reference [7]. The planar projections are from Reference [3].

It was demonstrated in [7] that the A and B tubules of the outer doublet in flagella also have a B lattice. However, the rows of both tubules match in such a way that the whole doublet exhibits a symmetric A type structure[3].

An object of intense investigations has been the composition of MT ends. It is known from many experiments that one MT end is more active than the other which suggests that the knowledge about the structure of the MT ends may explain other aspects of the MT behaviour. The more active MT end is termed the plus end and the less active MT end is termed the minus end. The tubulin monomers at the two ends of the MT protofilaments can be arranged in two possible ways which are

[3]The notation A and B tubules in flagella is not related to the A and B lattices in MTs.

shown in Figure 1.5. Either α-tubulin is exposed at the minus end and β-tubulin at the plus end or *vice versa*. Experiments reported in [7] strongly support the second alternative: α-tubulin was detected at the plus end and β-tubulin at the minus end.

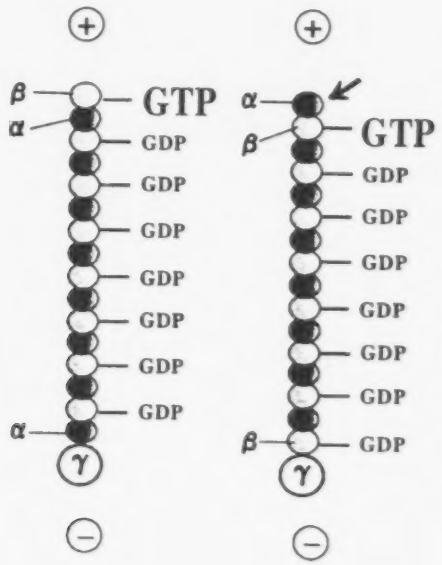

Figure 1.5: Two possible arrangements of the ends of a MT protofilament. On the left, the protofilament ends at the plus end with the β-tubulin. On the right, the exposed monomer at the plus end is the α-tubulin. The exchangeable guanosine 5' triphosphate (GTP) binds to the β-tubulin at the plus end of the protofilament. On the β-tubulin inside the protofilament GTP hydrolyses and the product of the hydrolysis is guanosine 5' diphosphate (GDP). γ-tubulin is located near the minus end. (From Reference [7].)

However, it is known that the attachment of the tubulin dimers at the assembling MT end (plus end) is followed by the hydrolysis of the exchangeable GTP which binds to β-tubulin (see section 1.4.3). Since the β-tubulin is partially buried in the MT lattice at the plus end, the observed structure of the MT ends may seem to contradict the observation that the plus end is more active. On the other hand, current opinion is that β-tubulin is genetically linked with the third variant of tubulin, γ-tubulin, which has been found recently [8]. γ-tubulin is not present in MTs; however, it has been detected in MT nucleating (organizing) centers (centrioles and basal bodies, see sections 1.4 and 1.5.3) at, or near, the minus ends [4]. This supports

the finding that the terminal monomer at the minus end is the β-tubulin.

1.4 Microtubule Assembly and Disassembly

1.4.1 Dynamic Instability

MTs in animal cells continuously grow and shrink. This phenomenon was discovered by M. Kirschner and T. Mitchison and it is known as **dynamic instability** [9].

Most of the knowledge about dynamic instability came from experiments with purified tubulin molecules *in vitro* [1]. In these experiments it was found that MTs start to polymerize from the pool of free tubulin when the concentration of Mg^{2+} and GTP exceeds a critical value. A MT can start growing either spontaneously or from a nucleation site [10]. After some time, the growth is stopped and the MT begins to shrink until it depolymerizes completely or it starts to grow again. While growth seems to be a linear function of time, shrinkages happen randomly and at a much higher rate. The transitions from shrinking to growing are termed "rescues", while the transitions from growing to shrinking are called "catastrophes". An experimental measurement of the dynamics of a single MT is shown in Figure 1.6.

The net growth or net shrinkage of a single MT is a result of the growth or shrinkage at both MT ends. According to observations the transitions between the growing and shrinking phases at a MT end are stochastic. The two ends behave independently of each other, that means, the frequencies of transitions between growing and shrinking and the rates of these processes at both ends are uncorrelated [11].

The dynamic behaviour of MTs in the cell is similar to that observed *in vitro*. The polymerization/depolymerization at both ends result in shrinkage or growth of the whole MT. Shrinkage happens suddenly and much faster than growth. Once a MT starts shrinking, it either partially shortens and then starts growing or it completely disassembles. The average half-life time of an individual cellular MT is about 10 minutes [1].

Most cellular MTs originate at the centrosome [1]. They extend from the centrosome in all directions towards the cell periphery (Figure 1.7). The MT end attached

This figure has been removed due to copyrights. The figure can be found in Reference 10 at page 1579.

Figure 1.6: The observed time change of the net length of a single MT. (From Reference [10].)

to the centrosome grows three times slower than the free end. The attached end is the minus end and the free end is the plus end. Due to dynamic instability the array of MTs concentrated around the centrosome is continuously changing as new MTs grow and replace the MTs that have depolymerized.

Dynamic instability is a mechanism by means of which the cell organizes such important activities as polarization and division. Polarization can be observed in most animal cells. The cell is polarized when the cell elements order themselves in a preferred direction. MTs play an important role in this process when they grow preferably in one direction due to mechanisms that are largely not understood. For example, crawling of the cell is achieved when a leading edge is created by MTs that point mainly in the direction towards the edge.

1.4.2 Cell Division[4]

MTs play a significant role in cell division, which is the most important event during the life time of the cell. Cell division consists of two phases: **mitosis**, when the cell nucleus is divided into two daughter nuclei, and **cytokinesis**, when the cell membrane and cytoplasm divide to form two daughter cells around the new nuclei. The time between two divisions is called **interphase**. During this stage the cell

[4]Based on Reference [1].

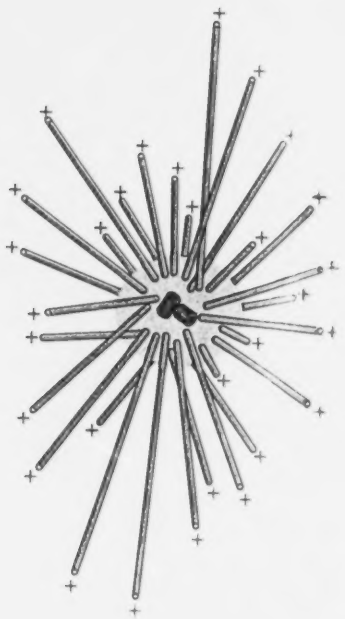

Figure 1.7: A schematic illustration of the array of MTs radiating from the centrosome. The MTs are attached to the centrosome at the minus end, the end growing out of the centrosome is the more active plus end. (From Reference [1].)

grows and prepares for the next division which includes the replication of DNA in the cell nucleus.

MTs are mainly involved in mitosis. Mitosis is initiated by a cascade of protein phosphorylations triggered by the activation of the mitosis inducing protein kinase called M-phase promoting factor (MPF), and terminates by dephosphorylations that follow inactivation of MPF. Mitosis consists of 5 stages: prophase, prometaphase, metaphase, anaphase and telophase (Figure 1.8 and Figure 1.9).

In **prophase**, chromatin that is dispersed during interphase in the cell nucleus condenses into chromosomes. Each chromosome consists of two sister chromatids, one for each of the two new cells. The cytoplasmic MTs that have been part of the cytoskeleton in interphase, disassemble. The centrosome duplicates into two. Each of the two new centrosomes moves towards the opposite poles of the cell and starts to nucleate MTs. The resulting structure is called mitotic spindle and it is the main apparatus of cell division. While in interphase MTs are relatively few and quite

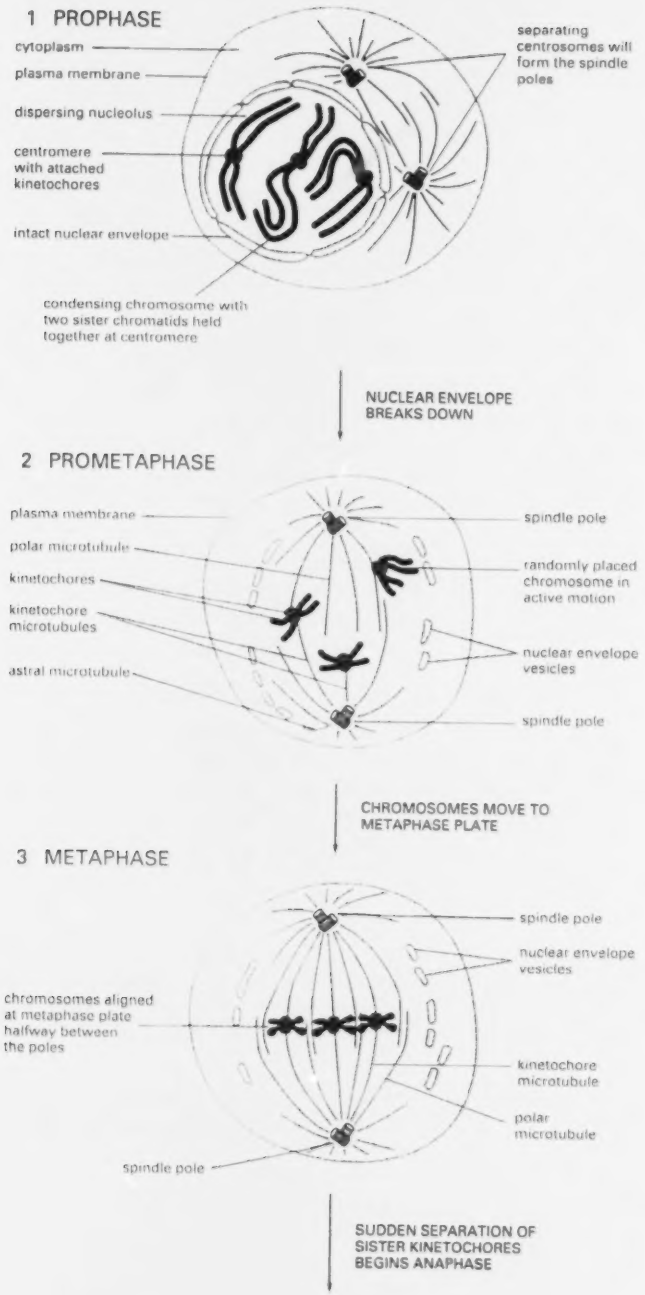

Figure 1.8: Prophase, prometaphase and metaphase. (From Reference [1].)

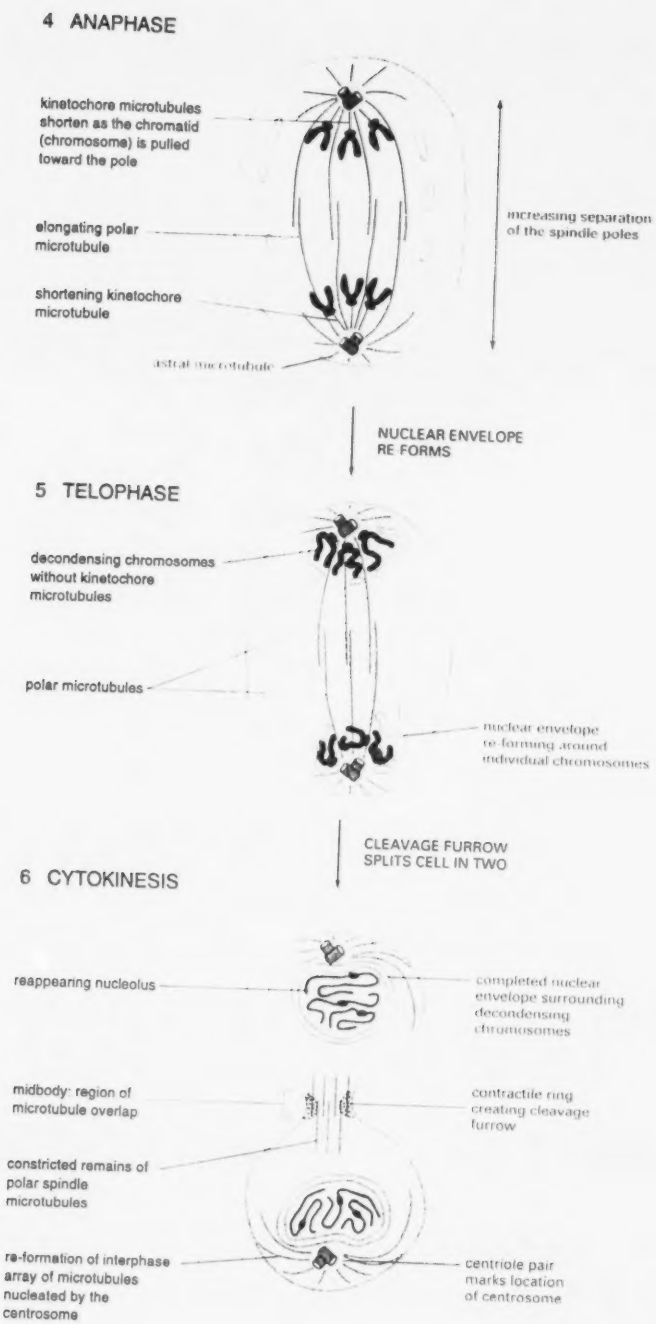
4 ANAPHASE
kinetochore microtubules shorten as the chromatid (chromosome) is pulled toward the pole
elongating polar microtubule
shortening kinetochore microtubule
astral microtubule
increasing separation of the spindle poles
NUCLEAR ENVELOPE RE-FORMS
5 TELOPHASE
decondensing chromosomes without kinetochore microtubules
polar microtubules
nuclear envelope re-forming around individual chromosomes
CLEAVAGE FURROW SPLITS CELL IN TWO
6 CYTOKINESIS
reappearing nucleolus
completed nuclear envelope surrounding decondensing chromosomes
midbody: region of microtubule overlap
contractile ring creating cleavage furrow
constricted remains of polar spindle microtubules
re-formation of interphase array of microtubules nucleated by the centrosome
centriole pair marks location of centrosome

Figure 1.9: Anaphase, telophase, cytokinesis. (From Reference [1].)

long with the average half-life time of about 5 minutes, prophase is characterized by large numbers of short MTs that surround each centrosome and exist for only about 15 seconds.

In **prometaphase**, the nuclear envelope breaks down and the chromosomes become accessible to the mitotic spindle. The plus ends of the continuously changing MTs probe the space in the cell at random until some of them attach to the chromosomes. The places at which MTs attach to the chromosomes are called kinetochores. One kinetochore is placed at each of the two chromatids. Both chromatids of each chromosome eventually connect to the MTs from the opposite poles of the mitotic spindle. According to the estimate made in [12] a connection of a MT to a kinetochore is made within 2 minutes. In this process errors can occur, most frequently when both chromatids of the same chromosome attach to the MTs from the same pole, but usually these errors are quickly corrected. MTs attached to the kinetochores are called kinetochore MTs. Kinetochore MTs are not static. While the kinetochore maintains its mechanical attachment to the MT plus end, there is a constant loss and addition of tubulin subunits at this end.

In the third stage of mitosis, **metaphase**, kinetochore MTs align the chromosomes in a plane that is halfway between the two poles of the mitotic spindle so that the chromosomes become ready for segregation. The kinetochore MTs continuously lose tubulin subunits at the minus end and gain them at the plus end keeping the net length constant.

Inactivation of MPF triggers the beginning of **anaphase**. The two sister chromatids of each chromosome are freed from the bond that has held them together and are pulled towards the opposite poles of the mitotic spindle. This process is accompanied by depolymerization of the kinetochore MTs. From 60% to 80% of the assembled tubulin is depolymerized at the kinetochores and the rest at the minus ends.

The mechanism that causes the sister chromatids to move towards the spindle poles is not exactly known. One possible hypothesis is that the kinetochore of a sister chromatid is attached to the MT plus end through a motor protein that moves towards the MT minus end by hydrolysing adenosine $5'$ triphosphate (ATP) (see section 1.5.2). As the motor protein moves, it pulls the chromatid. At the same time the MT plus end becomes exposed and disassembles molecules of tubulin. Another possible explanation of the poleward movement of the chromatids is that the kinetochores are attached to the MT plus end through a protein which has

high affinity for polymerized tubulin. Hence, as the MT plus end is disassembling, both the protein and the chromatid follow the shortening MT. In recent experiments minus-end-directed movement of motor proteins in the kinetochore has been detected. This finding favours the first hypothesis.

In the second stage of anaphase, the kinetochore MTs are completely depolymerized. The two poles of mitotic spindle are moved apart by elongation of polar MTs. The process of nuclear division is ended by **telophase** in which the nuclear envelope forms around each group of daughter chromosomes.

The division of the cell is completed by cytokinesis (Figure 1.9). The cell membrane and the cytoplasm divide into two halves by means of the contractile ring that starts to assemble in the middle of the cell during anaphase from actin and myosin-II. The contractile ring pushes the cell membrane inwards perpendicular to the rests of the mitotic spindle. The cleavage furrow created in this way gradually deepens and eventually breaks down resulting in a final formation of two new daughter cells.

1.4.3 GTP Hydrolysis in Microtubule Assembly/Disassembly

According to *in vitro* observations, MT polymerization takes place when the concentration of free tubulin molecules that bind at their exchangeable nucleotide binding site GTP reaches a certain critical value. The attachment of a tubulin dimer to a MT is accompanied by the **hydrolysis of GTP** bound at the exchangeable binding site. In the GTP hydrolysis, a molecule of water breaks the bond between the high energy phosphate group of GTP (Figure 1.10) and the rest of the molecule which results in a formation of GDP and a phosphate group.

It should be pointed out that according to standard view, the exchangeable nucleotide binding site is placed at the β monomer of the tubulin dimer [4, 11, 13]. After GTP hydrolyses, this site binds GDP[5]. GDP on the β-tubulin is exchanged for GTP after a MT depolymerizes. In this way the pool of free tubulin that binds exchangeable GTP is regenerated and the MT assembly followed by the GTP hydrolysis can start again. The α monomer binds GTP as well but with a much greater affinity than the β monomer. Due to this the GTP on the α monomer is bound permanently and can not be exchanged.

[5]Tubulin which binds on the exchangeable nucleotide binding site GTP will be termed GTP tubulin and tubulin which binds on the exchangeable nucleotide binding site GDP will be termed GDP tubulin.

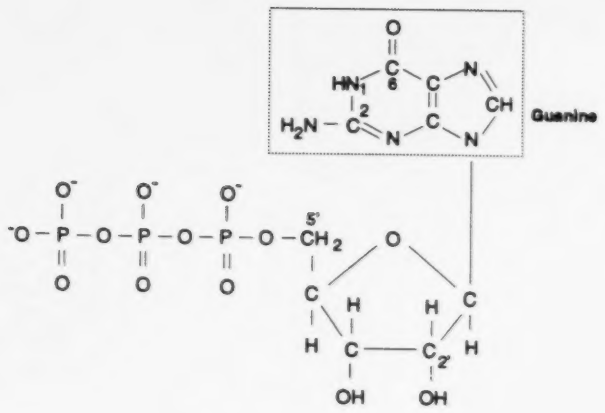

Figure 1.10: Guanosine 5′ triphosphate. Drawn according to [14].

At pH=7, the GTP hydrolysis reaction can be written as

$$GTP^{4-} + H_2O \rightarrow GDP^{3-} + HPO_4^{2-} + H^+ + \Delta E\,. \tag{1.1}$$

At pH=9, the result of the GTP hydrolysis is a phosphate group PO_4^{4-} and two protons H^+. In both cases, the standard free energy ΔE is released.

The energy ΔE is the same as the energy of the ATP hydrolysis, $\Delta E = 8.7\,\mathrm{kcal/mol}$ [15]. The ATP hydrolysis is a major source of free energy utilized by biological systems. However, the free energy can also be supplied by the hydrolysis of other nucleoside 5′ triphosphates[6], among them GTP [14]. Other nucleoside 5′ triphosphates are present in the cell in much lower concentrations than ATP. This implies that they are specific only for some biological activities.

A number of experiments have shown that the GTP hydrolysis is linked to MT assembly and disassembly processes. This phenomenon has been studied by examining the MT assembly from tubulin molecules that bind to their exchangeable nucleotide binding sites very slow hydrolysable GTP analogues. Such a GTP analogue is, for example, guanylyl-(α,β)-methylene-diphosphate (GMPCPP) that hydrolyses very slowly into GMPCP [16,17]. The half-life time of the GMPCPP hydrolysis is about 10 hours, which is very long compared to the half-life of a MT. Consequently during MT polymerization from GMPCPP tubulin, GMPCPP doesn't hydrolyse. Such

[6]Nucleoside is the base of the nucleoside 5′ triphosphate molecules, for example, guanine in GTP or adenin in ATP. Nucleotide is the whole molecule, *i.e.*, GTP, ATP, *etc.*

MTs were found to be very stable. The rate of dissociation of GMPCPP tubulin is 100 times slower than the rate of dissociation of MTs composed of GMPCP and GDP tubulin. These observations imply that the GTP hydrolysis is not necessary for the MT assembly, but it is essential for the disassembly.

In [16] the measurements of the standard free energy of the GMPCPP hydrolysis are reported. This energy is 5.18 kcal/mol (0.21 eV) in solution, 3.79 kcal/mol when GMPCPP is bound within a free tubulin molecule and only 0.9 kcal/mol when the tubulin is bound in a MT. It can be assumed that the energies of the GTP hydrolysis are in a similar ratio. Then the values above imply that most of the energy freed during the GTP hydrolysis in the process of the MT assembly is stored in the assembled MT. The way this energy is stored could be a conformational change of tubulin molecules induced after the GTP hydrolysis. The stored energy must be released during the MT disassembly. If it is larger than the energy needed for the breakage of the bonds between the tubulin molecules in the disassembling MT, the surplus can be used to do mechanical work, for example, by coupling disassembly to the vesicle or chromosome movement [18]. This conjecture was supported by the finding that in the chromosome movement during mitosis no exogenous energy is supplied [19].

1.4.4 Tubulin Conformational States and Microtubule Assembly/Disassembly

Observations of the MT assembly/disassembly indicate that the conformation of the tubulin molecule changes after the exchangeable GTP hydrolyses. In other words, the conformational states of the GTP tubulin and GDP tubulin are different which may be closely linked with the MT assembly/disassembly.

In experimental measurements no GTP tubulin has been detected in MTs until now. This finding suggests that GTP hydrolysis takes place soon after a tubulin dimer attaches to the growing MT end. Due to this, the tubulin subunits in the interior of a MT bind GDP and so do the molecules of tubulin from the disassembled MTs. Furthermore, it has been observed that at the growing MT end the protofilaments are straight, while at the disassembling end they tend to uncoil [2, 18, 19]. After disassembly, rings and double rings composed of GDP tubulin are often observed. The possible explanation of these experimental facts could be the following:

At the growing end, the tubulin protofilaments are capped with GTP tubulin. The GTP tubulin promotes formation of straight and stable protofilaments that are favourable for growth. The disassembling end consists mostly of GDP tubulin. Due to the different conformation of the GDP tubulin the protofilaments uncoil as the MT disassembles and form rings composed of GDP tubulin (Figure 1.11).

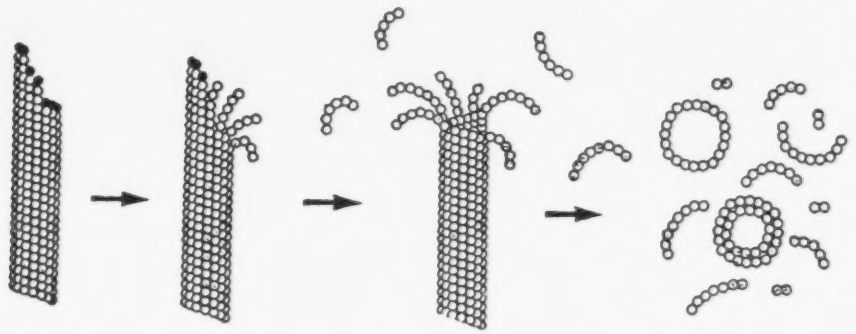

Figure 1.11: The growing MT end is capped with the GTP tubulin (solid circles). After GTP hydrolyses the tubulin binds GDP (open circles). When the protofilaments are not capped with tubulin GTP they start to uncoil and the MT disassembles. The disassembled GDP tubulin molecules associate themselves into rings and double rings. (From Reference [19].)

The concept above is known as the conformational (lateral) cap hypothesis. It may provide a possible explanation of the experiments discussed in the previous section according to which most of the energy of the GTP hydrolysis is stored in the MT in the form of the conformational states of the tubulin molecules. The interior of MTs is formed mainly of GDP tubulin which has the intrinsic tendency to coil. On the other hand, the lateral bonds between the neighbouring protofilaments stabilize the MT. Thus there is a competition between the tendency of tubulin GDP to curve and the stabilizing effect of the lateral bonds and most of the energy of the GTP hydrolysis is stored in the MT as a mechanical strain due to this competition.

On the basis of the considerations and observations above a mechanism of the MT disassembly has been suggested in [19]. In the interior of the MT the protofilaments are stabilized by the lateral bonds. However, the ends are exposed and if they are not capped by a sufficient fraction of the GTP tubulin molecules it is more likely that the tendency of the GDP tubulin to uncoil overpowers the stabilizing effect of

the lateral bonds and the end starts to disassemble. The mechanical energy stored in the MT lattice of tubulin dimers is freed and the unwinding of protofilaments propagates inwards along the MT. Similarly, a defect inside the MT that destabilizes the bonds between the tubulin dimers can propagate along the MT and cause an overall internal breakage of the MT [4]. This direct route, rather than dynamic instability could be utilized by the cell when MTs undergo quick reorganization.

The growing MT ends have been observed in a tubular form but as well as in the form of a sheet of protofilaments [20, 21]. The reason for this behaviour is unclear. The experiments in [19] showed that the growing MT ends are usually smooth but some protofilaments can protrude straight out up to 100-200 nm. This means that a MT grows along the protofilaments and not along the helix and thus doesn't behave in a helical manner. Secondly, there must be cooperative interactions between the neighbouring protofilaments that don't let a single protofilament grow too long.

The conformational cap hypothesis can be connected with the GTP cap hypothesis. The GTP cap hypothesis postulates that a MT end grows when it is capped at least by one layer of tubulin GTP. This means that the rate of GTP hydrolysis must be smaller than the rate of attachment of the GTP tubulin dimers to the MT.

Numerical simulations of MT assembly/disassembly based on the GTP cap have successfully reproduced the dynamic behaviour of MTs [3, 18, 22]. However, these models have not taken into account some observed features of the assembly/disassembly of a MT such as coiling of protofilaments at the disassembling ends or the anisotropy of the tubulin-tubulin bonds.

Figure 1.12 shows the length versus time plot of a MT with A and B lattices obtained from the simulations presented in [3]. The simulated growth and shrinkage behaviour of the MT is very similar to that observed for a real MT shown in Figure 1.6. The calculated plots show that the type of the lattice and the number of protofilaments have an effect on the overall growth but they don't change the nature of the dynamic instability.

Figure 1.13 represents the simulated effect of a nonhydrolysable analogue of GTP and GDP tubulin on the assembly of a single MT. As the plots show, a fraction of GMPPNP or GDP tubulin introduced into the pool of free GTP tubulin suppresses considerably the dynamics of the MT.

However, neither cap hypothesis has been confirmed yet. The fact that no GTP has been detected in MT tubulin may mean that either the size of the GTP cap is so small that it is below detectable limits or it is nonexistent. There is also evidence

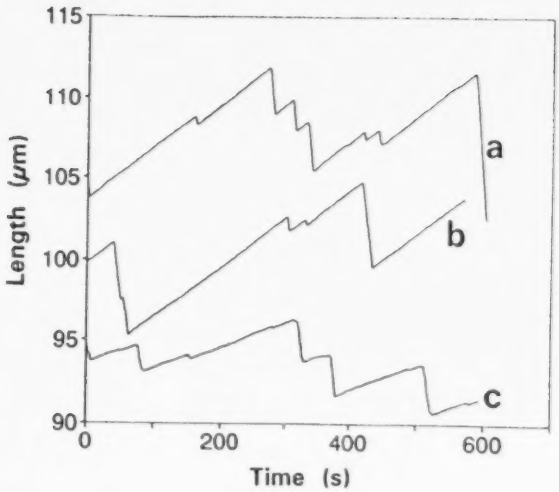

Figure 1.12: Numerically calculated length changes as a function of time for the MT lattices (a) A with 13 protofilaments, (b) A with 14 protofilaments, (c) B with 13 protofilaments. (From Reference [3].)

that some fraction of tubulin GDP can be used in the assembly of MTs [18, 23]. In [21] observations of shrinking MT ends that are blunt, not coiled, were reported.

It also has been suggested that the behaviour at the MT ends depends on the communication between them by means of diffusion of tubulin subunits. According to [10], the diffusion of free tubulin molecules towards the growing end of a MT is faster than the rate of incorporation of the molecules into the MT. This means that there is another mechanism necessary for attaching the tubulin dimers to the MT.

It should be pointed out that under favourable combination of the free GTP tubulin concentration, presence of microtubule associated proteins (see section 1.5), the rate of GTP hydrolysis, *etc.*, a MT can exhibit treadmilling.

1.4.5 Microtubule Oscillations

In vitro experiments have shown that under certain conditions the dynamic instability in an assembly of MTs can be synchronized. In other words, the amount of tubulin can oscillate in regular time intervals between a phase when almost all tubulin is bound in MTs and a phase when almost all tubulin is free [18, 19, 24].

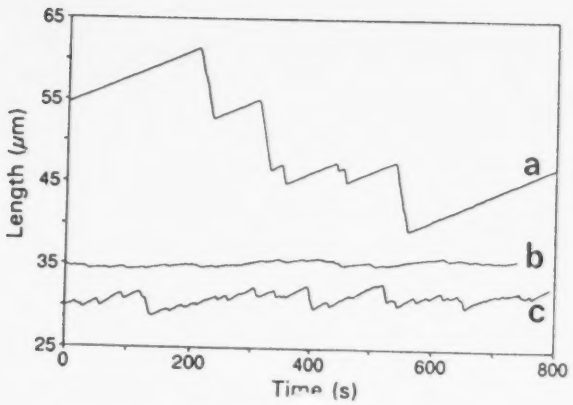

Figure 1.13: Numerically calculated length changes of a MT with the A lattice with 13 protofilaments as a function of time. The pool of free GTP tubulin contains (a) tubulin GTP only (b) 20% of GMPPNP, (c) 10% of tubulin GDP. (From Reference [3].)

In order for the oscillations of the assembly of MTs to be synchronized the disassembled tubulin can not be used immediately in the new MT assembly. As follows from the previous sections, MTs can assemble only in the presence of tubulin GTP and the product of disassembly is tubulin GDP. This implies that the condition for synchronized oscillations is that the regeneration of the GTP tubulin from the GDP tubulin has to be sufficiently slow. When the MTs have used all GTP tubulin and the GTP tubulin within the MTs hydrolyses there won't be any stabilizing cap and the MTs disassemble. If the rate of regeneration of the GTP tubulin from the GDP tubulin is slow, all tubulin will bind GDP on its exchangeable binding site and the MTs won't be able to start to assemble immediately after the disassembly, but only after a sufficient amount of GTP tubulin is regenerated from the GDP tubulin.

The regeneration of GTP tubulin from the GDP tubulin can be limited due to several factors. One is the rate of exchange of GDP for GTP on the disassembled tubulin. However, numerical simulations indicate that the rate of this process is too high to slow down the assembly significantly [18]. Therefore it was proposed that the regeneration of the GTP tubulin is prevented by binding GDP tubulin in the disassembly products. These could be rings or curved protofilaments that were observed to coexist with oscillating MTs in a substantial fraction [19]. Since it is known that GDP can be exchanged for GTP only on free tubulin the regeneration of

GTP tubulin is limited by the rate of dissociation of the curved oligomers. Indeed the numerical simulations presented in [19] have shown that curved oligomers oscillate in antiphase with MTs.

Figure 1.14 shows the reaction cycle for the synchronized oscillations of the MT assembly which was proposed in [19]. MTs start growing from the nucleation sites. These could be oligomers of globular form that have been observed to appear when MTs start growing. These globular structures could be associations of tubulin dimers that look like small parts of MT walls. Under favourable conditions determined mainly by the GTP tubulin concentration, a MT grows capped with GTP tubulin molecules. After the growing phase the MT starts shrinking due to lack of GTP tubulin. The protofilaments at the disassembling ends coil and form curved oligomers. Oligomers transiently bind GDP tubulin so that GDP can not be exchanged for GTP. After oligomers depolymerize, GTP tubulin is recovered and MTs start assembling again.

An example of simulated oscillations compared with the real oscillations observed *in vitro* is shown in Figure 1.15. The calculations are based on the reaction cycle drawn in Figure 1.14. The amount of tubulin molecules polymerized in MTs is plotted versus time. The calculated oscillations fit very well the observed oscillations of the assembly of MTs.

However, according to simulations presented in [24] oscillations can be also produced when the rate of dissociation of the oligomers is not limiting and thus the rate of exchange of GDP for GTP on the free tubulin is the crucial mechanism for generating synchronized oscillations. The authors of [24] also suggest that the destabilization and consecutive depolymerization of a MT is not connected to the GTP hydrolysis but to the release of the phosphate group HPO_4^{2-}. Thus the tubulin that binds the GTP hydrolysis products GDP+HPO_4^{2-} forms stable MTs.

Other mechanisms that could destabilize MTs and consequently prevent the MT polymerization were proposed in [18]. One is the interaction of the MT ends with curved oligomers. If the ends of a MT are slightly bent (marginally stable MT), the probability for switching to shrinkage is higher. If curved oligomers attach to a curved protofilament at one of the MT ends, there is a competition between the lateral interactions between the oligomers and the protofilaments and the longitudinal interactions in the protofilament. This can eventually make the catastrophe probability sufficiently high and the MT starts to disassemble.

As was shown in the previous section, the presence of a fraction of free GDP

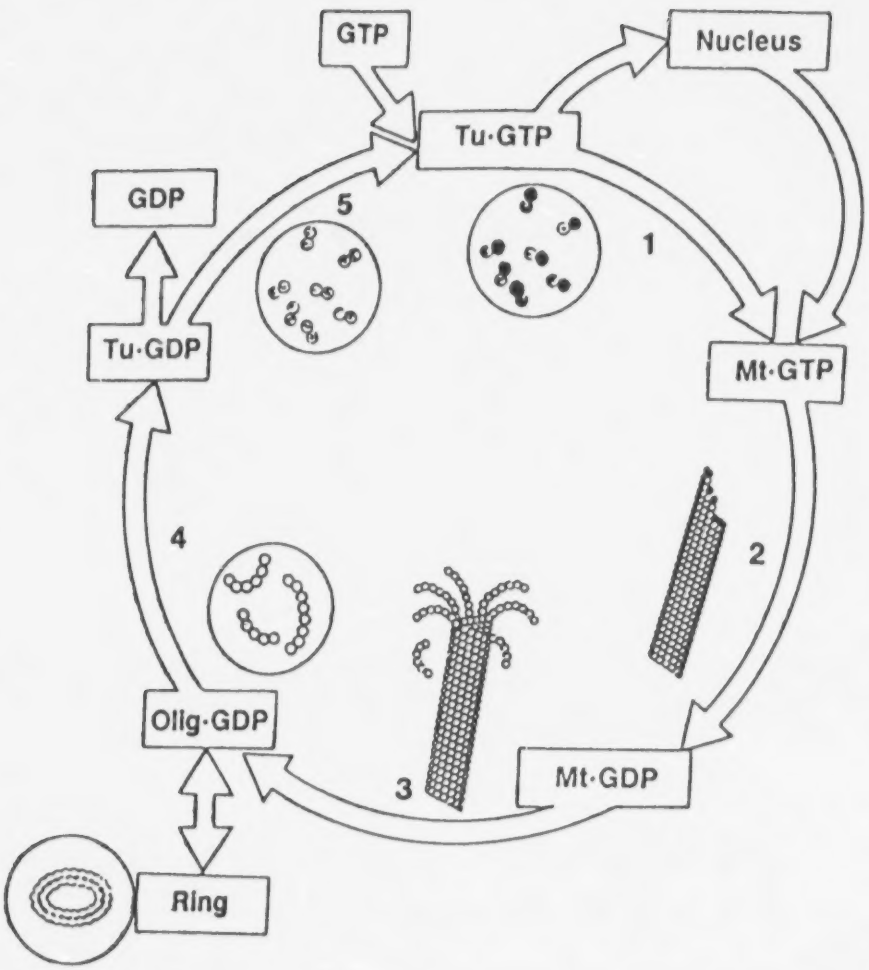

Figure 1.14: The oscillation cycle of an assembly of MTs. (From Reference [19].)

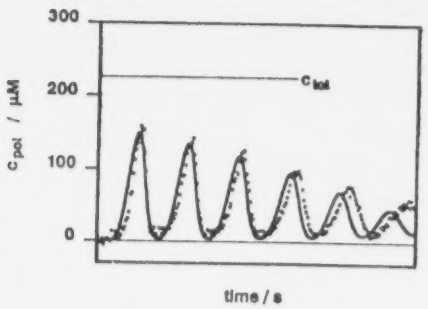

Figure 1.15: Regular oscillations of the MT assembly. c_{pol} is the concentration of the tubulin GTP in the MT polymer, c_{tot} is the total concentration of tubulin, the solid line is the calculated MT dynamics and the dotted line represents *in vitro* observations. (From Reference [18].)

tubulin considerably suppresses the dynamic instability. This means that incorporation of GDP tubulin at the growing MT end may be a factor which destabilizes MTs since it prevents them from growing. Destabilization could be also caused by the direct interaction between MTs. Such an interaction exists since regular spatial patterns formed by MTs have been observed (see Chapter 3). However, it is not clear how these interactions could influence the regular transitions between the two phases in the MT assemblies.

The dependence of the rate of growth of an assembly of MTs on the GTP concentration was numerically studied in [3]. Figure 1.16 shows the plots of growth rate of a MT assembly as a function of free GTP tubulin concentration. Below the concentration at which the point on the curve corresponds to the zero growth rate the MTs will disassemble, above this concentration the population of MTs will exhibit assembly. At a certain concentration, called the critical concentration, the growth rate doesn't change any more as a function of the GTP tubulin concentration.

Here it should be pointed out that the GTP tubulin concentration depends on various factors, *e.g.*, concentration of different ions (Ca^{2+}, Mg^{2+}), temperature, the presence of microtubule associated proteins, drugs, *etc.*, [3]. The effects of these factors on the dynamic instability can be multiple and interrelated. For example, high Mg^{2+} concentration increases the critical concentration of tubulin GTP, but at the same time it is favourable for forming oligomers which prevents the regeneration of the GTP tubulin from the GDP tubulin.

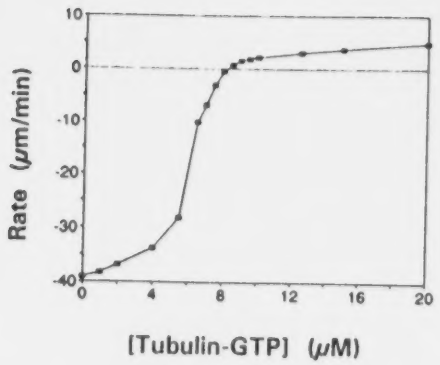

Figure 1.16: The rate of growth of the assembly of MTs with the A lattice which consists of 13 protofilaments as a function of the tubulin GTP concentration. (From Reference [3].)

1.5 Microtubule Associated Proteins

Microtubule associated proteins are special groups of proteins which bind to MTs. They are characteristic for specific cellular functions of MTs and can be divided into two main classes, MAPs and motor proteins [1, 25].

1.5.1 MAPs

MAPs are mainly known as promoters of the MT assembly *in vitro* and as bridges that interconnect MTs and also determine spacing between them [25]. MAPs so far identified have been termed MAP1, MAP2, MAP3, MAP4 and tau, each of which represents a family of isoforms[7]. Different MAP isoforms exist in different parts of cells and in different stages of cell morphogenesis.

MAPs are several times heavier than tubulin molecules. Their molecular weight ranges from 200 to 420 kilodaltons with the exception of tau whose molecular weight is between 59 and 62 kilodaltons. MAP1, MAP2 and tau have been detected mainly in neuronal cells. MAP4 has been found in many types of mammalian cells. The biochemical properties and the tissue distribution of MAP3 are similar to those of

[7]Isoforms or isotypes of a protein molecule differ by a small fraction of residues, but a substantial fraction of residues is the same. (For the definition of a residue see section 1.6.)

MAP4 which has lead to the conclusion that MAP3 and MAP4 are very likely the same proteins [25].

MAPs can be posttranslationally modified. Different modifications are associated with different functions. The best known modification of MAPs is phosphorylation by protein kinases. Phosphorylated MAPs are known to be less efficient in binding to MTs compared to the unphosphorylated forms. Phosphorylation/dephosphorylation of MAPs is also associated with different stages of cell morphogenesis [25].

The tau protein is the most efficient assembly promoter among MAPs. Because tau significantly increases the rate of MT polymerization and decreases the rate of MT depolymerization it has been suggested that neurites grow as a consequence of MT polymerization promoted by tau [25].

MAP4 has been detected along all cellular MTs during all stages of the cell cycle. Since MAP4 is widely distributed in many types of cells, it is likely to be involved in a number of MT functions such as transport of organelles or cell motility. Growing experimental evidence indicates that MAP4 could be the regulator of the MT behaviour during the interphase-mitosis transition. It is known that MAP4 becomes phosphorylated at the onset of mitosis. It interacts with cyclin B which together with $p34^{cdc2}$ kinase constitutes MPF [1]. This reaction could serve to target MPF to mitotic MTs. Since MAP4 is the predominant MAP in many types of dividing cells, its phosphorylation may indeed be an important factor in the dramatic changes in the dynamics and organization of MTs during cell division [25].

MAP molecules are composed of two domains, one with which they bind to MTs and a side arm by means of which the MAP binds to other cell components. Since MAPs are larger than tubulin dimers except for tau, they most likely bind to more than one molecule of tubulin. This may be one of the reasons why MAPs speed up the nucleation and assembly of MTs [1].

Different forms of MAPs with different size of side arms can determine different spacing between MTs. For example, in dendrites where MTs are closely spaced, the main MAP is a short-armed tau while in axons where the spaces between MTs are larger, high levels of long-armed MAP2 have been detected. It has been suggested that different spacings between MTs may be also achieved by means of different forms of the same MAP. This has been demonstrated for tau whose phosphorylation causes enlargement of its projection arms [25].

MAPs are associated with cylindrical structures of tubulin as tubulin forms a

large variety of other structures which are not cylindrical and whose formation depends on the presence of various drugs. MTs with bound MAPs usually have 13 protofilaments while MTs assembled from pure tubulin consist of 14 protofilaments [4].

Observations show that the patterns of MAPs bound to MTs in the brain cells are irregular. However, it has been suggested that MAPs can also form regular patterns, some of which are shown in Figure 1.17 [26]. This suggestion is supported by experiments which indicate that MAP2 may bind to the MT surface cooperatively. The measured ratio of MAPs to the number of tubulin molecules at which the binding of MAP4 to MTs is saturated was found to range from 1:2.3 to 1:20. The saturation level of MAP2 was reported to be 1:4.3 [25].

1.5.2 Motor Proteins

Motor proteins are involved in MT-based motility and the motions of cilia and flagella. Two classes of MT-associated motor proteins have been identified, kinesins and dyneins. Dyneins which bind to MTs within the cytoskeleton are called cytoplasmic dyneins while ciliary dyneins are bound to the MTs in cilia and flagella [1]. Both kinesins and dyneins are families of structurally different proteins. The family of kinesins is much more diverse than the family of dyneins. Binding of kinesin and dynein to distinct cellular sites may be determined by structurally different subdomains of these molecules [25].

Numerous experiments have shown that kinesins are mainly associated with movement of organelles and axoplasmic vesicles towards the MT plus end (away from the cell body) while the cytoplasmic transport mediated by dynein is directed mainly towards the MT minus end (towards the cell body). However, some observations indicate that the transport in the opposite direction for both kinesin and dynein can not be excluded [25]. For example, a *Drosophila* kinesin *Ncd* moves towards the MT minus end [1].

Kinesin is a prolonged molecule with molecular weight of about 200 kilodaltons. It consists of two heads, a long rod-like domain and a tail (Figure 1.18). The tail is composed of several heavy chains and several light chains. Besides axoplasmic and organelle transport, kinesin has also been detected in other cell activities. It seems to participate in the interaction of organelles and intermediate filaments. There is

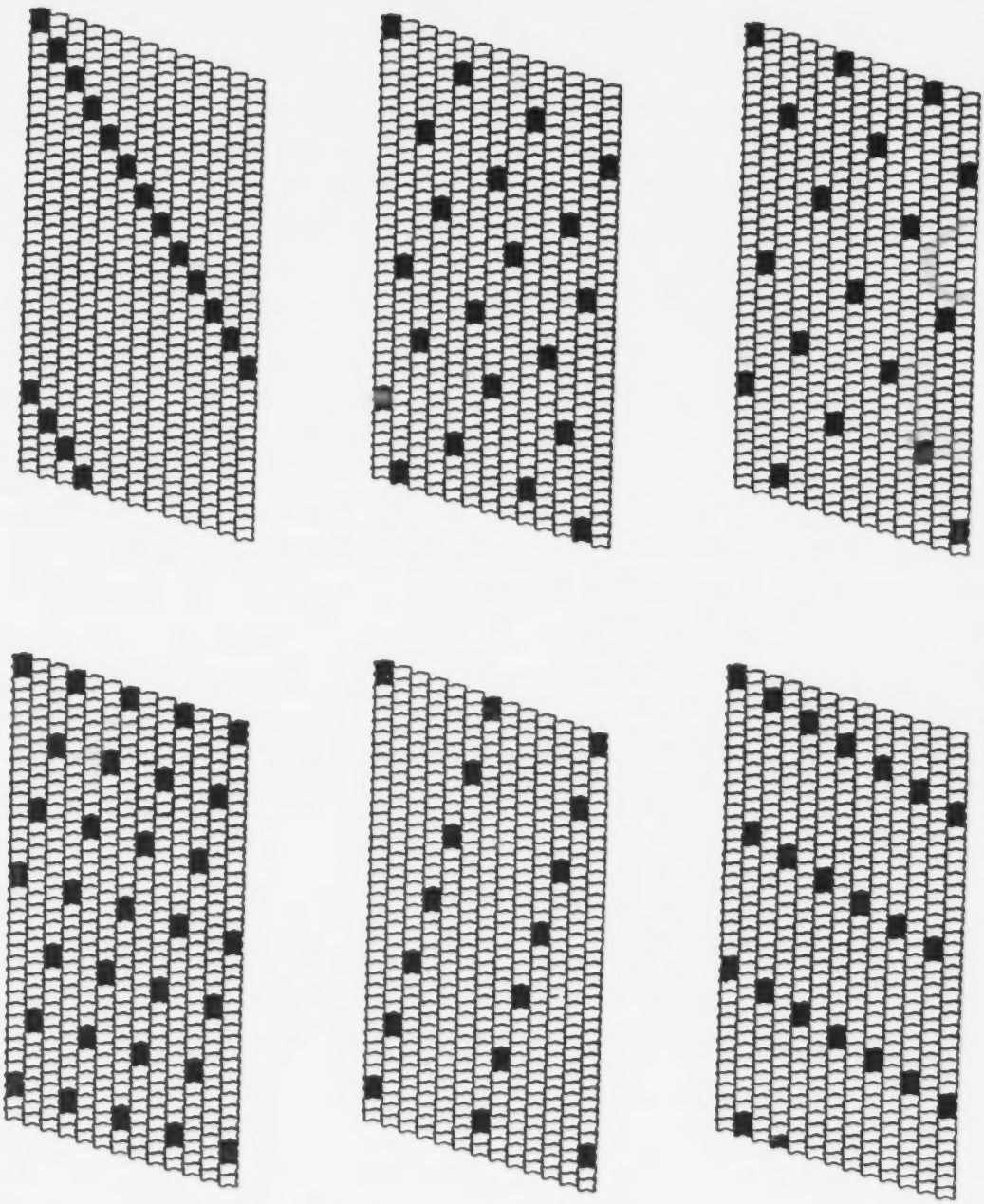

Figure 1.17: MAP attachment patterns observed by electron microscopy. (From Reference [26].)

strong experimental evidence that kinesins are involved in mitosis. It was found that a special group of kinesins keeps the two spindle poles apart until anaphase [25].

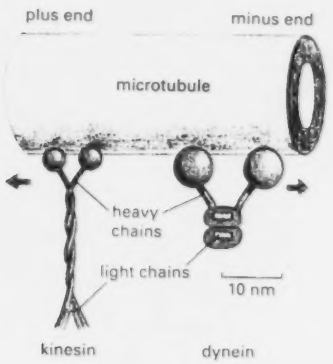

Figure 1.18: A schematic drawing of kinesin and cytoplasmic dynein. The direction of movement along MTs is indicated by arrows. (From Reference [1].)

The rate of kinesin associated transport has been measured for several species. Kinesin purified from squid axons has been observed to move MTs at a velocity $0.5\,\mu\text{ms}^{-1}$ [25]. Experiments show that the cytoplasmic transport along MTs with bound kinesin occurs at 4 nm steps which suggests that kinesin binds to each MT monomer. Other observations indicate that only 1 to 5 kinesin molecules are involved in the transport along MTs [25].

Kinesin has been observed in two forms, inactive folded and active extended. This feature may be important in regulation of the cytoplasmic transport when the activation of kinesin can be achieved by means of posttranslational modifications such as phosphorylation. It is known that organelle transport activity is high during interphase but is very low during cell division, while the concentration of kinesin doesn't change during the cell cycle. This means that there must be a regulatory mechanism which activates the organelle transport mediated by kinesin [25].

A molecule of cytoplasmic dynein consists of two heads connected to the common base that is composed of heavy chains and light chains. Each head has a molecular weight of about 400 kilodaltons and the molecular weight of the entire molecule is about 1.2 megadaltons [25].

Cytoplasmic dynein was detected along axonal MTs, kinetochores, spindle poles and spindle MTs. The poleward movement of chromosomes in prometaphase has

been found to have rates associated with cytoplasmic dynein which are in the range 1.25-2 μms^{-1}. In axons, the transport of vesicles from the synapse towards the cell body is most likely mediated by dynein. Since all proteins are made in the cell body, dynein must be first carried along the axon to the synapse, most likely by kinesin, in order to pass the vesicles back to the cell body [1]. Similarly to other associated proteins, cytoplasmic dynein can be phosphorylated which may be important in the regulation of dynein function [25].

The movement of kinesin and cytoplasmic dynein is driven by the hydrolysis of ATP that is bound to the heavy chains of both motors. However, the mechanism of conversion of the chemical energy of the ATP hydrolysis into the mechanical movements is not known [1].

1.5.3 Cilia and Flagella

Ciliary dynein is associated with motions of cilia and flagella [1, 2, 25]. Cilia are projections from the cell surface that are used to move the fluids and other particles around the cell and sometimes the whole cell. Fields of cilia move in coordinated unidirectional waves which are the result of a whiplike motion of each cilium. Flagella are very similar to cilia but usually they are much longer. They are the tails that propel sperm and their motions resemble quasi-sinusoidal waves. The coordinated character of the ciliary and flagellar movement suggests that it originates from cooperative interactions within these structures.

The movement of a cilium or a flagellum is produced by the bending of its core called the axoneme. The usual length of an axoneme is 10 μm but it can be as long as 200 μm. The axoneme is composed of MTs and their associate proteins. In the center of the axoneme is a central pair of MTs around which are positioned 9 MT doublets (Figure 1.19). The central MTs are complete and each consists of 13 protofilaments. In each doublet, one MT is complete and is composed of 13 protofilaments. This is the A tubule. The other tubule, B tubule, is incomplete. It shares part of its wall with the A tubule and consists of 10 protofilaments [1].

Ciliary dynein binds to the MT doublets and forms outer and inner arms. This dynein is a larger and more complex molecule than the cytoplasmic dynein. Its molecular weight is nearly 2 megadaltons. The molecule consists of 2 or 3 heavy chains and about 10 light chains that form two or three head domains attached by stems to a common base. The head of the molecule binds to the B tubule while

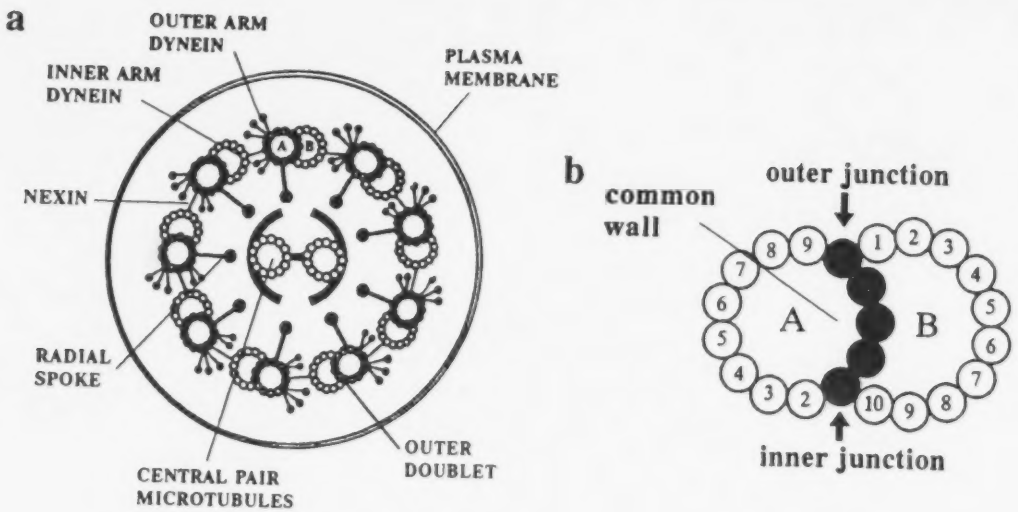

Figure 1.19: A schematic cross-section through a flagellum (a) and the MT doublet (b). (From Reference [7].)

the tail binds to the A tubule [25]. By hydrolysing ATP in the head the dynein molecules produce movement of MTs which would be sliding if the MTs were free, but becomes a bending movement because of the many links between MTs in the axoneme. This is the basis of the coordinated motions of cilia or flagella. However, the mechanism of the interactions between the MTs and the motor proteins which leads to such a regular behaviour is so far unexplained.

It has been found in experiments that the outer arm dynein binds to the MT doublets every 24 nm. The binding is cooperative. That means if a molecule of outer arm dynein binds to a MT, it is more likely that another one will bind next to it. The inner arms form a pattern where the dynein with three heads is followed by the dynein with two heads and the whole sequence repeats every 96 nm [25].

The rates of movement associated with ciliary dynein have been found to be higher than the rates of movement produced by kinesin and cytoplasmic dynein. MTs added to the mixture of ATP and outer arm dynein from sea urchin sperm flagella, were gliding on a glass surface at rates up to $7\,\mu\text{ms}^{-1}$. The rate of gliding didn't depend on the length of the MT, *i.e.*, on the number of outer arms. This means that the generation of force by the outer dynein arms must be very synchronized. In experiments with *Chlamydomonas* the measured rates of translocation of

MTs with their inner arms ranged from 2.7 to 11.5 μms^{-1}. Both outer and inner arm dynein have been found to be the MT minus end motors [25].

Other experiments indicate that the number of outer arms affects the frequency of the ciliary and flagellar motion but it is not responsible for the waveform. On the other hand, structurally different inner arm dyneins can be distributed along the axoneme which may be connected with the determination of the waveform and also with the initiation of bending. Different dyneins also produce different rates of MT gliding [25].

All cilia and flagella grow from basal bodies [1,2]. Basal bodies are constructed from 9 triplets of MTs which are arranged in a ring and tilted as the blades of a turbine. Each triplet is comprised of one complete A tubule and two incomplete tubules B and C. The triplets are interconnected with a central core so that the cross-section of a basal body resembles a cartwheel [2]. Adjacent triplets are cross-linked at regular distances. The structure of basal bodies is the same as the structure of centrioles. Both cell components are about 0.2 μm wide and 0.4 μm long [1].

1.6 Structure of Proteins and Structure of Tubulin.

Proteins are chain-like molecules that form from amino acids. At present time 22 amino acids are known that constitute the protein polymers [26]. A general structure of an amino acid molecule is shown in Figure 1.20. All amino acids have an amino group NH_2, a carboxyl group COOH and they differ by their radical. The atomic structure of 20 most common amino acids can be found, *e.g.*, in [14].

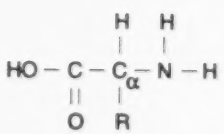

Figure 1.20: An amino acid molecule.

Amino acids can join together by releasing an H_2O group and forming a covalent C-N bond called peptide bond as is shown in Figure 1.21. The result of such reactions

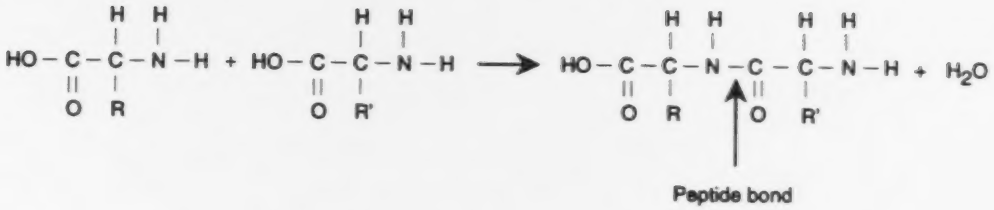

Figure 1.21: Formation of a dipeptide.

are polypeptide chains called proteins. Sequences of amino acid units or residues in a protein molecule determine the primary protein structure.

Some bonds in the polypeptide chain can rotate freely, changing the spatial arrangement of the chain resulting in the secondary protein structure or conformation. The most common protein conformations are random coils, α-helices and β-sheets [14]. Among them the α-helix is the most frequently found polypeptide arragement. It is a helical structure which is created by forming H-O bonds between every 3-rd or 4-th residue of the polypeptide chain. β-sheets arise by forming bonds between parallel polypeptide chains.

According to present experiments α-tubulin consists of four α-helices, two β-sheets and two random coils. β-tubulin is comprised of six α-helices, one β-sheet and seven random coils [27]. Each monomer has about 450 residues and is divided into two domains. The larger domain is called the amino terminal (N) and the smaller domain is called the carboxyl terminal (C) (Figure 1.22). Binding of MAP2 takes place at the C terminal of β-tubulin, tau binds at the N terminal of α- and C terminal of β-tubulin. GTP is bound on the N terminal of both α- and β-tubulin [11,28].

All three tubulins, α, β and γ, contain areas in which they differ but also possess highly conserved areas. The similarities between these areas undoubtedly point out that the tubulins are closely related [8]. The differences between various tubulin isoforms occur mostly in the C terminal region which is larger in the β-tubulin compared to the α-tubulin.

The primary structure of tubulin has been identified only for several species. The sequences of amino acids found in the tubulin extracted from chick brain and sea-urchin are listed in [2]. The similarities between the amino acid sequences of α- and β-tubulin of these two widely separated species confirm that the two tubulins belong to the same family of proteins.

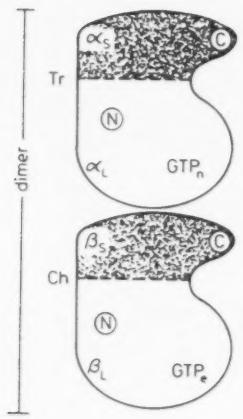

Figure 1.22: The domain structure of α- and β-tubulin. Nonexchangeable GTP (GTP_n) is bound to the α monomer. Exchangeable GTP (GTP_e) binds to the β monomer. (From Reference [13].)

Compared to the α- and β-tubulin, γ-tubulin doesn't appear to be a building block of MTs. This tubulin is located in the MT nucleating centers. It has been found that the disruption of γ-tubulin causes the inhibition of nuclear division, weaker inhibition of nuclear migration and the disassembly of most mitotic and all cytoplasmic MTs [29]. This suggests that γ-tubulin is closely related to these cell processes.

Tubulin is a complex chemical structure and several different isoforms of tubulin have been found in various organisms and cells. In [30] the results of experiments are reported in which 12 different subspecies of β-tubulin have been detected in mammalian brain and fewer in other tissues. Other experiments have shown that different isoforms of α- and β-tubulin can copolymerize so that they don't necessarily form specific subsets of MTs [11].

Similarly to the MT associated proteins, tubulin can be posttranslationally modified [4, 11]. The modifications are not determined by genetic factors but by local conditions in the cytoplasm [26]. The most common are the phosphorylation of β-tubulin, acetylation of α-tubulin, removal or readdition of the C-terminal tyrosine of α-tubulin and glutamylation of α- and β-tubulin [28].

The specific functions of different tubulin isoforms and posttranslational modi-

fications in MTs are at present not very well understood. Observations show that there is not a significant difference between the distribution of modified and unmodified cytoplasmic MTs [11]. On the other hand, there is increasing evidence that the diversity of tubulin isoforms and modifications is connected with specific MT functions. A number of studies have shown that stable MTs are mostly acetylated and detyrosinated. However, this may be due to different functions the modifying enzymes have in free tubulin and in MTs [11, 28]. In squid axons, different subsets of MTs have been identified in different cytoskeletal regions corresponding to differences in MAPs, β-tubulin isoforms and phosphorylation [31]. In *Drosophila*, a mutation of the testis β_2-tubulin has been found that fails to form closed tubes but it assembles into S shaped sheets instead. The tubulin has only one amino acid substitution at residue 288 which must be essential for the correct curvature of the MT wall [32].

Since protein chains can form different spatial arrangements, or conformations, it has been suggested that the different conformations of tubulin dimers in a MT are also associated with a specific MT behaviour [26]. The ways the conformational states of tubulin dimers could be linked to the physical properties of MTs and their functions in the cell are discussed in the following chapters of this work.

References

[1] B. Alberts, D. Bray, J. Lewis, M. Raff, K. Roberts, and J. D. Watson, *Molecular Biology of the Cell*, 3-rd edition (Garland Publishing, New York and London, 1994)

[2] P. Dustin, *Microtubules* (Springer, Berlin, 1984)

[3] S. R. Martin, M. J. Schilstra, and P. M. Bayley, Dynamic Instability of Microtubules: Monte Carlo Simulation and Application to Different Types of Microtubule Lattice, *Biophysical Journal* **65**, p. 578-596 (1993)

[4] E. Mandelkow , E.-M. Mandelkow, Microtubule structure, *Current Opinion in Structural Biology* **4**, p. 171-179 (1994)

[5] Y-H Song and E. Mandelkow, Recombinant kinesin motor domain binds to β-tubulin and decorates microtubules with a B surface lattice, *Proceedings of the National Academy of Sciences of the USA* **90**, p. 1671-1675 (1993)

[6] S. Kamimura and E. Mandelkow, Tubulin Protofilaments and Kinesin-dependent Motility, *Journal of Cell Biology* **118**, p. 865-875 (1992)

[7] Y-H Song and E. Mandelkow, The Anatomy of Flagellar Microtubules: Polarity, Seam, Junctions, and Lattice, *Journal of Cell Biology* **128**, p. 81-94 (1995)

[8] C. E. Oakley and B. R. Oakley, Identification of γ-tubulin, a member of the tubulin superfamily encoded by *mip*A gene of *Aspergillus nidulans*, *Nature* **338**, p. 662-664 (1989)

[9] T. J. Mitchison and M. W. Kirschner, Microtubule assembly nucleated by isolated centrosomes, *Nature* **312**, p. 232-237 (1984); Dynamic instability of microtubule growth, *Nature* **312**, p. 237-242 (1984)

[10] D. K. Fygenson, E. Braun, and A. Libchaber, Phase diagram of microtubules, *Physical Review E* **50**, p. 1579-1588 (1994)

[11] E. Mandelkow and E.-M. Mandelkow, Microtubular structure and tubulin polymerization, *Current Opinion in Cell Biology* **2**, p. 3-9 (1990)

[12] M. Kirschner and T. Mitchison, Beyond Self-Assembly: From Microtubules to Morphogenesis, *Cell* **45**, p. 329-342 (1986)

[13] K. Kirchner and E.-M. Mandelkow, Tubulin domains responsible for assembly of dimers and protofilaments, *EMBO Journal* **9**, p. 2397-2402 (1985)

[14] A. L. Lehninger, *Principles of Biochemistry* (Worth, New York, 1982)

[15] B. Mickey and Jonathon Howard, Rigidity of Microtubules Is Increased by Stabilizing Agents, *Journal of Cell Biology* **139**, p. 909-917 (1995)

[16] M. Caplow, R. L. Ruhlen, and J. Shanks, The Free Energy for Hydrolysis of a Microtubule-Bound Nucleotide Triphosphate Is Near Zero: All of the Free Energy for Hydrolysis Is Stored in the Microtubule Lattice, *Journal of Cell Biology* **127**, p. 779-788 (1994)

[17] A. A. Hyman, D. Chretien, I. Arnal, and R. H. Wade, Structural Changes Accompanying GTP Hydrolysis in Microtubules: Information from a Slowly Hydrolyzable Analogue Guanylyl -(α,β)-Methylene-Diphosphonate, *Journal of Cell Biology* **128**, p. 117-125 (1995)

[18] A. Marx, E. Mandelkow, A model of microtubule oscillations, *European Biophysics Journal* **22**, p. 405-421 (1994)

[19] E.-M. Mandelkow, E. Mandelkow, and R. A. Milligan, Microtubule dynamics and microtubule caps: A time-resolved cryo-electron microscopy study, *Journal of Cell Biology* **114**, p. 977-991 (1991)

[20] D. Chrétien, S. D. Fuller, and E. Karsenti, Structure of Growing Microtubule Ends: Two-Dimensional Sheets Close Into Tubes at Variable Rates, *Journal of Cell Biology* **129**, p. 1311-1328 (1995)

[21] J. R. Simon and E. D. Salmon, The structure of microtubule ends during the elongation and shortening phases of dynamic instability examined by negative-stain electron microscopy, *Journal of Cell Science* **96**, p. 571-582 (1990)

[22] P. M. Bayley, M. J. Schilstra and S. R. Martin, Microtubule dynamic instability: numerical simulation of microtubule transition properties using a Lateral Cap model, *Journal of Cell Science* **95**, p. 33-48 (1990)

[23] J. F. Diaz and J. M. Andreu, Assembly of Purified GDP-Tubulin into Microtubules Induced by Taxol and Taxotere: Reversibility, Ligand Stoichiometry, and Competition, *Biochemistry* **32**, p. 2747-2755 (1993)

[24] R. Melki, M.-F. Carlier and D. Pantaloni, Oscillations in microtubule polymerization: the rate of GTP regeneration on tubulin controls the period, *EMBO Journal* **7**, p. 2653-2659 (1988)

[25] *Microtubules*, editors J. S. Hyams and C. W. Lloyd (Wiley-Liss, 1994)

[26] S. Hameroff, *Ultimate Computing* (North-Holland, Amsterdam, 1987)

[27] D. Koruga, Neuromolecular Computing, *Nanobiology* **1**, p. 5-24 (1992)

[28] *Guidebook to the Cytoskeletal and Motor Proteins*, editors T. Kreis and R. Vale (University Press, Oxford, 1993)

[29] B. R. Oakley, C. E. Oakley, Y. Yoon, and M. K. Jung, γ-tubulin Is a Component of the Spindle Pole Body That Is Essential for Microtubule Function in Aspergillus nidulans, *Cell* **61**, p. 1289-1301 (1990)

[30] J. C. Lee, D. J. Field, H. J. George, and J. Head, Biochemical and Chemical Properties of Tubulin Subspecies, *Annals of the New York Academy of Sciences* **466**, p. 111-128 (1986)

[31] T. Arai and G. Matsumoto, Subcellular Localization of Functionally Differentiated Microtubules in Squid Neurons: Regional Distribution of Microtubule Associated Proteins and β-Tubulin Isotypes, *Journal of Neurochemistry* **51**, p. 1825-1838 (1988)

[32] M. T. Fuller, J. H. Caulton, J. A. Hutchens, T. C. Kaufman, and E. C. Raff, Mutations that encode partially functional β_2-tubulin subunits have different effect on structurally different microtubule arrays, *Journal of Cell Biology* **107**, p. 141-152 (1988)

2 Dielectric Phases in Microtubules

Experiments strongly indicate that tubulin molecules, like many other biological molecules, carry permanent dipole moments [1]. Based on this a MT can be viewed as a ferroelectric crystal. Ferroelectric crystals are composed of particles which carry permanent dipole moments. They are known to undergo a phase transition from a low temperature state in which all dipoles are aligned in the same direction to a high temperature state in which the dipoles are oriented at random. The goal in this chapter is to investigate the possibility of such a transition in MTs and its significance for the biological functions of MTs.

2.1 Some Features of Phase Transitions

Systems that possess very strong interactions between their constituent particles are known to exhibit phase transitions. This phenomenon can be observed in the condensation of gases, melting of liquids, ferromagnetism and antiferromagnetism, ferroelectric crystals, order-disorder transitions in alloys, and many other physical systems [2–5].

A phase transition is manifested by discontinuities in thermodynamic functions and the emergence of a non-zero order parameter at a transition temperature T_c. The thermodynamic functions mentioned above are, for example, the free energy, specific heat or susceptibility of a ferromagnetic or ferroelectric material, specific heat and compressibility of a gas, *etc.*

The concept of an order parameter is associated with the critical behaviour of many systems. The order parameter is a quantity that is nonzero below T_c and zero above T_c. Examples of an order parameter are the difference in the densities of gas and liquid phases, spontaneous magnetization of a ferromagnet, spontaneous polarization of a ferroelectric crystal, the displacement of atoms in alloys [3, 4].

Depending on the character of the discontinuities in the thermodynamic functions and the order parameter, phase transitions are usually classified as first order or second order. Since the investigation presented in this chapter is based on the assumption that a MT can be viewed as a two-dimensional ferroelectric crystal, in what follows, the concept of first and second order phase transition is explained for a ferroelectric system.

As was mentioned earlier, a ferroelectric crystal is composed of particles that possess permanent dipole moments. If the crystal is not exposed to an external electric field the overall configuration of the dipole moments results in a non-zero net spontaneous polarization.

A first order phase transition in a ferroelectric crystal is characterized by a discontinuous jump in the spontaneous polarization and a finite discontinuity in the electric susceptibility. In a second order phase transition, the spontaneous polarization decreases continuously until it reaches zero at T_c and the electric susceptibility is divergent at T_c. The character of the discontinuities in both spontaneous polarization and electric susceptibility for a first and second order phase transition is illustrated in Figure 2.1.

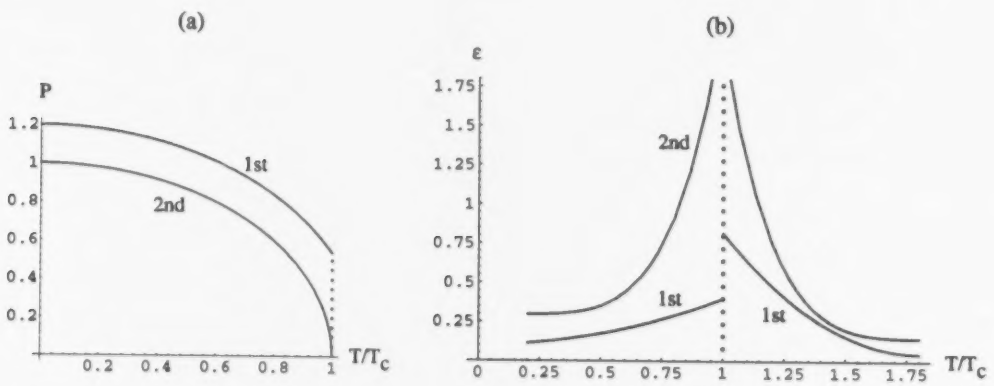

Figure 2.1: Spontaneous polarization (a) and electric susceptibility (b) for a first and second order phase transition.

Corresponding to the change in spontaneous polarization, the minima of the free energy of the ferroelectric system change as the temperature increases as shown in Figure 2.2. The plotted curves were calculated using the Landau free energy expansion [3, 6]

$$F = \frac{\alpha}{2}P^2 + \frac{\beta}{4}P^4 + \frac{\gamma}{6}P^6 + \ldots, \tag{2.1}$$

where $\alpha = a(T - T_0)$, $a > 0$, β and γ are temperature independent constants and P is the spontaneous polarization.

The equation above is often used to describe a phase transition which can be well characterized by an order parameter. It contains only even powers of P because it is assumed that the free energy is the same regardless of the sign of P. The minima of

the free energy (2.1) determine the equilibrium value, *i.e.*, the most probable value of the spontaneous polarization P at a temperature T. They can be obtained by solving the equation

$$(\frac{\partial F}{\partial P})_T = 0 = a(T - T_0)P + \beta P^3 + \gamma P^5 + \ldots . \tag{2.2}$$

When $T > T_0$ and a, β and γ are all positive, the only solution of equation (2.2)

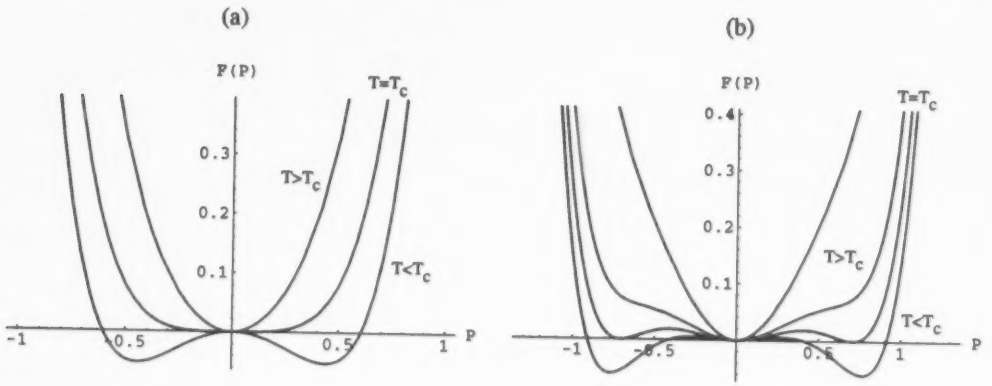

Figure 2.2: The free energy of a ferroelectric crystal as a function of spontaneous polarization for a first (a) and second order (b) phase transition.

is $P = 0$. In a second order phase transition $T_0 = T_c$. For positive β below T_c, equation (2.2) has two other symmetric solutions

$$P_{\pm} = \pm[\frac{-a(T - T_c)}{\beta}]^{1/2} . \tag{2.3}$$

The solutions (2.3) were obtained when the term γP^5 was neglected since P is small in the vicinity of T_c. This shows that in the second order phase transition the minima of the free energy change continuously from two values symmetric about the origin for $T < T_c$ to zero for $T > T_c$.

Consider now the first order phase transition and $T_0 < T_c$. For negative β and after neglecting the term γP^5, the nonzero solutions of (2.2) for $T_0 < T < T_c$ are

$$P_{\pm} = \pm[\frac{a(T - T_0)}{\beta}]^{1/2} . \tag{2.4}$$

This means that in the first order phase transition just above T_c the minimum of the free energy is at $P = 0$ and after the temperature decreases just below T_c this minimum changes discontinuously into two finite minima symmetric about the origin.

The free energy shown in Figure 2.2 can, for example, describe a ferroelectric crystal in which each particle can be in one of two dipole states that are parallel to the same axis but point in the opposite directions. The finite value of the spontaneous polarization below T_c results from ordering of dipoles in a preferred direction due to the interaction between them. This state is called the ferroelectric phase. When the temperature in the crystal is increased, the thermal energy increases as well and eventually at T_c becomes larger than the interaction energy between the dipoles. Due to this the dipoles cease to be aligned and become oriented randomly which results in a zero net spontaneous polarization. This state of a ferroelectric crystal is called the paraelectric phase.

2.2 Phase Transitions in Lattices

A number of physical systems that undergo phase transitions can be represented, to a varying degree of accuracy, by an array of lattice sites. Although this is a simplified description, it has been successfully used to study a variety of phenomena such as ferromagnetism and antiferromagnetism, gas-liquid and liquid-solid transitions, transitions in binary alloys, *etc.*, [2].

The problem of phase transitions on a lattice is usually formulated for the case of ferromagnetism. A magnetic solid can be viewed as a collection of magnetic spins distributed on sites of a crystal lattice. If only the interaction energy between the atoms in the solid is considered, the Hamiltonian of the system can be assumed in the following form [7]

$$H_H = -2\sum_{i>j} J_{ij}\vec{S}_i.\vec{S}_j\,. \tag{2.5}$$

This Hamiltonian is called the **Heisenberg Hamiltonian**. The variables $\vec{S}_i$ are quantum mechanical operators that represent the spins on lattice sites $\vec{R}_i$. Their Cartesian components $S_{i\alpha}$ obey the following commutation relation

$$[S_{i\alpha}S_{l\beta}] = \delta_{il}i\hbar\epsilon_{\alpha\beta\gamma}S_{i\gamma}\,. \tag{2.6}$$

The operator $\vec{S}_i^{\,2}$ commutes with the Hamiltonian (2.5) and its eigenvalue is $S_i(S_i+1)$. J_{ij} are the exchange constants that represent the interaction between spins located at sites i and j. They depend on the distance between sites i and j and can be calculated from the spin wave functions [2, 7]. The sign in the Hamiltonian

(2.5) is chosen in such a way that for J_{ij} all positive the groundstate of the system is ferromagnetic. If J_{ij} are not all positive, a much more complicated situation may occur, one possibility is antiferromagnetism.

When the magnetic crystal is subjected to an external magnetic field the interaction of each spin i with the magnetic field leads to a potential energy [2]

$$E_{pi} = g\frac{e}{2mc}\vec{S}_i.\vec{B}\,, \tag{2.7}$$

where e and m are the charge and mass of an electron, $\vec{B}$ is the external magnetic field and g is Lande's factor which for the spin electron angular momentum has a value very close to 2. Based on (2.7) and (2.5) the Hamiltonian that describes an assembly of magnetic spins which are exposed to an external magnetic field $\vec{B}$ is

$$H_H = -2\sum_{i>j} J_{ij}\vec{S}_i\vec{S}_j - g\frac{e}{2mc}\vec{B}.\sum_i \vec{S}_i\,. \tag{2.8}$$

If quantization takes place only along the z-axis and the magnitude of the spin is $\frac{1}{2}$, then only two orientations of the spin are possible and the vector $\vec{S}_i$ has two components $S_{zi} = -\frac{1}{2}$ and $S_{zi} = +\frac{1}{2}$. In such case the Hamiltonian (2.8) becomes

$$H_I = -\sum_{i>j} J_{ij}\sigma_i\sigma_j - \mu_B B\sum_i \sigma_i\,, \tag{2.9}$$

where $\mu_B = e\hbar/2mc$ is the Bohr magneton, $\sigma_i = \pm 1$ are classical variables and $g = 2$. The fraction $\frac{1}{2}$ that should be in front of the sum in (2.9) was included in the interaction constants, *i.e.*, one can put $J'_{ij} = J_{ij}/2$ and then drop the prime. The model based on the Hamiltonian (2.9) is known in the physical literature as the **Ising model**. It is a classical model and can be used to study phase transitions in systems whose components can be in two distinct microstates.

As was explained in the previous section, a phase transition is characterized by discontinuities in the thermodynamic functions of a system. These functions can be evaluated using the partition function. For the Ising Hamiltonian (2.9) the partition function is given by the formula [2,4]

$$Q_N(B,T) = \sum_{\{\sigma_i\}} \exp\,[-\frac{H_I\{\sigma_i\}}{k_B T}] = \sum_{\{\sigma_i\}} \exp[\frac{1}{k_B T}\sum_{i>j} J_{ij}\sigma_i\sigma_j + \frac{\mu_B B}{k_B T}\sum_i \sigma_i]\,, \tag{2.10}$$

where the sum goes over all possible configurations of the spin variables $\{\sigma_i\}$, $H_I\{\sigma_i\}$ is the Hamiltonian for a configuration of the spin variables $\{\sigma_i\}$, and k_B is the Boltzmann constant.

To evaluate the partition function (2.10) exactly is a difficult mathematical problem since the Hamiltonian (2.9) is still very complicated. Because of that, further simplifications have to be introduced. A standard approach is to take into consideration only the nearest-neighbour interactions. However, even under this simplification an analytical expression for the partition function in zero magnetic field could be found only for two cases - for the one-dimensional lattice (Ising in 1925) and a two-dimensional square lattice (Onsager in 1944). Evaluation of magnetization and magnetic susceptibility on the basis of the resulting partition function showed that the one-dimensional lattice doesn't exhibit any phase transition but the two-dimensional lattice undergoes a second order phase transition at a transition temperature T_c which is proportional to the interaction constant J.

2.3 Calculation of Polarization and Electric Susceptibility of the Microtubule Lattice

As was mentioned earlier, tubulin is a dipolar molecule. Since the tubulin dimers in a MT are arranged in a regular manner, the dipoles on the dimers form a regular two-dimensional lattice. As will be discussed in the following section, it will be assumed that the dipole on each tubulin dimer can be in one of two distinct states.

According to Chapter 1, two possible geometrical arrangements of the tubulin dimers in a MT are considered at present and they are termed the A and B lattice. Sections of both lattices for a MT with 13 protofilaments are drawn in Figure 2.3 where each tubulin dimer is represented as a site. Both lattices are hexagonal; each site has six nearest neighbours. When the lattices are folded into a tube, column (protofilament) number 13 becomes adjacent to column number 1. Since the A lattice with 13 protofilaments is symmetric, the geometrical structure of this lattice between columns 1 and 13 is the same as inside the lattice. The B lattice is not symmetric and the mismatch of the rows results in a structural discontinuity or seam. Due to this, the arrangement of lattice sites at the boundaries of the B lattice is different from that inside the lattice.

It is obvious from Figure 2.3 that each three nearest sites in the hexagonal MT lattice form a triangle and all triangles formed in this way are equivalent (except for those along the seam in the B lattice). This means that the MT lattice can be treated as a triangular lattice. Depending on the way the hexagonal lattice is transformed

into the triangular lattice and on the type of the lattice, at the boundaries along the MT, the end of the i-th row matches with the beginning of the (i+n)-th row and the beginning of the i-th row matches with the end of the (i-n)-th row. The boundary conditions at the ends of the MT can be set up so that the first row is adjacent to the last row. These boundary conditions are toroidal boundary conditions.

The exact partition function for a triangular lattice in the absence of an external field and with the inclusion of only nearest-neighbour interactions, hasn't been found yet. However, the average spontaneous polarization of an assembly of dipoles which are placed at sites of a regular lattice, can be calculated precisely at each temperature as a weighted average

$$< P >= \frac{\sum_{\{\sigma_i\}} P\{\sigma_i\} \exp[-\frac{1}{k_B T} H\{\sigma_i\}]}{\sum_{\{\sigma_i\}} \exp[-\frac{1}{k_B T} H\{\sigma_i\}]}. \tag{2.11}$$

In (2.11) the sum goes over all possible configurations of the spin variables $\{\sigma_i\}$, where σ_i represents dipole states of each dipole. $H\{\sigma_i\}$ is the potential energy of a configuration of dipoles which is due to the interactions between them and with an external electric field.

In this chapter, calculations were performed for the MT lattices with 13 columns and a number of rows ranging from 100 up to 3000. To find all possible configurations of dipoles for lattices of this size would take an unreasonably long time. However, from statistical mechanics it is known that a statistical system which consists of N particles, spends the majority of its time in states whose parameters are within $O(1/\sqrt{N})$ of those in thermal equilibrium [5]. Since these are the states with the highest weight, it is reasonable to use only these to calculate the statistical average of a thermodynamic quantity. This approach is called importance sampling.

To find the states with the highest weight, the Monte Carlo procedure of the importance sampling has been used. This procedure generates a Markov chain of states which has the property that the average of a thermodynamic quantity over these states converges to the exact thermal average defined in (2.11). The chain of states is generated according to the transition probabilities which are not defined uniquely.

An often used choice for realization of the Monte Carlo procedure is the Metropolis algorithm, which has been also utilized in the simulations presented below [8]. According to this algorithm a new state in the Markov chain is generated when the probability of transition into this state is greater than a random number whose value

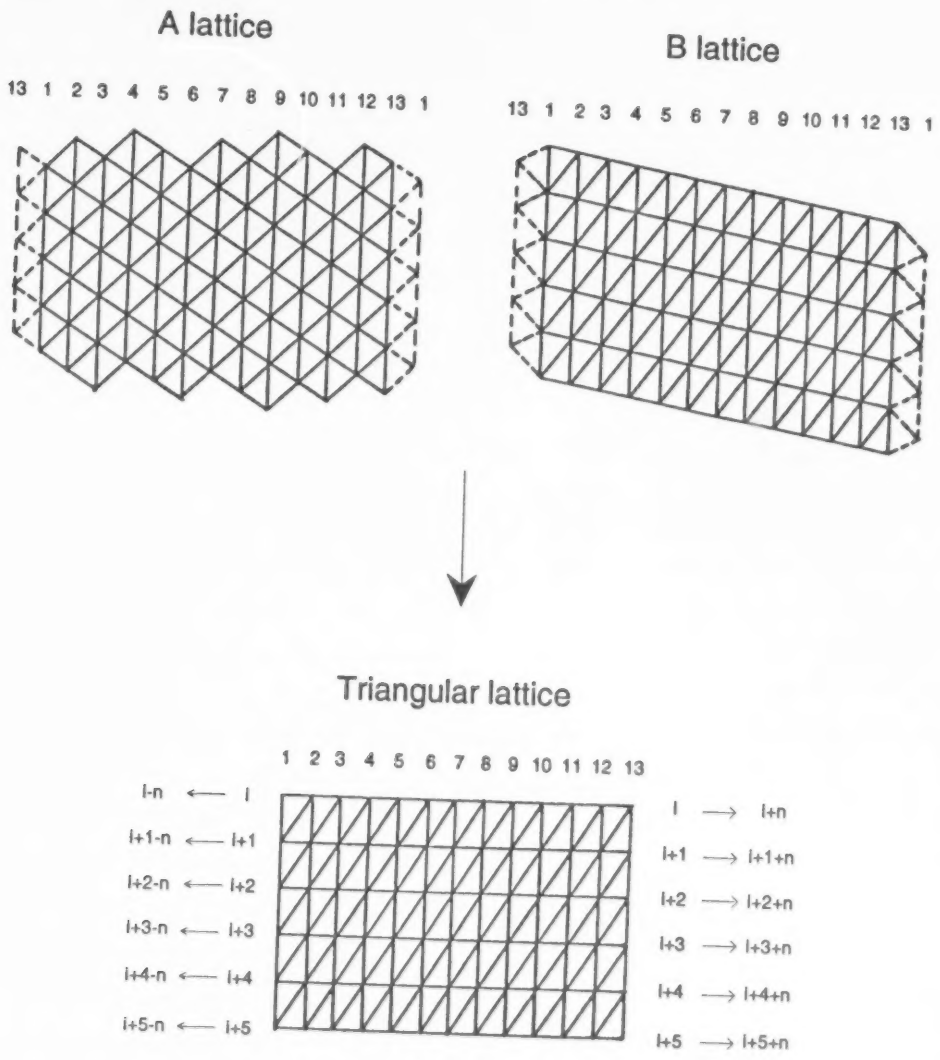

Figure 2.3: The geometrical configuration of the A and B lattice for a MT with 13 protofilaments. The hexagonal lattices can be transformed into triangular lattices in which the hexagonal arrangement of sites in the MT lattices is taken into account by shifting the rows at the boundaries by a number of rows n.

is between 0 and 1. This transition probability is calculated as

$$\exp[-\frac{(E_{new} - E_{old})}{k_B T}], \tag{2.12}$$

where E_{new} is the energy of the possible new state and E_{old} is the energy of the old state. In an assembly of dipoles the possible new state is obtained from the previous state by changing the value of the spin variable σ_{ij} which represents the dipole at a site (i, j). In a MT lattice of dipoles the spin variable at each lattice site can assume values +1 or -1 corresponding to the two states of the dipole on the tubulin dimer.

In the actual computer simulation the Markov chain begins from a chosen initial configuration. In the calculations presented here, at each temperature all dipoles were initially completely ordered, that means, all σ_{ij}'s were put equal to either +1 or -1. After the initial configuration is determined, at each lattice site (i, j) the transition probability (2.12) is calculated. If this number is greater than a generated random number the dipole at this site is flipped, *i.e.*, σ_{ij} changes its value from +1 to -1 or *vice versa*. If the transition probability is smaller than the random number the dipole is not flipped and the same procedure repeats at the next lattice site. At each temperature, the whole lattice is examined in this way a number of times so that the state of the system is not correlated with its initial state. One examination of the whole lattice is called one Monte Carlo step.

When such a number of Monte Carlo steps is performed that the state of the lattice is not correlated with its initial state, the spontaneous polarization is found at the end of each of the following Monte Carlo steps from the configuration of dipoles in the lattice. In the calculations presented here the polarization was calculated as a sum of the projections of the dipole moments of the dipoles on the MT axis. The values of polarization obtained in a sufficiently large number of Monte Carlo steps were then used to calculate the required thermal average of polarization at temperature T.

The electric susceptibility can be calculated from the known values of polarization according to the formula [2,4]

$$\epsilon = \frac{\partial < P >}{\partial E} = \frac{1}{k_B T}(< P^2 > - < P >^2). \tag{2.13}$$

2.4 Two Models of the Dipole States of the Tubulin Dimer

A model of the tubulin electric states is presented in [9] and related works in

Figure 2.4: The α and the β state of the tubulin dimer. In the β state the tubulin dimer is shifted with respect to the vertical axis by about 29°. (From Reference [9].)

which it is used to simulate the MT behaviour by means of cellular automata (see Chapter 4). A tubulin electric state is represented by a mobile electron, the average position of which can be located either more towards the α or more towards the β monomer (Figure 2.4). The states of the tubulin dimer are then correspondingly named the α and β state. Experiments indicate that when the electron moves from the α to the β monomer, the tubulin dimer undergoes a conformational shift of about 29° with respect to the vertical axis [10].

In analogy with these considerations, two dipole states of the tubulin dimer have been defined here, the α state, when the dipole moment is pointing towards the α monomer and the β state, when the dipole moment is pointing towards the β monomer. The α state will be also referred to as the "up" state and the β state will be referred to as the "down" state.

Two models of the tubulin dipole states have been considered here and are shown in Figure 2.5. These models differ by the orientation of the dipole in the β state. In the model called the model with nontilted states, the dipoles in the α and β states are oriented along the vertical axis and in the opposite directions. In the second model called the model with tilted states, the α dipole states are the same as in the model with nontilted states, but the dipoles in the β state are tilted by 29° with respect to the vertical axis (the MT axis). In both models, the magnitudes of the dipole moments in the up and down states are assumed to be equal.

Since in the model with nontilted dipoles it is assumed that the dipoles are oriented along the MT axis, the polarization of the lattice is also oriented along the MT axis, and it can be calculated as a sum of the dipole moments $\pm p$ corresponding to the up and down states of the dipoles. Because the magnitudes of the dipole moments are equal, they can be represented by the values of the spin variables +1 or -1. Then by summing up the values of the spin variables at all lattice sites the

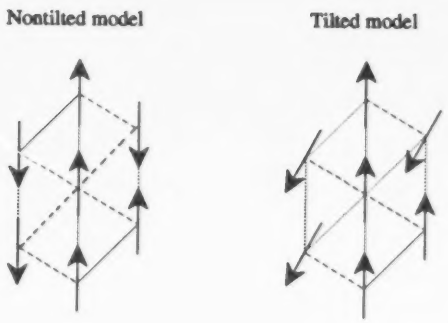

Figure 2.5: The hexagonal nearest-neighbour cluster for the model with nontilted and tilted states. The corresponding up and down states are at the same sites in the cluster.

polarization of the whole lattice is obtained in the units of the dipole moment. Dividing this number by the total number of dipoles in the lattice N gives polarization per site (relative polarization)

$$P = \frac{N^{\uparrow} - N^{\downarrow}}{N}. \tag{2.14}$$

In (2.14), $N^{\uparrow}$ is the number of dipoles in the up state, $N^{\downarrow}$ is the number of dipoles in the down state.

In the model with tilted dipoles, the dipoles in the β state are not oriented along the MT axis. Therefore, to calculate the component of the polarization along the MT axis the magnitude of the dipole moment in the β state has to be projected on the MT axis and the formula (2.14) is modified as follows

$$P = \frac{N^{\uparrow} - N^{\downarrow}\cos 29^{\circ}}{N}. \tag{2.15}$$

2.5 Model with Nontilted States

If it is assumed that each dipole in a MT interacts only with its nearest neighbours, the potential energy of the whole assembly of dipoles in the MT due to the

dipole-dipole interactions and a non-zero external electric field E is

$$H = -\sum_{j=1}^{NC}\sum_{i=1}^{NR}(J_1\sigma_{i,j}\sigma_{i+1,j} + J_2\sigma_{i,j}\sigma_{i-1,j+1} + J_3\sigma_{i,j}\sigma_{i,j+1}) - pE\sum_{j=1}^{NC}\sum_{i=1}^{NR}\sigma_{i,j}\,. \quad (2.16)$$

In (2.16) the interaction constants J_1 and J_3 represent the interaction in the vertical and horizontal direction, respectively. J_2 represents the interaction along the diagonal (Figure 2.6). The dipoles are placed at sites of a triangular lattice with NR rows and NC columns and the toroidal boundary conditions are assumed. It can be noted that the equation above is the same as the Ising Hamiltonian (2.9) for the case when only nearest-neighbour interactions are included and the potential energy $\pm\mu_B B$ is replaced by $\pm pE$.

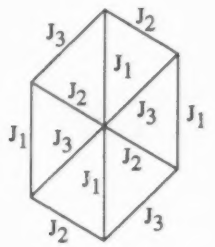

Figure 2.6: The interact n constants in the three directions that characterize the MT lattice.

The interaction constants J_1, J_2, J_3 were calculated according to the expression

$$W_n^{\uparrow\uparrow} - W_n^{\uparrow\downarrow} = -2J_n\,, \quad (2.17)$$

where $W_n^{\uparrow\uparrow}$ is the interaction energy between two neighbouring dipoles in the n-th direction when they are both in the up state and $W_n^{\uparrow\downarrow}$ is the interaction energy between two neighbouring dipoles in the n-th direction when one dipole is in the up state and the other dipole is in the down state. $W_n^{\uparrow\uparrow}$ and $W_n^{\uparrow\downarrow}$ were calculated using the classical formula for the interaction energy between two dipoles

$$W_n = \frac{1}{4\pi\epsilon_0\epsilon_r}\frac{(\vec{p}_1.\vec{p}_2)_n - 3(\vec{u}.\vec{p}_1)_n(\vec{u}.\vec{p}_2)_u}{\mid(\vec{x}_1 - \vec{x}_2)_n\mid^3}\,. \quad (2.18)$$

In (2.18), $\vec{p}_1 = q_1\vec{s}_1$, $\vec{p}_2 = q_2\vec{s}_2$ are the dipole moments, q_1, q_2 are the charges of the dipoles, s_1, s_2 are the dipole lengths, $\vec{u}$ is a unit vector that connects the centers of

the two dipoles, $\vec{x}_1$, $\vec{x}_2$ are their position vectors, ϵ_0 is the permittivity of vacuum, and ϵ_r is the relative permittivity of the medium.

As was stated earlier, the dipole moments in the up and down states can differ by their directions, but they are assumed to have the same charge and length, *i.e.*, $q_1 = q_2$ and $s_1 = s_2$. Using this assumption in (2.17) and (2.18) gives the following formula for the interaction coefficients J_n

$$J_n = \frac{q^2 s^2}{4\pi\epsilon_0\epsilon_r} \frac{3\cos^2\theta_n - 1}{r_n^3}, \quad n = 1, 2, 3, \tag{2.19}$$

where θ_n are the angles between $\vec{u}$ and positive vertical axis and $r_n = |\,(\vec{x}_1 - \vec{x}_2)_n\,|$ (Figure 2.7).

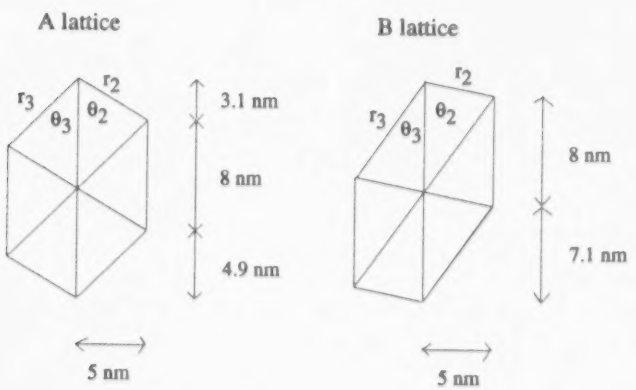

Figure 2.7: The geometrical configuration of the A lattice and inside the B lattice.

On the basis of the dimensions of the A lattice and inside the B described in Chapter 1, the angles θ_n and the lengths of the sides of the triangular cell r_n have the following values

$$\begin{aligned} \theta_1^A &= 0^\circ, & \theta_1^B &= 0^\circ, \\ \theta_2^A &= 58.2^\circ, & \theta_2^B &= 79.8^\circ, \\ \theta_3^A &= 45.6^\circ, & \theta_3^B &= 35.2^\circ, \end{aligned} \tag{2.20}$$

$$\begin{aligned} r_1^A &= 8.00 \times 10^{-9}\,\mathrm{m}, & r_1^B &= 8.00 \times 10^{-9}\,\mathrm{m}, \\ r_2^A &= 5.88 \times 10^{-9}\,\mathrm{m}, & r_2^B &= 5.08 \times 10^{-9}\,\mathrm{m}, \\ r_3^A &= 7.00 \times 10^{-9}\,\mathrm{m}, & r_3^B &= 8.68 \times 10^{-9}\,\mathrm{m}. \end{aligned} \tag{2.21}$$

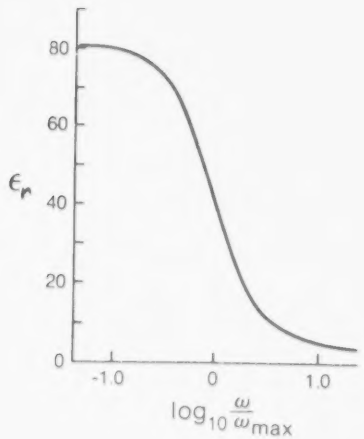

Figure 2.8: Relative permittivity of free water as a function of frequency at 20°. (From Reference [11].)

Along the boundaries in a MT with the B lattice the angles θ_2 and θ_3 and the distances r_2 and r_3 are different from those listed in (2.20) and (2.21). This means that the values of the interaction constants J_n^B at the boundaries of the B lattice will be different from the interaction constants inside the B lattice.

From equation (2.19) it is obvious that for fixed θ_n's and r_n's, that means, for a fixed type of the lattice A or B, the interaction energies J_n depend only on the parameters q, s and ϵ_r. This dependence can be reduced to a dependence on the single parameter $\bar{Q} = q^2 s^2 / \epsilon_r$.

In a realistic model, q should have a value of the order of one electronic charge 1.602×10^{-19} C and s should be of the order of several nanometers The relative permittivity of the medium surrounding a MT can be approximated by the permittivity of free water since the bulk of the cell's mass is due to free water [11]. The relative permittivity of free water as a function of frequency of oscillations of the dipoles in the medium is plotted in Figure 2.8. For a static case, *i.e.*, for no oscillations, $\epsilon_r(0)$ is close to 80. With increasing frequency ϵ_r rapidly decreases and in the limit $\omega \to \infty$, $\epsilon_r(\infty) = 4.5$. At body temperature these values would drop by about 10 %.

For the value $\bar{Q} = 12 \times 10^{-56}\,\mathrm{C^2 m^2}$ which is consistent with the above estimates

as will be shown later, the interaction constants for the A lattice and inside the B lattice are

$$\begin{aligned} J_1^A &= +4.21 \times 10^{-21}\,\mathrm{J}, & J_1^B &= +4.21 \times 10^{-21}\,\mathrm{J}, \\ J_2^A &= -0.89 \times 10^{-21}\,\mathrm{J}, & J_2^B &= -7.46 \times 10^{-21}\,\mathrm{J}, \\ J_3^A &= +1.48 \times 10^{-21}\,\mathrm{J}, & J_3^B &= +1.66 \times 10^{-21}\,\mathrm{J}. \end{aligned} \tag{2.22}$$

In both lattices two interaction constants are positive and one is negative. If one of the positive interaction constants and the negative interaction constant had the same magnitude, the assembly of dipoles in a MT would be frustrated.

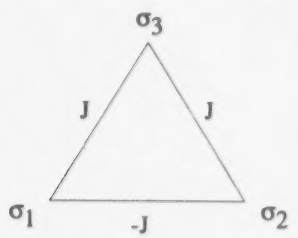

Figure 2.9: A system of three frustrated spins.

An example of a frustrated system is shown in Figure 2.9. The figure depicts a system of three spins (dipoles) characterized by three interaction constants that have the same magnitude but one of them is negative. The spins are placed in the corners of a triangle and they are represented by a spin variable σ_i which can have values $+1$ (up state) or -1 (down state). If only the nearest-neighbour interactions are taken into account the potential energy due to the interaction between the spins is

$$H_\triangle = -J \sum_{i=1}^{3} \sigma_i \sigma_{i+1} = +J\sigma_1\sigma_2 - J\sigma_2\sigma_3 - J\sigma_1\sigma_3\,. \tag{2.23}$$

Suppose that spin 1 is in the up state. In order for the interaction energy between spins 1 and 2 and 1 and 3 to be the lowest, spin 2 has to be in the down state and spin 3 has to be in the up state. However, according to (2.23), the interaction energy between spins 2 and 3 is the lowest when they are in the same states which is in conflict with the state of spin 1. A system with such a property is called a frustrated system.

In the frustrated system of spins in Figure 2.9, there are 6 configurations of spins for which the system will be in its ground state. However, the three interaction

constants that characterize the MT lattice have different magnitudes which means that there is only one state with the lowest energy. For example, the ground state of a triangular cell of the A lattice is the state when the two dipoles which interact through J_1 are both up and the third dipole is up as well. This gives the interaction energy of the three dipoles -9.61×10^{-21} J. Such a state is in conflict with the interaction through J_2 which requires the third dipole to be down. In that case the interaction energy of the three dipoles would be -7.25×10^{-21} J. Since this state has higher energy compared to the ground state, it is much less likely for the three dipoles to be in it. Similar considerations can be done for a larger lattice.

These considerations show that the MT lattice of dipoles (in which the dipoles are nontilted) is not really frustrated even though the concept of frustration in MTs is very appealing. Frustration is a feature of the class of magnetic systems called spin glasses [12–14]. In spin glasses, each spin is frozen in a random direction for a certain period of time but it changes its direction after a very long time. This is a characteristics of metastable systems. Due to metastability and frustration spin glasses possess a multitude of relatively long-lived ground states separated by only small potential barriers. Switching between two states can happen either at no or very little energy cost. If such properties existed in MTs they could be very well suited for information processing. (In the triangle in Figure 2.9, the number of states with the lowest energy is 6. In a MT the number of triangles is of the order of the number of lattice sites, that means, $N \sim 2 \times 10^4$. This gives the degeneracy of the ground state 6^N which is a very large number [15].)

Based on the considerations above, the expected dielectric behaviour in the MT lattice of dipoles is the following: At low temperatures the behaviour of the system of dipoles will be dominated in the A lattice by the two directions which possess positive interaction constants J_1^A and J_3^A and in the B lattice by the direction characterized by the negative interaction constant J_2^B. Hence, all dipoles will tend to align themselves in the same direction. At high temperatures, the dominant effects in the lattice are thermal effects since the thermal energy is larger than the interaction energies between dipoles. These effects will cause disorder of dipoles resulting in a net zero polarization.

The dielectric behaviour in a MT can also be influenced by external electric fields. An electric field the direction of which is the same as the direction of dipoles at low temperatures, will force the dipoles to keep their original orientation. On the other hand, the electric field applied in the opposite direction will force the dipoles

to switch their orientation. In both cases the external electric field will act against the thermal fluctuations and will promote ordering of dipoles in the MT.

As will be discussed in the next chapter, the background of ordered dipoles in the ferroelectric phase can serve for propagation of kink-like waves of tubulin dipole states that are coupled to the tubulin conformational states. Such excitations can be bits of information that signal other cellular events. Another effect of the dipole ordering in the ferroelectric phase is that the net dipole moment of a MT may couple with the dipole moment of a nearby MT [16]. Therefore, the dynamical behaviour of assemblies of MTs in which the MTs are concentrated with high density should be different from the dynamical behaviour of an individual MT. Here it can be recalled that assemblies of MTs *in vitro* exhibit oscillatory behaviour while the growth dynamics of a single MT is a stochastic process (see Chapter 1).

At higher temperatures the ferroelectric phase can become destroyed since, due to thermal fluctuations, clusters of dipoles with different orientation of dipole moments start to form. A MT in such a state may be able to store information by means of the patterns of the clusters. This possibility will be studied in Chapter 4.

The discussion above implies that the dipolar order in the MT lattice can be determined by such parameters as temperature or presence of external electric fields. The effect of these parameters as well as MAPs on the ordering of dipoles in a MT is studied in the following sections of this chapter.

2.5.1 A Lattice

Figure 2.10 shows plots of the spontaneous polarization per site (relative polarization) and the electric susceptibility (normalized to unity) of a MT with the A lattice. The size of the lattice is 13 columns and 100 rows[1], and the value of the parameter $\bar{Q} = q^2 s^2/\epsilon_r$ is $12 \times 10^{-56}\,\mathrm{C^2m^2}$. The figure shows that the MT lattice of dipoles undergoes a transition from a ferroelectric phase at low temperatures to a paraelectric phase at high temperatures. The transition between the the two phases is gradual with a number of excursions. The transition temperature was taken as a temperature at which the electric susceptibility has its maximum. For this lattice $T_c = 300\,\mathrm{K}$.

[1]The type and size of the MT lattice will be also written as 13x100B, 13x3000A, *etc.*, where the first number is the number of columns, the second number is the number of rows, and A or B stand for the lattice type.

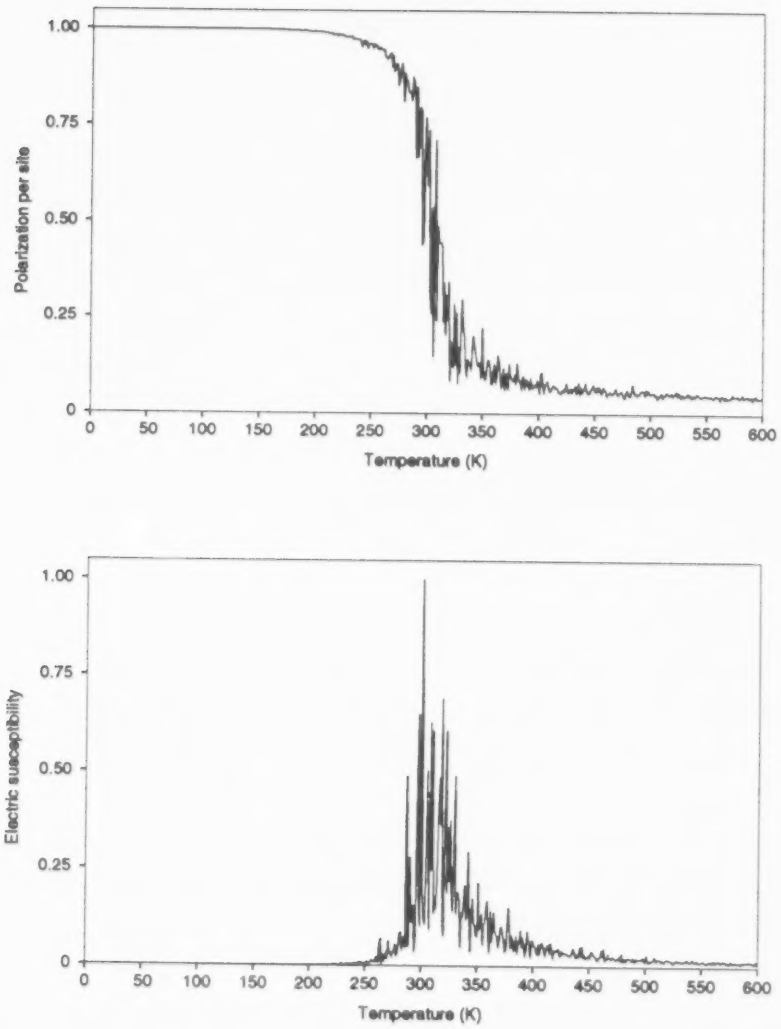

Figure 2.10: Dielectric transition in a MT with the A lattice. The size of the lattice is 13x100 and $\bar{Q} = 12 \times 10^{-56}\,\mathrm{C^2m^2}$. The spontaneous polarization per site decreases from $P = 1$ at low temperatures to almost zero at high temperatures. The transition temperature is indicated by the peak of the electric susceptibility, $T_c = 300\,\mathrm{K}$.

Figure 2.11 is a plot of the spontaneous polarization per site of a MT with the A lattice and 13 columns and 3000 rows. The value of $\bar{Q}$ is the same as for the plots in Figure 2.10. The transition is similar to that in Figure 2.10, but the polarization curve is much smoother. This implies that the excursions of polarization observed in the lattice 13x100 are due to the smaller size of the lattice.

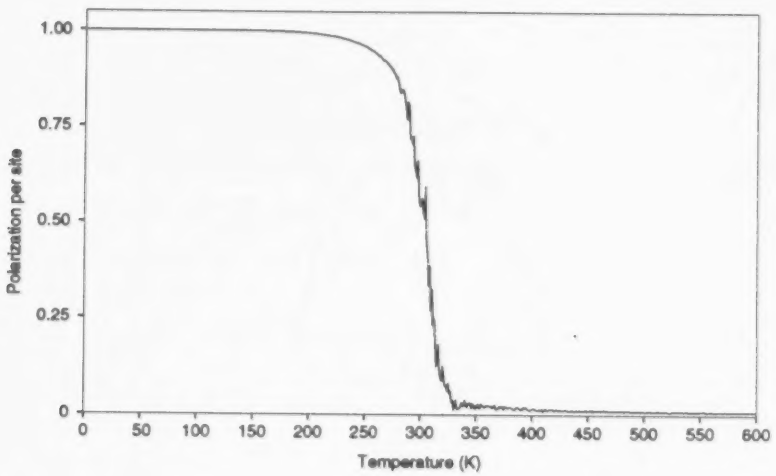

Figure 2.11: Spontaneous polarization per site in a MT with the lattice 13x3000A for $\bar{Q} = 12 \times 10^{-56}\,\mathrm{C^2m^2}$. The excursions of polarization are almost removed due to the large size of the lattice.

The critical temperature of the transition in Figure 2.11 obtained from the calculation of the electric susceptibility is 311 K. This is close to the T_c of the lattice with 100 rows. For a lattice with 500 rows the critical temperature was 306 K. This shows that T_c doesn't significantly change as a function of the MT length but it seems to increase with the increasing size of the MT. The magnitude of the maximum of the electric susceptibility was also found to increase when the number of rows in the lattice increased. In the lattice with 3000 rows the susceptibility was two orders of magnitude larger than in the lattice with 100 rows. Investigations with other finite systems have revealed that such behaviour is characteristic for a phase transition. A phase transition is defined in an infinite system. Since the MT lattice is finite, its electric susceptibility doesn't diverge as it is in a second order phase transition. However, with increasing size of the MT lattice the temperature

at which the electric susceptibility peaks, approaches the critical temperature and the maximum of the electric susceptibility approaches infinity.

Figure 2.12 shows plots of the spontaneous polarization per site in the MT lattice 13x100A when the values of $\bar{Q}$ are $10 \times 10^{-56}\,\mathrm{C^2m^2}$, $12 \times 10^{-56}\,\mathrm{C^2m^2}$ and $14 \times 10^{-56}\,\mathrm{C^2m^2}$. As can be seen from the figure, with increasing $\bar{Q}$ the transition temperature increases as well and *vice versa*. The corresponding electric susceptibilities peaked at temperatures 264 K, 300 K and 361 K.

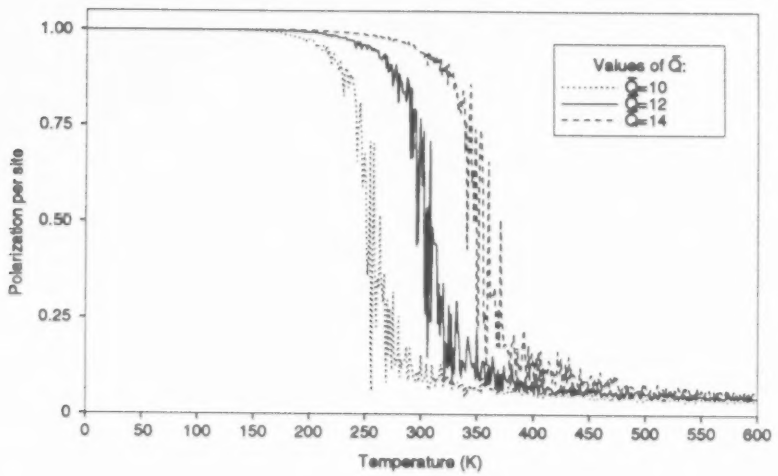

Figure 2.12: Transition in the MT lattice 13x100A when $\bar{Q}$ is $10 \times 10^{-56}\,\mathrm{C^2m^2}$, $12 \times 10^{-56}\,\mathrm{C^2m^2}$ and $14 \times 10^{-56}\,\mathrm{C^2m^2}$. As $\bar{Q}$ increases the transition moves towards higher temperatures. The values of $\bar{Q}$ are given in $10^{-56}\,\mathrm{C^2m^2}$.

Hence, for different configurations of q, s and ϵ_r the critical temperatures of the dielectric transition in a MT are different. The range of different T_c's is given by the range of possible values of q, s and ϵ_r. As was mentioned in the previous section, q should be of the order of the electronic charge and the value of s is up to a few nanometers. The relative permittivity ϵ_r could have different values if the lattice of dipoles were capable of oscillations at different frequencies.

For the value $\bar{Q} = q^2s^2/\epsilon_r = 12 \times 10^{-56}\,\mathrm{C^2m^2}$, the transition temperature of the A lattice is in the range of body temperature, $T_B = 310\,\mathrm{K}$. For the static value of the relative permittivity $\epsilon_r \simeq 70$ and the value of the charge $q = 2 \times 1.602 \times 10^{-19}\,\mathrm{C}$ the dipole length would be $s = 9 \times 10^{-9}\,\mathrm{m}$, which is close to the acceptable limits.

Increasing q or decreasing ϵ_r will require smaller s if the transition temperature is to be close to body temperature. It should be noted that the fluid surrounding MTs is cytosol which is a solution of water, ions and other molecules and that, except for free water, there exists bound water in the cell as well. These fluids may have somewhat different ϵ_r from that of free water.

As has been shown here, not a substantial change of the parameters q, s and ϵ_r may cause a shift of the transition region towards higher or lower temperatures. When the critical temperature is higher than body temperature, the assembly of MT dipoles is in the ferroelectric phase. When a MT is in this phase it may be able to propagate kink-like excitations of tubulin dipole states, and also to interact with other MTs by means of electric fields. When T_c is less than body temperature, a MT may store information in the form of patterns of clusters of dipoles with different orientation of polarization. The calculations shown here suggest that if there are such mechanisms in the cell which control the values of the parameters q, s and ϵ_r and consequently the interaction constants J_n in the MT with the A lattice, these mechanisms determine the dielectric state of the MT which may be linked to a different mode of operation of the MT.

It can be noted that the values of the interaction constants J_n can also be altered by changing the geometrical arrangement of the tubulin dimers in the MT lattice which results in different values of the angles θ_n and distances r_n (see equation (2.19)). Even though the arrangement of the tubulin dimers in a MT with either A or B lattice is fixed, changes can occur due to the twisting of the MT or defects in the MT lattice, *etc.*

The effect of external electric fields on the dielectric transition in MTs is studied in this work for the values of E found in the literature. The results of the experiments *in vitro* reported in [17] imply that MTs can interact with electric fields as small as $1\,\mathrm{Vm}^{-1}$. The authors of [18] reported that naturally occurring fields may be in the range $2 - 50\,\mathrm{Vm}^{-1}$. In the cell membranes, the magnitude of the membrane potential was measured in the range $0.02 - 0.2\,\mathrm{V}$ [19]. The thickness of the the cell membranes is about 5 nm. This gives the electric fields across the membrane in the range $4 \times 10^6\,\mathrm{Vm}^{-1}$ to $4 \times 10^7\,\mathrm{Vm}^{-1}$.

In Figure 2.13 the polarization per site is plotted in the MT lattice 13x100A which is subjected to external electric fields $0\,\mathrm{Vm}^{-1}$, $10^3\,\mathrm{Vm}^{-1}$, $10^4\,\mathrm{Vm}^{-1}$, $10^5\,\mathrm{Vm}^{-1}$, $10^6\,\mathrm{Vm}^{-1}$. The electric fields point in the direction in which the dipoles are aligned in the ferroelectric phase. For all curves $\bar{Q} = 12 \times 10^{-56}\,\mathrm{C}^2\mathrm{m}^2$. The figure shows

that the external electric field tends to order the dipoles in the MT lattice in the same direction. The larger the field, the larger the degree of ordering.

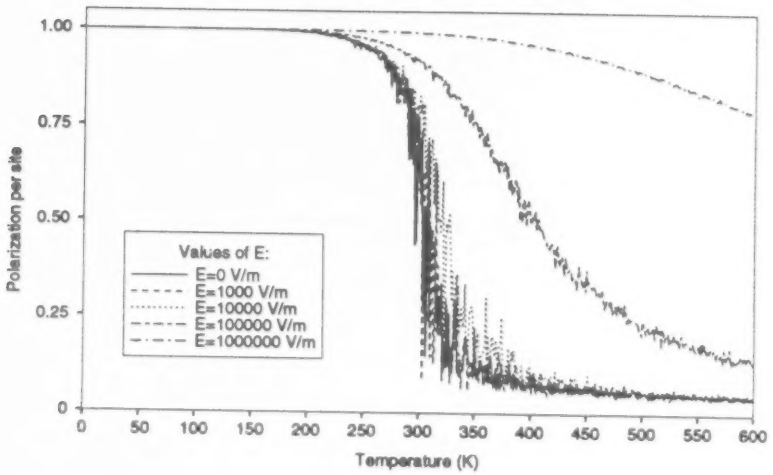

Figure 2.13: Polarization per site in the MT lattice 13x100A when the external electric fields are $0\,\mathrm{Vm}^{-1}$, $10^3\,\mathrm{Vm}^{-1}$, $10^4\,\mathrm{Vm}^{-1}$, $10^5\,\mathrm{Vm}^{-1}$, $10^6\,\mathrm{Vm}^{-1}$. $\bar{Q} = 12 \times 10^{-56}\,\mathrm{C}^2\mathrm{m}^2$ for all curves. As the external electric field increases, the ordering of dipoles in the lattice in the direction along the field increases as well.

The effect of the external electric field on the ordering of dipoles in a MT, shown by the Monte Carlo calculation in Figure 2.13, can be estimated qualitatively by comparing the potential energy associated with each dipole due to its interaction with the electric field and the interaction energy between two dipoles. If the static value of the relative permittivity of free water $\epsilon_r = 70$ is assumed then for $\bar{Q} = 12 \times 10^{-56}\,\mathrm{C}^2\mathrm{m}^2$ the product $qs = 2.9 \times 10^{-27}\,\mathrm{Vm}^{-1}$. Choosing $q = 4 \times 1.602 \times 10^{-19}\,\mathrm{C}$ gives the dipole length $s = 4.5 \times 10^{-9}\,\mathrm{m}$. Assuming that the magnitude of the dipole moment is $2.9 \times 10^{-27}\,\mathrm{Vm}^{-1}$, the contribution to the potential energy due to the interaction with the electric field from each dipole is $\pm pE = \pm qsE = 2.9 \times 10^{-27}E$. For $E = 10^3\,\mathrm{Vm}^{-1}$, the potential energy is $\pm qsE = \pm 0.0029 \times 10^{-21}\,\mathrm{J}$. This is very small compared to the interaction energies given in (2.22) and the dielectric transition in the MT is not affected. With increasing external electric field the magnitude of the potential energy $\pm qsE$ increases as well, and the electric field will start to have an effect on the ordering of dipoles. For $E = 10^6\,\mathrm{Vm}^{-1}$ the potential

energy due to the electric field is $\pm qsE = \pm 2.9 \times 10^{-21}$ J which is almost as large as the largest interaction constant J_1^A in (2.22). When the electric field is so large that the potential energy due to the interaction of the dipoles with the field is larger than the energies due to the dipole-dipole interaction, the lattice will be completely ordered at all temperatures. It should be pointed out that for smaller electric fields to be effective, the value qs would have to be larger which is possible only up to a certain limit as was discussed before.

The calculation for the case when the lattice of dipoles is subjected to an external electric field which points in the direction opposite to the direction in which the dipoles are aligned in the ferroelectric phase is shown in Figure 2.14 for the MT lattice 13x100A and $\bar{Q} = 12 \times 10^{-56}\,\mathrm{C^2m^2}$. All dipoles are initially in the up state and the fields are $-10^4\,\mathrm{Vm^{-1}}$ and $-10^6\,\mathrm{Vm^{-1}}$. The plots show that the assembly of dipoles switches into the branch with the opposite sign of polarization and then undergoes a transition into the paraelectric phase.

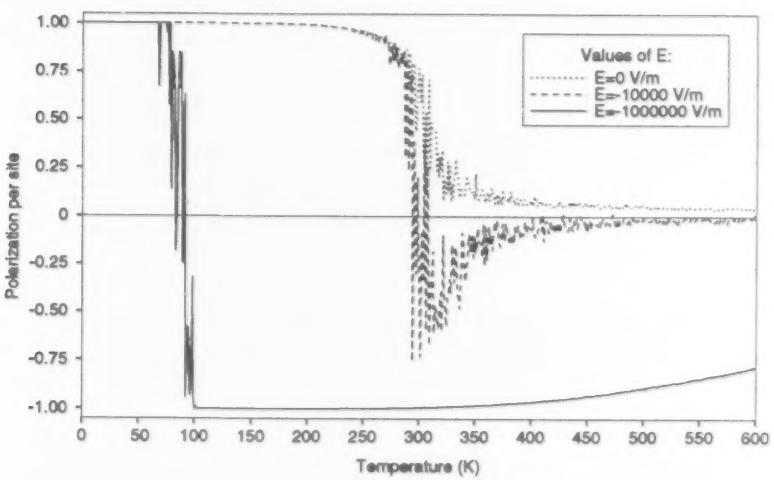

Figure 2.14: Polarization per site in the MT lattice 13x100A when the external electric fields are $-10^4\,\mathrm{Vm^{-1}}$ and $-10^6\,\mathrm{Vm^{-1}}$ and $\bar{Q} = 12 \times 10^{-56}\,\mathrm{C^2m^2}$ for both curves.

Such behaviour is due to the properties of the model, in which each dipole can be in two states of equal magnitude that are parallel but point in the opposite directions. In a lattice which is not subjected to a external electric field, the two

orientations of dipoles are energetically equivalent (see Figure 2.2). An electric field applied in the direction antiparallel to the orientation of dipoles produces additional potential energy. This energy lowers the potential energy of the dipoles which point in the same direction as the electric field. Consequently, this state becomes the state with lower energy and the assembly of dipoles switches into this state.

According to Figure 2.14 the effect described above depends on the magnitude of the electric field. This is because an insufficient number of Monte Carlo steps was performed at low temperatures in order for the state of the assembly of dipoles to become uncorrelated with its initial state. If a sufficient number of Monte Carlo steps had been performed, the assembly of dipoles would have switched into the state with opposite orientation already at the lowest temperature independently of the magnitude of the electric field.

To study the influence of MAPs on the dielectric behaviour of a MT with the A lattice, three regular MAP distributions were constructed according to Figure 1.17. The patterns are shown in Figure 2.15. The sites (dimers) at which MAPs are attached, are represented by 0's and the rest of the sites are represented by 1's. The ratios of the number of MAP attachment sites to the total number of sites are 1/11, 1/22 and 1/48, respectively.

The effect of a MAP attached on a tubulin dimer may be to prevent it from changing its conformational state. Since the conformation of the tubulin is coupled to its dipole state, the dipole on the tubulin dimer on which a MAP is attached, won't be able to flip. In the Monte Carlo procedure this was taken into account by putting the value of the spin variable equal to 1 at the sites with attached MAPs and during the importance sampling these sites weren't examined. For comparison, calculations were also performed when at the sites on which MAPs were attached the spin variable was put equal to 0. For this case, the initial value of polarization in the lattice is smaller due to the zero dipole moment at the sites of attached MAPs.

Figure 2.16 shows the results of Monte Carlo simulations for the MT with the A lattice in which attached MAPs form three patterns depicted in Figure 2.15 and for the lattice without MAPs. The parameter $\bar{Q}$ is set to $12 \times 10^{-56}\,\mathrm{C^2m^2}$ for all curves. As can be seen, the effect of MAPs is similar to the effect of the external electric field. With the increasing number of MAPs attached to the MT the number of dipoles aligned in the same direction at a temperature T increases. Since MAPs are assembly promoters, this suggests that the ferroelectric phase may be the phase suitable for the assembly of MTs.

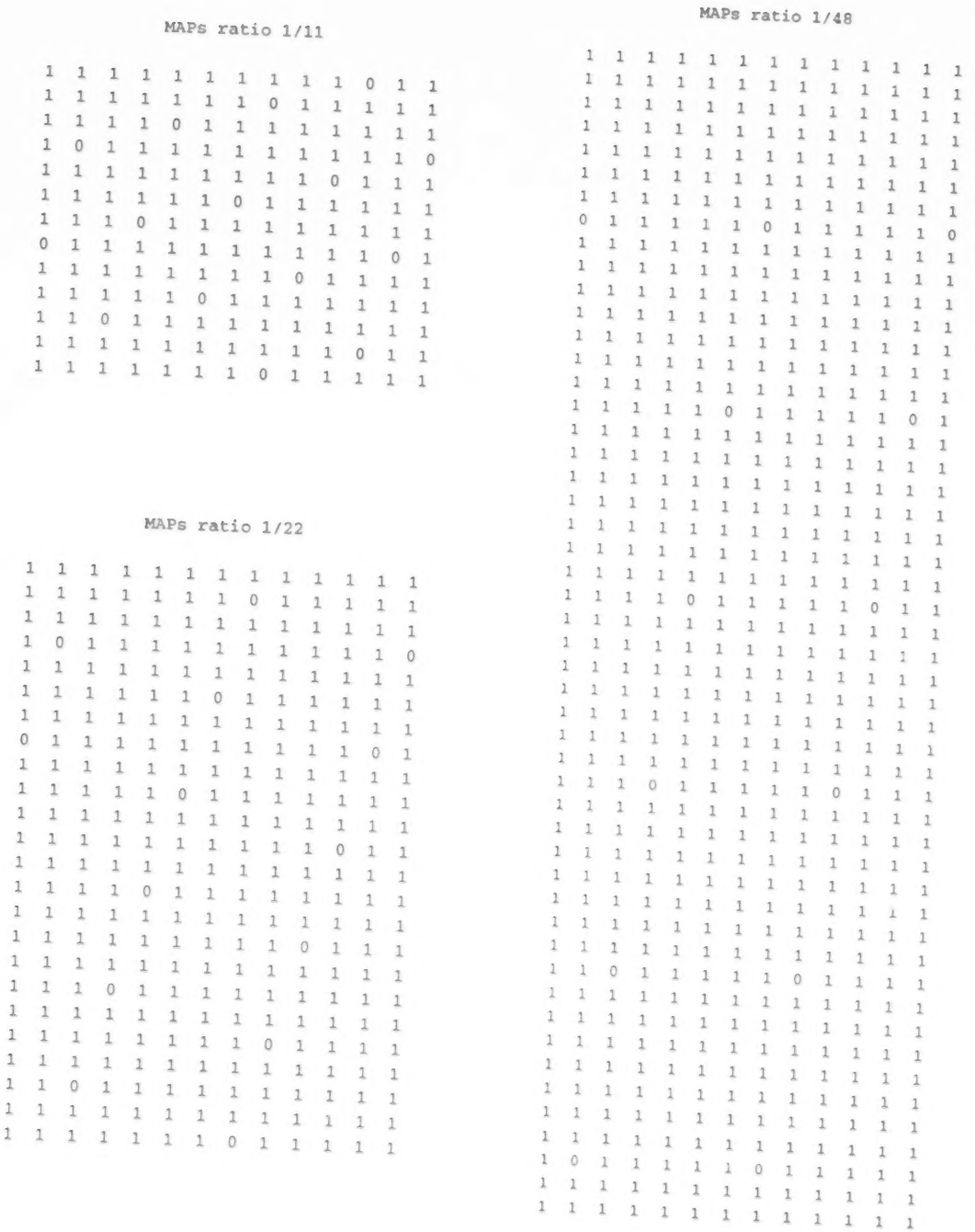

Figure 2.15: Three MAP patterns in a MT with the A lattice and 13 protofilaments. The ratios of the number of sites at which MAPs are attached to the total number of sites in the lattice are 1/11, 1/22, 1/48.

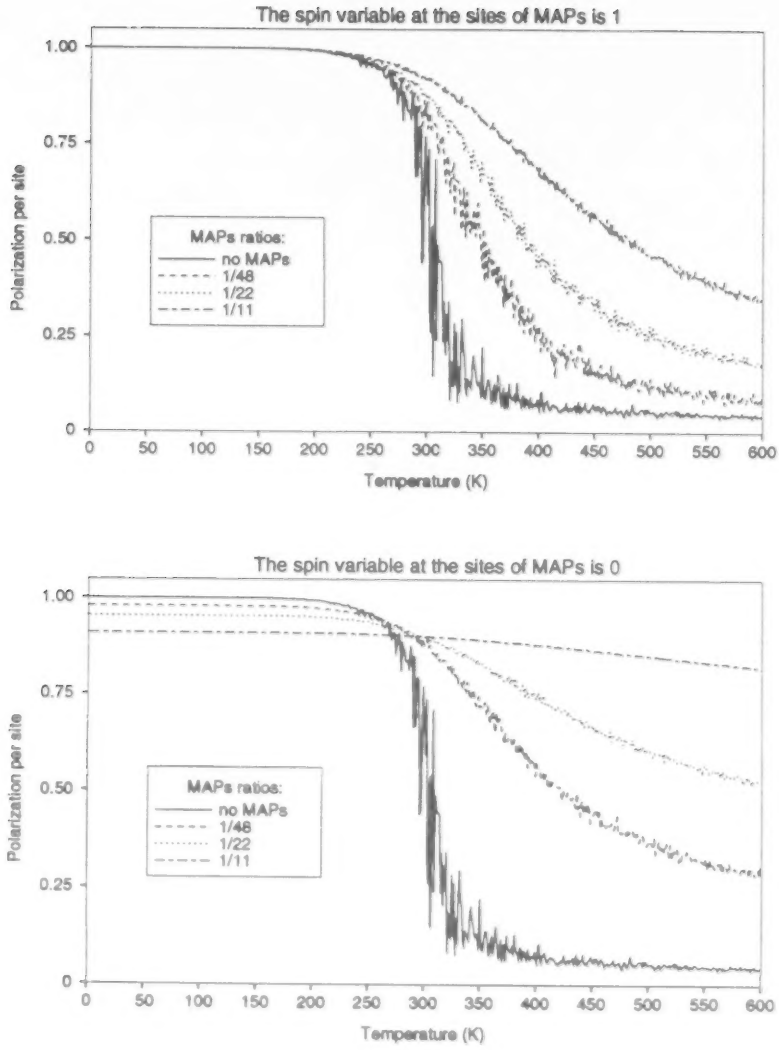

Figure 2.16: The effect of MAPs attached to the MT A lattice in the three regular patterns shown in Figure 2.15. The lattices consist of 13 columns and 99, 110 and 96 rows for the corresponding ratios 1/11, 1/22 and 1/48. $\bar{Q} = 12 \times 10^{-56}\,\mathrm{C^2m^2}$ for all curves. The values of the spin variable at the MAP attachment sites are +1 and 0.

2.5.2 B-lattice

When the arrangement of the tubulin dimers in a MT is of the B type the distances r_2 and r_3 and the angles θ_2 and θ_3 in the triangular cells formed between the 1-st and 13-th column are different from those inside the lattice. According to (2.22) this gives different interaction constants J_2^B and J_3^B associated with the interaction between dipoles placed at the boundaries. For $\bar{Q} = 12 \times 10^{-56}$ C^{2}m^2, the interaction constants at the boundaries of the B lattice are

$$\begin{aligned} J^B_{1,boundary} &= +4.21 \times 10^{-21}\,\mathrm{J}\,, \\ J^B_{2,boundary} &= -1.63 \times 10^{-21}\,\mathrm{J}\,, \\ J^B_{3,boundary} &= +1.61 \times 10^{-21}\,\mathrm{J}\,. \end{aligned} \tag{2.24}$$

They correspond to the angles and distances

$$\begin{aligned} \theta^B_{1,boundary} &= 0^\circ\,, & r^B_{1,boundary} &= 8.00 \times 10^{-9}\,\mathrm{m}\,, \\ \theta^B_{2,boundary} &= 43.9^\circ\,, & r^B_{2,boundary} &= 7.21 \times 10^{-9}\,\mathrm{m}\,, \\ \theta^B_{3,boundary} &= 60.8^\circ\,, & r^B_{3,boundary} &= 5.73 \times 10^{-9}\,\mathrm{m}\,. \end{aligned} \tag{2.25}$$

It can be noted that the magnitudes of the interaction constants J^B_{bound2} and J^B_{bound3} are almost the same due to which the B lattice can be frustrated along its boundaries.

Figure 2.17 depicts spontaneous polarization per site for lattices with a stagger 3.1 nm (A lattice), 2.9 nm, 2.3 nm, 1.5 nm and 0.9 nm (B lattice). The lattices consist of 13 columns and 100 rows and the value of $\bar{Q}$ is 12×10^{-56} C^{2}m^2. As can be seen from the curves, with the decreasing stagger of the lattice the transition temperature moves towards lower temperatures. In the B lattice the assembly of dipoles is in a state with almost zero polarization at all temperatures, that means, it doesn't undergo a dielectric transition. This result was found for several different values of $\bar{Q}$ up to 1000×10^{-56} C^{2}m^2. Figure 2.17 also illustrates how the transition in the MT lattice depends on the geometrical arrangement of the tubulin dimers and the degree of mismatch of the successive rows in the MT since these are characteristics given by the stagger of the lattice.

2.6 Model with Tilted States

In the MT lattice in which the dipoles are tilted in the β state, the potential

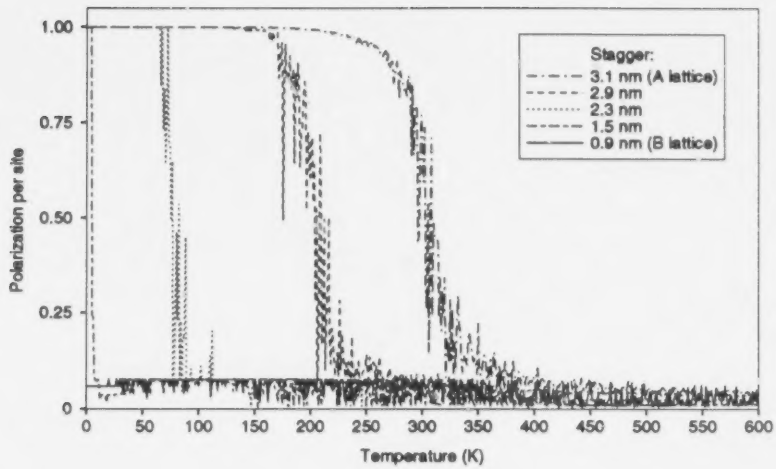

Figure 2.17: Spontaneous polarization per site for the values of the stagger of the MT lattice 3.1 nm (A lattice), 2.9 nm, 2.3 nm, 1.5 nm, 0.9 nm (B lattice). The size of the lattice is 13x100 and $\bar{Q} = 12 \times 10^{-56}\,\mathrm{C^2m^2}$ for all curves.

energy due to the interaction between the dipoles can be expressed as [5]

$$H = \frac{1}{4}\sum_{n=1}^{3}\sum_{<nn>} J_{n1}(1+s_k)(1+s_l)+J_{n2}(1-s_k)(1-s_l)+J_{n3}[(1+s_k)(1-s_l)+(1-s_k)(1+s_l)]. \tag{2.26}$$

The expression above represents the interaction energy between particles which can be in two distinct states (they can also be two different particles). The particles are placed at sites which form a triangular lattice and interact only with their nearest neighbours. The sum over n in (2.26) is a sum over the sides of a triangular cell of this lattice and the sum over $< nn >$ runs over the nearest neighbours. The variable s_k can have two values +1 or -1 which correspond to the two different states of each particle. Each direction n of the triangular cell is characterized by three interaction constants J_{nm}.

If the particles are dipoles on the tubulin dimers that compose a MT then the two values of s_k represent the tilted (α) and nontilted (β) state, respectively. J_{n1} is the interaction energy between two dipoles that are in the nontilted state, J_{n2} is the interaction energy between two dipoles that are both tilted and J_{n3} is the interaction energy between a dipole in the tilted and a dipole in the nontilted state. Thus, the

MT lattice in which the dipoles are tilted in the β state possesses altogether 9 interaction constants.

After rearranging terms in equation (2.26), the potential energy of the assembly of dipoles which are tilted in the β state has the form

$$H = H_{int} + V_{eff} \sum_{j=1}^{NC} \sum_{i=1}^{NR} \sigma_{ij} + C\,. \tag{2.27}$$

In (2.27), H_{int} is the same as the interaction part of (2.16) but with a plus sign, V_{eff} is an effective potential energy, NR and NC are the number of rows and number of columns in the lattice, and C is a constant.

The three interaction constants J_n in H_{int} are given by the equations

$$\begin{aligned} J_1 &= \tfrac{1}{4}(J_{11} + J_{12} - 2J_{13})\,, \\ J_2 &= \tfrac{1}{4}(J_{21} + J_{22} - 2J_{23})\,, \\ J_3 &= \tfrac{1}{4}(J_{31} + J_{32} - 2J_{33})\,. \end{aligned} \tag{2.28}$$

where the interaction energies J_{nm} were calculated from the formula (2.18) and they are of the following form

$$J_{nm} = \frac{q^2 s^2}{4\pi\epsilon_0\epsilon_r} \frac{\cos\alpha_{nm} - 3\cos\beta_{nm}\cos\gamma_{nm}}{r_n^3}\,, \quad n = 1,2,3,\ m = 1,2,3\,. \tag{2.29}$$

The variables α_{nm}, β_{nm} and γ_{nm} in (2.29) are given in terms of the angles θ_n that characterize the MT lattice and the angle θ_{tilt} by which the dipoles are tilted in the β state with respect to the MT axis as follows

$$\begin{gathered} \alpha_{n1} = \alpha_{n2} = 0\,, \quad \alpha_{n3} = \pi - \theta_{tilt}\,, \\ \beta_{11} = \gamma_{11} = 0\,, \quad \beta_{21} = \gamma_{21} = \theta_2\,, \quad \beta_{31} = \gamma_{31} = \theta_3\,, \\ \beta_{12} = \gamma_{12} = \theta_{tilt}\,, \quad \beta_{22} = \gamma_{22} = \theta_2 - \theta_{tilt}\,, \quad \beta_{32} = \gamma_{32} = \theta_{tilt} + \theta_3\,, \\ \beta_{13} = \theta_1\,, \quad \gamma_{13} = \pi - \theta_{tilt}\,, \\ \beta_{23} = \theta_2\,, \quad \gamma_{23} = \pi - (\theta_2 - \theta_{tilt})\,, \\ \beta_{33} = \theta_3\,, \quad \gamma_{33} = \pi - \theta_3\,. \end{gathered} \tag{2.30}$$

The effective potential energy V_{eff} and the constant term C have the following form

$$V_{eff} = \frac{1}{2}(J_{11} - J_{12} + J_{21} - J_{22} + J_{31} - J_{32}) \tag{2.31}$$

and

$$C = \frac{N}{4} \times (J_{11} + J_{12} + 2J_{13} + J_{21} + J_{22} + 2J_{23} + J_{31} + J_{32} + 2J_{33})\,. \tag{2.32}$$

In the latter equation $N = NC \times NR$ is the total number of lattice sites.

It should be pointed out that all terms in (2.27) are exactly valid for the A lattice, but they have to be modified for the B lattice for which the interaction constants at the boundaries are different from those inside the lattice.

Based on (2.28) and (2.18) for the value of $\bar{Q} = 12 \times 10^{-56}\,\mathrm{C^2m^2}$, the values of the interaction constants J_n of the A lattice and inside the B lattice for the model with dipoles tilted in the β state by 29° to the left with respect to the MT axis[2] are

$$\begin{aligned} J_1^A &= -3.58 \times 10^{-21}\,\mathrm{J}, & J_1^B &= -3.56 \times 10^{-21}\,\mathrm{J}, \\ J_2^A &= -2.82 \times 10^{-21}\,\mathrm{J}, & J_2^B &= +3.67 \times 10^{-21}\,\mathrm{J}, \\ J_3^A &= -0.75 \times 10^{-21}\,\mathrm{J}, & J_3^B &= -0.40 \times 10^{-21}\,\mathrm{J}. \end{aligned} \tag{2.33}$$

Similarly to the model with nontilted dipoles the interaction constants have different signs and different magnitudes. However, inside the B lattice the magnitudes of the constants J_1^B and J_2^B are very close. This means that by tilting the dipoles on the tubulin dimers the MT can become frustrated. On the other hand, the effective potential energy (2.31) can be viewed as a consequence of the interaction of dipoles with an effective electric field which suppresses frustration. For $\bar{Q} = 12 \times 10^{-56}\,\mathrm{C^2m^2}$ the values of V_{eff} for the A lattice and inside the B lattice are

$$V_{eff}^A = +1.13 \times 10^{-21}\,\mathrm{J} \qquad V_{eff}^B = +2.61 \times 10^{-21}\,\mathrm{J} \tag{2.34}$$

In the next two sections, the effect of tilting the dipoles on the tubulin dimers in the β state on the dielectric transition in a MT is studied and compared with the results for the model with nontilted dipoles.

2.6.1 A Lattice

In Figure 2.18 are plotted two curves which represent the spontaneous polarization in the 13x100A lattice of dipoles that are tilted in their β state by 29° to the left with respect to the MT axis. The solid line corresponds to the simulation when in the starting configuration at each temperature all dipoles are in the nontilted state, *i.e.*, $\sigma_{ij} = +1$ at each lattice site. The dotted line shows the calculation when the initial state of all dipoles at each temperature was tilted, *i.e.*, all $\sigma_{ij} = -1$. The

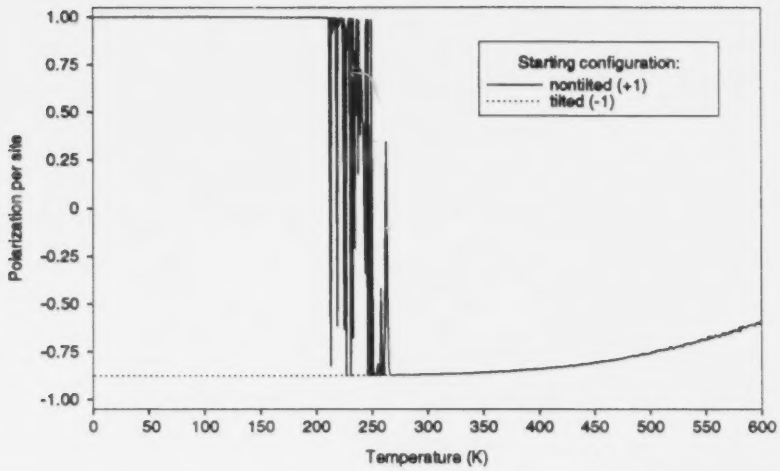

Figure 2.18: Polarization per site in a MT with 13x100A lattice for $\bar{Q} = 12 \times 10^{-56}\,\mathrm{C^2m^2}$ and $\theta_{tilt} = 29^{\circ}_{+}$. The two curves correspond to the tilted and nontilted starting configuration of dipoles, respectively.

value of the parameter $\bar{Q}$ is $12 \times 10^{-56}\,\mathrm{C^2m^2}$.

The figure shows that when all dipoles are initially in the up state, that means, the spontaneous polarization per site is $P = +1$, the lattice switches into the opposite state in which all dipoles are tilted and corresponding value of $P = -\cos 29^{\circ} = -0.875$. This happens because the configuration in which all dipoles are tilted has a lower energy compared to that in which all dipoles are nontilted. Using the values of the interaction energies J_1, J_2, J_3, J_{12}, J_{22} and J_{32} for $\bar{Q} = 12 \times 10^{-56}\,\mathrm{C^2m^2}$, the energy of a dipole in the A lattice due to the interactions with its nearest neighbours is $E^{\uparrow} = -9.61 \times 10^{-21}\,\mathrm{J}$ when all dipoles are nontilted (up) and $E^{\downarrow} = -14.13 \times 10^{-21}\,\mathrm{J}$ when all dipoles are tilted (down) (Figure 2.19). This means that unlike the model with nontilted dipoles, in the model with tilted dipoles the up and down configurations of dipoles are not energetically equivalent and due to this the assembly of dipoles in a MT will always tend to be in the state which has a lower energy.

It should be pointed out that if at low temperatures a sufficient number of Monte

[2]Tilting to the left/right with respect to the MT axis in the β state will be written with a subscript +/-. For example, 29°_{+} means tilting by 29° to the left with respect to the MT axis, 5°_{-} means tilting by 5° to the right with respect to the MT axis, *etc.*

Carlo steps had been performed, the assembly of dipoles in the up state would have switched into the state when all dipoles are down already at the lowest temperature, *i.e.*, no transition from the state with $P = +1$ to the state with $P = -0.875$ would have been observed.

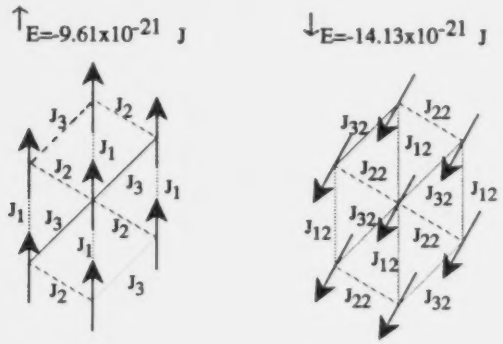

Figure 2.19: A dipole in the MT A lattice and its nearest neighbours in the tilted and nontilted configuration, respectively. The energy of the central dipole due to the interaction with its nearest neighbours is calculated for $\bar{Q} = 12 \times 10^{-56}\,\mathrm{C^2m^2}$ and $\theta_{tilt} = 29^\circ_+$.

So far no experiments have been done in which the orientation of the dipole on the tubulin dimer was measured. In this work the assumption has been made that the angle θ_{tilt} by which the dipole on the tubulin dimer is tilted with respect to the MT axis in the β state is the same as the conformational shift of the dimer in the β state, *i.e.*, $\theta_{tilt} = 29^\circ$ to the left with respect to the MT axis.

Figure 2.20 shows a set of calculations when θ_{tilt} is assumed to be either 5° or 29° both to the left and to the right with respect to the MT axis. When $\theta_{tilt} = 5^\circ_+$ or $\theta_{tilt} = 29^\circ_+$, the tilted configuration is the configuration with a lower energy and in the Monte Carlo simulations this is the starting configuration. The corresponding polarizations per site are $P = -\cos 5^\circ = -0.996$ and $P = -\cos 29^\circ = -0.875$. In a lattice in which $\theta_{tilt} = 5^\circ_-$ and $\theta_{tilt} = 29^\circ_-$, the energies of a tilted dipole due to the interaction with its nearest neighbours that are all tilted, are $E^\downarrow = -8.79 \times 10^{-21}\,\mathrm{J}$ and $E^\downarrow = -5.99 \times 10^{-21}\,\mathrm{J}$, respectively. This shows that the nontilted configuration has a lower energy compared to the tilted one and it is the starting configuration in the Monte Carlo simulations with the corresponding value of the spontaneous

polarization per site $P = +1$.

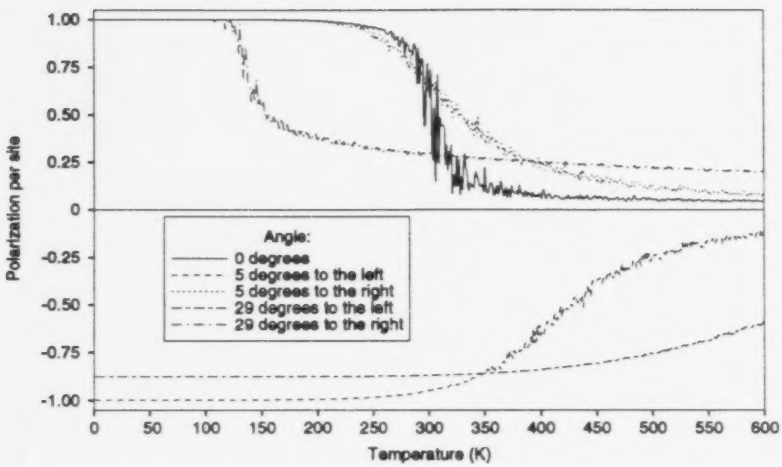

Figure 2.20: Polarization per site in the MT lattice 13x100A for $\theta_{tilt} = 5^{\circ}_{\pm}$ and $29^{\circ}_{\pm}$ and $\bar{Q} = 12 \times 10^{-56}\,\mathrm{C^2m^2}$.

As can be seen from Figure 2.20, tilting the dipoles in the MT lattice to the left with respect to the MT axis results in a dielectric transition with a higher T_c compared to the transition in a lattice in which the dipoles are nontilted. On the contrary, tilting the dipoles to the right with respect to the MT axis moves the transition from the ferroelectric to the paraelectric phase towards lower temperatures.

The effect of external electric fields on a MT A lattice of dipoles that are tilted in the β state is shown in Figure 2.21. In the starting configuration at each temperature $\theta_{tilt} = 29^{\circ}_{+}$, $\bar{Q} = 5 \times 10^{-56}\ \mathrm{C^2m^2}$ and the size of the lattice is 13x100. The calculation was performed for the values of the external electric fields $-10^6\,\mathrm{Vm^{-1}}$, $-10^5\,\mathrm{Vm^{-1}}$, $-10^4\,\mathrm{Vm^{-1}}$, $+10^4\,\mathrm{Vm^{-1}}$, $+10^5\,\mathrm{Vm^{-1}}$, and $+10^6\,\mathrm{Vm^{-1}}$. According to the figure, the lattice with tilted dipoles behaves similarly to the lattice with nontilted dipoles. When the external electric field points in the negative direction, *i.e.*, in the direction of the projection of the dipoles in the tilted state on the MT axis, the dipoles tend to be ordered in the tilted state. The larger is the field, the larger is the degree of ordering of dipoles in this state at each temperature.

This result can be explained by calculating the potential energy of interaction of the dipoles with the external electric field and comparing this energy to the energy of

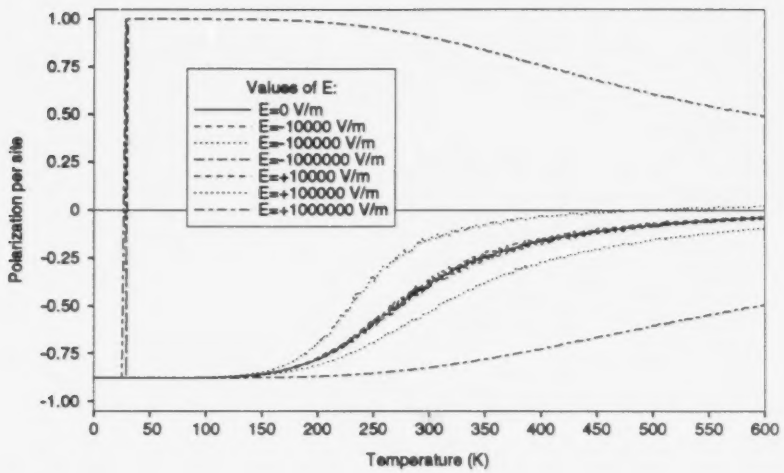

Figure 2.21: Dielectric transition in the MT lattice 13x100A in which $\theta_{tilt} = 29^{\circ}_{+}$, $\bar{Q} = 5 \times 10^{-56}\,\mathrm{C^2m^2}$ and the external electric field is present. The values of the external electric fields are $-10^{6}\,\mathrm{Vm^{-1}}$, $-10^{5}\,\mathrm{Vm^{-1}}$, $-10^{4}\,\mathrm{Vm^{-1}}$, $+10^{4}\,\mathrm{Vm^{-1}}$, $+10^{5}\,\mathrm{Vm^{-1}}$, and $+10^{6}\,\mathrm{Vm^{-1}}$.

each dipole which is due to the interaction with its nearest neighbours. The relevant interaction energies in the A lattice for $\bar{Q} = 5 \times 10^{-56}\,\mathrm{C^2m^2}$ and $\theta_{tilt} = 29^{\circ}_{+}$ are

$$\begin{aligned} J^{A}_{11} &= -1.76 \times 10^{-21}\,\mathrm{J}, & J^{A}_{12} &= -1.14 \times 10^{-21}\,\mathrm{J}, \\ J^{A}_{21} &= +0.37 \times 10^{-21}\,\mathrm{J}, & J^{A}_{22} &= -2.84 \times 10^{-21}\,\mathrm{J}, \\ J^{A}_{31} &= -0.62 \times 10^{-21}\,\mathrm{J}, & J^{A}_{32} &= +1.03 \times 10^{-21}\,\mathrm{J}. \end{aligned} \tag{2.35}$$

In (2.35), the interaction energies J^{A}_{n1} represent the interaction between two nontilted dipoles, *i.e.*, they are the same as the interaction energies J^{A}_{n} that characterize the model with nontilted dipoles. The interaction energies J^{A}_{n2} represent the interaction between two tilted dipoles.

If the static value of the relative permittivity $\epsilon_r = 70$ is assumed and $\bar{Q} = 5 \times 10^{-56}\,\mathrm{C^2m^2}$ then the magnitude of the dipole moment on a tubulin dimer is $qs = 1.87 \times 10^{-27}\,\mathrm{Cm}$. Based on these values, for $E = -10^{4}\,\mathrm{Vm^{-1}}$ the potential energy due to the interaction of a dipole in the β state with this electric field is $-pE\cos 29^{\circ} = -0.0164 \times 10^{-21}\,\mathrm{J}$. This potential energy is only a small fraction of the interaction energies listed in (2.35) and consequently it won't significantly affect the dielectric state of the MT lattice of dipoles. However, when $E = -10^{6}\,\mathrm{Vm^{-1}}$

the potential energy is $-pE\cos 29° = -1.64 \times 10^{-21}$ J which is comparable to the interaction energies (2.35) and the assembly of dipoles in the MT exhibits a high degree of ordering in the tilted state.

When the external electric field points in the same direction as the dipoles in the nontilted state, it forces the dipoles to change their orientation from the tilted into the nontilted state. Compared to the model with nontilted dipoles, however, in the model with tilted dipoles the two orientations of dipoles are not energetically equivalent: the state when all dipoles are nontilted has higher energy. This means that in order for the dipoles to switch into this state the external electric field must be so large that the potential energy of the assembly of nontilted dipoles becomes lower than the potential energy of the assembly of tilted dipoles. This can be shown as follows:

Using the values of the interaction energies (2.35), the energy of a dipole due to the interaction with its nearest neighbours is $E^{\downarrow} = -5.9 \times 10^{-21}$ J in a lattice in which all dipoles are tilted and $E^{\uparrow} = -4.02 \times 10^{-21}$ J in a lattice in which all dipoles are nontilted (Figure 2.20). The potential energy due to the interaction of a dipole which is in the nontilted (up) state with the electric field $E = +10^6\,\mathrm{Vm}^{-1}$ is $-pE = -1.87 \times 10^{-21}$ J. This energy lowers the value of the energy $E^{\uparrow}$ to -5.89×10^{-21} J. The potential energy of a tilted dipole due to the interaction with the electric field $E = +10^6\,\mathrm{Vm}^{-1}$ is $+pE\cos 29° = 1.64 \times 10^{-21}$ J which brings the value of $E^{\downarrow}$ up to -4.27×10^{-21} J. Hence, the assembly of nontilted dipoles compared to the assembly of tilted dipoles is in a state with lower energy when subjected to the external electric field $E = +10^6\,\mathrm{Vm}^{-1}$. Consequently, the array of tilted dipoles switches into the state in which all dipoles are nontilted when it interacts with this field or a sufficiently large external electric field.

On the basis of the calculations above it is easy to see that in the external electric field $E = +10^5\,\mathrm{Vm}^{-1}$ the assembly of tilted dipoles has lower potential energy compared to the assembly of nontilted dipoles. Due to that, the dipoles remain in the state with negative polarization, that means, in the tilted state, but as can be seen from Figure 2.20 the transition from the ferroelectric to the paraelectric phase shifts towards lower temperatures. The effect of the electric field $E = +10^4\,\mathrm{Vm}^{-1}$ is very small because the potential energy of a dipole in the MT lattice due to the interaction with this field is negligible.

The results of the calculations for the model with tilted dipoles when MAPs are

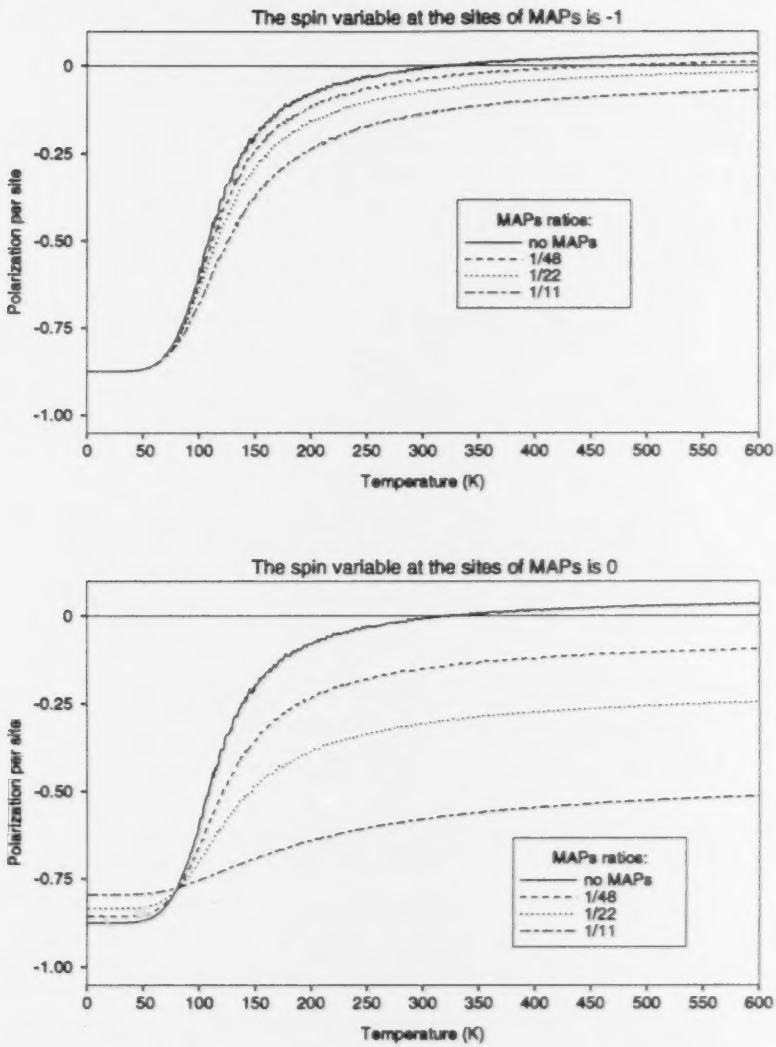

Figure 2.22: Dielectric transition in the MT A lattice to which MAPs are attached according to the patterns shown in Figure 2.15. The corresponding lattice sizes are 13x99, 13x110, and 13x96. $\theta_{tilt} = 29^{\circ}_{+}$ and $\bar{Q} = 2 \times 10^{-56}\,\mathrm{C^2m^2}$ for all curves. The value of the dipole variable at a MAP attachment site is -1 or 0.

attached to the MT A lattice are presented in Figure 2.22. The MAP patterns were programmed as for the model with nontilted dipoles according to Figure 2.15. The sites at which MAPs are attached are represented by the value of the dipole variable -1 and 0. The plots show that the effect of attached MAPs is similar as in the lattice in which the dipoles are nontilted. The presence of MAPs increases the number of dipoles aligned in the same direction, which is the tilted direction in this case. This effect is larger when the dipole variable on the MAP attachment site is represented by a 0.

2.6.2 B Lattice

Spontaneous polarization in the B lattice, in which the dipoles are tilted by 29° to the left with respect to the MT axis, is plotted in Figure 2.23. The lattice has

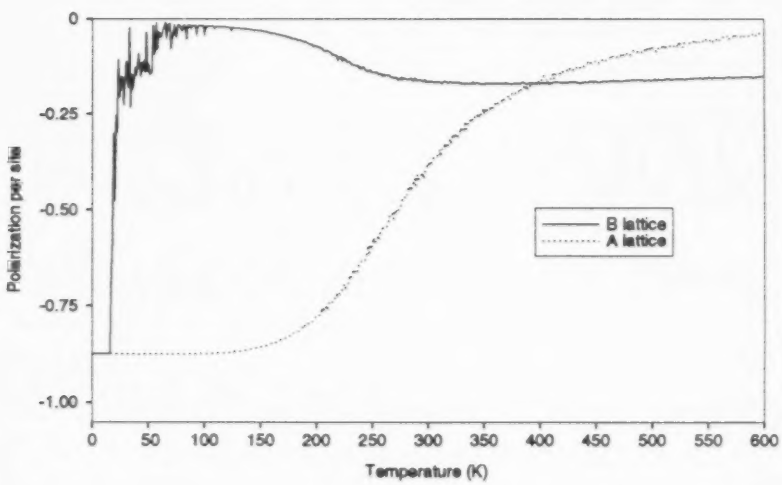

Figure 2.23: Spontaneous polarization per site in the MT lattice 13x100B in which $\theta_{tilt} = 29^{\circ}_{+}$ and $\bar{Q} = 5 \times 10^{-56}\,\mathrm{C^2m^2}$. For comparison, the corresponding curve for the A lattice is also shown.

13 columns and 100 rows and $\bar{Q} = 5 \times 10^{-56}\,\mathrm{C^2m^2}$. The values of the interaction

constants at the boundaries for this value of $\bar{Q}$ are

$$\begin{aligned} J^B_{1,boundary} &= -3.58 \times 10^{-21}\,\mathrm{J}\,, \\ J^B_{2,boundary} &= -2.34 \times 10^{-21}\,\mathrm{J}\,, \\ J^B_{3,boundary} &= +0.37 \times 10^{-21}\,\mathrm{J}\,. \end{aligned} \tag{2.36}$$

For comparison, a curve for the A lattice with the same parameters is shown as well. Unlike the model with nontilted dipoles, this lattice undergoes a transition from the ferroelectric to the paraelectric phase. However, after the transition into the paraelectric phase at some temperature the polarization increases to a value of about -0.2.

In Figure 2.24 are shown plots of the spontaneous polarization per site in the 13x100B lattice for $\bar{Q} = 5 \times 10^{-56}\,\mathrm{C^2m^2}$, $\bar{Q} = 25 \times 10^{-56}\,\mathrm{C^2m^2}$ and $\bar{Q} = 55 \times 10^{-56}\,\mathrm{C^2m^2}$. The corresponding critical temperatures are $T_c = 17\,\mathrm{K}$, $97\,\mathrm{K}$ and $210\,\mathrm{K}$

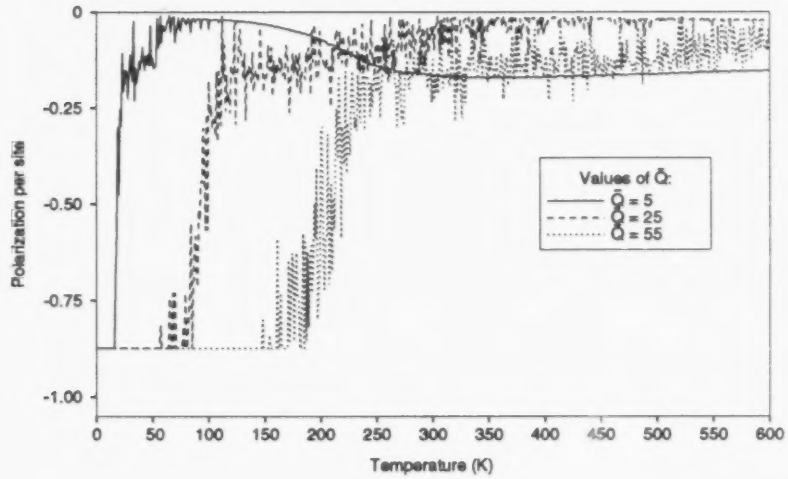

Figure 2.24: Dielectric transition in the MT lattice 13x100B for the values of $\bar{Q}$: $5 \times 10^{-56}\,\mathrm{C^2m^2}$, $25 \times 10^{-56}\,\mathrm{C^2m^2}$ and $55 \times 10^{-56}\,\mathrm{C^2m^2}$. The $\bar{Q}$'s are shown in units $10^{-56}\,\mathrm{C^2m^2}$ and $\theta_{tilt} = 29^\circ_+$.

and $\theta_{tilt} = 29^\circ_+$ for all curves. Similarly to the A lattice, when the value of $\bar{Q}$ increases the transition temperature increases as well. It can be noticed that the plots exhibit more excursions as the temperature increases. When $\bar{Q} = 25 \times 10^{-56}\,\mathrm{C^2m^2}$ and $\bar{Q} = 55 \times 10^{-56}\,\mathrm{C^2m^2}$ the polarization doesn't increase at high temperatures as it is for $\bar{Q} = 5 \times 10^{-56}\,\mathrm{C^2m^2}$.

The results above imply that a MT with the B lattice in which the dipoles are tilted in the β state can be in the ferroelectric phase, however, for quite high values of $\bar{Q}$ compared to those for the A lattice. If the smallest possible value of ϵ_r is about 4, then for $\bar{Q} = 55 \times 10^{-56}\,\mathrm{C^2m^2}$ the dipole length is about $4 \times 10^{-9}\,\mathrm{m}$ and the charge on the dipole would be about $3 \times 1.602 \times 10^{-19}\,\mathrm{C}$.

The calculations presented in this chapter demonstrate that a MT with 13 protofilaments may undergo a dielectric transition from a ferroelectric phase at low temperatures to a paraelectric phase at high temperatures. The existence and the character of the transition depend on the configuration of the parameters of the MT lattice of dipoles. These parameters are the geometrical arrangement of the lattice, the orientation of dipoles on the tubulin dimers, the magnitude of the dipole moments and the relative permittivity of the surrounding medium.

In the A lattice in which the dipoles are nontilted, the critical temperature of the transition is in the range of body temperature for acceptable values of the magnitude of the dipole moment of the dipoles and relative permittivity. In the B lattice in which the dipoles are nontilted no dielectric transition was found for any feasible values of the dipole moments and relative premittivity. Along the seam of the B lattice with nontilted dipoles two of the interaction constants have opposite signs but almost the same magnitude, which suggests that this lattice can be frustrated along the boundary.

The A lattice in which the dipoles are tilted in the β state undergoes a smooth transition between ferroelectric and paraelectric phases. In a MT with the B lattice in which the dipoles are tilted in the β state, the transition from the ferroelectric to the paraelectric phase was also found. However, in order for the critical temperature of the transition to be close to body temperature the values of the dipole moments have to be quite large or the relative permittivity has to be small. In this lattice, two interaction constants were found to have opposite signs and close values of their magnitudes. This means that depending on the angle by which the dipoles on the tubulin dimers are tilted, a MT with the B lattice can become frustrated.

When the MT with the A lattice is subjected to external electric fields which point in the same direction as the dipoles in the ground state, the critical temperature of the dielectric transition moves towards higher temperatures depending on the size of the electric field for both tilted and nontilted model. Similar is the effect of MAPs attached to the MT lattice at regular sites. The higher the ratio of attached MAPs to the total number of lattice sites, the higher is the degree of

alignment of dipoles in the direction they have in the ground state. Thus, both MAPs and external electric fields which point in the same direction as the dipoles in the ground state promote the existence of the ferroelectric phase in a MT.

When the external electric field is applied in the direction opposite to the direction of dipoles in the ground state of the MT A lattice, the assembly of nontilted dipoles switches into the state with opposite polarization (which becomes the ground state due to the external electric field) and then undergoes the transition into the paraelectric phase. In the assembly of tilted dipoles this effect is observed when the external electric field is sufficiently large since the state when all dipoles are nontilted has higher energy compared to the state when all dipoles are tilted.

The results above imply that MTs with the A lattice, rather than MTs with the B lattice, can exist in different dielectric states which can be linked to different biological functions of MTs. However, MTs with the A lattice haven't been experimentally observed yet. This may mean that they don't exist at all or that the MTs with the A lattice are present in the cell in a very small fraction or only in some sections of MTs. If the latter alternative is true then the occurrence of the A type arrangement of the tubulin dimers in the MTs may signal the onset of cellular events that result from the special dielectric properties of the MT A lattice which have been demonstrated here. On the other hand, MTs with the B lattice seem to exhibit frustration which is a feature that wasn't found in the A lattice. As was discussed earlier, this property may be very well suited for processing information.

References

[1] H. Athenstaedt, Pyroelectric and Piezoelectric Properties of Vertebrates, *Annals of the New York Academy of Sciences* **238**, p. 68-94 (1974)

[2] R. K. Pathria, *Statistical Mechanics* (Pergamon Press, 1993)

[3] G. Burns, *Solid State Physics* (Academis Press, 1985)

[4] H. E. Stanley, *Phase Transitions and Critical Phenomena* (Clarendon Press, Oxford, 1971)

[5] J. M. Yeomans, *Statistical Mechanics of Phase Transitions* (Clarendon Press, Oxford, 1992)

[6] J.-C. Tolédano, P. Tolédano, *The Landau Theory of Phase Transitions* (World Scientific, New Jersey, 1987)

[7] J. Callaway, *Quantum Theory of the Solid State* (Academic Press, 1991)

[8] K. Binder, D. W. Heermann, *Monte Carlo Simulation in Statistical Physics* (Springer-Verlag, Berlin, Heidelberg, 1988)

[9] S. Rasmussen, H. Karampurwala, R. Vaidyanath, K. S. Jensen and S. Hameroff, Computational Connectionism within Neurons: A Model of Cytoskeletal Automata Subserving Neural Networks, *Physica D* **42**, p. 428-449 (1990)

[10] S. N. Timasheff, R. Melki, M. F. Carlier, and D. Pantaloni, The geometric control of tubulin assemblies: cold depolymerization of microtubules into double rings, *Journal of Cell Biology* **107**, p. 243a (1988)

[11] H. Bolterauer, J. A. Tuszyński, M. V. Satarić, Fröhlich and Davydov regimes in the dynamics of dipolar oscillations of biological membranes, *Physical Review A* **44**, p. 1366-1380 (1991)

[12] M. Suzuki, Frustration, Metastability and Nonlinear Susceptibility in Spin Glasses, *Progress of Theoretical Physics*, Supplement No. 80, p. 195-202 (1984)

[13] K. Binder, A. P. Young, Spin glasses: Experimental facts, theoretical concepts, and open questions, *Reviews of Modern Physics* **58**, p. 801-976 (1988)

[14] G. Toulouse, Theory of the frustration effect in spin glasses: I, *Communications on Physics* **2**, p. 115-119 (1977)

[15] J. A. Tuszyński, B. Trpišová, D. Sept, M. V. Satarić, S. Hameroff, Microtubules: The cell's information processors?, proceedings of the Third International Conference on *Computational Physics: Nonlinear Dynamical Phenomena in Physical, Chemical and Biological Systems*, Lyngby, editors P. L. Christiansen and E. Mosekilde, IMACS, 1994, p. 144-149

[16] J. A. Tuszyński, B. Trpišová, D. Sept, M. V. Satarić, The Enigma of Microtubules and their Self-Organizing Behaviour in the Cytoskeleton, submitted in *Biosystems*

[17] P. M. Vassilev, R. T. Dronzine, M. P. Vassileva, and G. A. Georgiev, Parallel Arrays of Microtubules Formed in Electric and Magnetic Fields, *Bioscience Reports* **2**, p. 1025-1029 (1982)

[18] L. F. Jaffe and R. Nuccitelli, Electrical Controls of Development, *Annual Review of Biophysics and Bioengineering* **6**, p. 445-476 (1977)

[19] B. Alberts, D. Bray, J. Lewis, M. Raff, K. Roberts, and J. D. Watson, *Molecular Biology of the Cell*, 3-rd edition (Garland Publishing, New York and London, 1994)

3 Energy Transfer in Microtubules

As was discussed in the first chapter, the addition of a tubulin dimer at the assembling MT end is followed by the hydrolysis of exchangable GTP bound to the tubulin. Most of the standard free energy released in the hydrolysis is stored in the MT in the form of conformational changes of the tubulin molecules. A small portion of the free energy is freed and it is not known how is it utilized in the MT.

In this chapter it is argued that the free portion of the energy released in the GTP hydrolysis propagates along a MT in the form of solitary waves of tubulin dipole states coupled to tubulin conformational states. The existence of solitary waves in biological systems has been suggested before and it is briefly discussed in the next section.

3.1 Solitary Waves in Biological Systems

Many biological activities in the cell require input of energy. Examples of such activities include the synthesis of biomolecules from smaller precursors, the performance of mechanical work, for example, in muscle contraction, or transport of ions and biomolecules across membranes in the direction of increasing concentration [1]. The energy needed in these biological activities is supplied mainly from the hydrolysis of ATP but it could also be supplied by an electrical pulse or an electromagnetic wave [2].

However, little is known about the way the free energy is utilized by the biological structures or molecules. In other words, the mechanisms by means of which the free energy is transformed or transported in the biological systems haven't been elucidated yet. In 1973 A. Davydov showed that the transport of the chemical energy could be achieved by means of soliton-like excitations [3].

Solitons are a special class of solitary waves. Solitary waves are travelling localized waves which preserve their shape and velocity. They are particular solutions of quite a large number of partial differential equations that contain dispersive and nonlinear terms [4–6]. The solitary wave solutions of some of these equations preserve their shape and velocity also in collision with other solitary waves and they are called solitons. The most well-known solitary waves are depicted in Figure 3.1.

Solitary waves arise as a result of a delicate balance between dispersion and

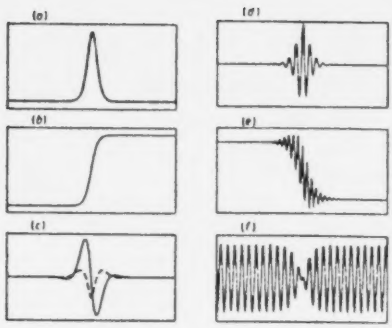

Figure 3.1: Possible types of solitary waves: (a) pulse, (b) kink, (c) breather, (d) symmetric envelope solitary wave, (e) asymmetric envelope solitary wave, (f) symmetric dark solitary wave. Asymmetric dark solitary wave and nonlinear periodic wave are not shown. (From Reference [7].)

nonlinearity [4]. Since a number of physical systems possess these properties, it is quite natural to expect that these characteristics will be also found in biological systems. Some indications that excitations of the solitary wave type may arise in biological systems are based on the dielectric properties of biological molecules. It is known that the structure of biomolecules is similar to the structure of ferroelectric crystals. Thus the models that describe these crystals can be adapted to describe biological systems. Such types of models are characterized by a nonlinear coupling between electric and elastic degrees of freedom which results in the formation of solitary waves. For example, in [8] by means of a two-dimensional smectic liquid crystal model it is shown that localized electric excitations can propagate along the cell membrane of a nerve axon. The model equations account for both electric and elastic properties of the studied system.

In another work [2], it is suggested how a model proposed for the ferroelectric phase transition in perovskites could explain some features of the behaviour of membranes and enzymes. A chain of positive and negative ions such as K^+, Na^+, Ca^{2+}, Ti^{4+}, H^-, O^{2-}, *etc.*, is described by the equations of motion that are nonlinear and contain both elastic and electric degrees of freedom. When this system of ions is in the ferroelectric phase the solutions of the equations of motion are kinks and pulses. Since biological systems contain similar types of ions as ferroelectrics, such localized excitations could exist in these systems.

An instructive example of how the nonlinear coupling between elastic and electric

degrees of freedom gives rise to localized travelling waves is the original model due to Davydov which describes the propagation of solitons along an α-helix . By means of this model Davydov attempted to explain the utilization of the energy of ATP hydrolysis in muscle contraction.

3.2 Davydov's Model of Propagation of Solitons along an α-Helix[1]

Davydov suggested that the energy of ATP hydrolysis can travel along one of the spines of an α-helix in the form of the amide-I bond vibrational energy which is about one half of the energy of the ATP hydrolysis. The amide-I bond is the double bond between a carbon atom and an oxygen atom which is located in each peptide group of the protein molecule (see section 1.6 in Chapter 1).

The α-helix is one of the possible conformational arrangements of a protein molecule. This arrangement arises by twisting the protein chain in a helical fashion and binding the hydrogen atom of the first peptide group to the oxygen atom of the fourth group, the hydrogen of the second group to the oxygen of the fifth group, *etc.*, (Figure 3.2). Such binding of the peptide groups results in the formation of three chains called spines which are parallel to the axis of the α-helix. The first spine consist of the first, fourth, seventh, ... peptide groups, the second spine is composed of of the second, fifth, eighth, ... peptide groups and the third spine contains the third, sixth, ninth, ... peptide groups.

Davydov based his suggestion, that the energy of the ATP hydrolysis can propagate along a spine of the α-helix in the form of a localized soliton excitation, on the following considerations. When the amide-I vibration in one of the peptide groups of one of the spines is excited, for example, by the energy of the ATP hydrolysis, the energy of this vibration will propagate through the dipole-dipole coupling between the neighbouring peptide groups in the spine. The energy of the electromagnetic dipole-dipole interaction between two amide-I bonds is given by the equation

$$J = \frac{1}{2\pi\epsilon}\frac{|\vec{d}|^2}{R^3}, \tag{3.1}$$

where $\vec{d}$ is the dipole moment of a peptide group bond and R is the separation between two neighbouring peptide groups.

[1]Based on [4].

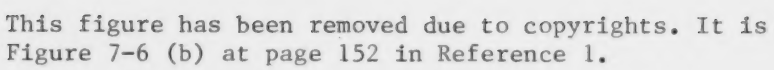

Figure 3.2: The α-helix conformation of a protein molecule. (From Reference [1].)

The coupling between the dipoles of the neighbouring peptide groups in the spine will cause the dispersion of the vibrational energy. However, stretching and contraction of the C=O bond in the vibration leads to the displacement of the peptide group from its equilibrium position resulting in deformation of the H-O bond between the neighbouring peptide groups in the spine. Since there are forces acting between the peptide groups (van der Waals forces, hydrogen bond, *etc.*), the displacement of one peptide group causes the displacement of the neighbouring peptide group and so on which results in the formation of a longitudinal sound wave.

Davydov pointed out that the electromagnetic wave and the sound wave are coupled since the vibrational energy of the amide-I bond changes due to the change of the distance R between two peptide bonds. Thus the longitudinal sound acts as a potential well that traps the electromagnetic energy of the amide-I vibration. The vibrational energy doesn't disperse but it travels localized together with the longitudinal displacement without loss of energy as a soliton.

The model originally developed by Davydov is a semi-classical model in which the amide-I vibration was treated quantum mechanically and the longitudinal sound

classically. In the continuum approximation this approach leads to a nonlinear Schrödinger equation.

In the special case of the travelling wave solutions the nonlinear Schrödinger equation obtained by Davydov for the system of peptide bonds in a spine of the α-helix has the following form

$$i\hbar\frac{\partial a(x,t)}{\partial t} + J\frac{\partial^2 a(x,t)}{\partial x^2} - E_0 a(x,t) + \kappa|a(x,t)|^2 a(x,t) = 0\,. \tag{3.2}$$

Equation (3.2) is the equation for the probability amplitude of the exciton $a(x,t)$. The energy constant E_0 is given by the formula

$$E_0 = E - 2J + \frac{1}{2}\int_{-\infty}^{\infty}[m(\frac{\partial u(x,t)}{\partial t})^2 + K(\frac{\partial u(x,t)}{\partial x})^2]dx\,, \tag{3.3}$$

where E is the energy of amide-I vibration, m is the mass of a peptide group, K is the strength of the spring that represents the H-O bond between the neighbouring peptide groups and $u(x,t) = u(x - vt)$ is the displacement at time t and at a point x along the chain of peptide groups. The nonlinearity constant κ is given by the expression

$$\kappa = \frac{4\chi^2}{K(1-s^2)}\,, \tag{3.4}$$

where $\chi = dE/dR$ is the parameter that characterizes the coupling between the amide-I vibration and the longitudinal sound wave, $s = v/v_s < 1$, where v is the velocity of the soliton and $v_s = R(K/m)^{1/2}$ is the velocity of sound.

The stationary solution of the equation (3.2) is obtained when $s = 0$ and it has the following form

$$a(x) = \frac{\chi}{(2KJ)^{1/2}}\,\mathrm{sech}[\frac{\chi^2}{KJ}(x - x_0)]\exp[-\frac{i}{\hbar}(E_0 - \frac{\chi^2}{K^2 J})t]\,. \tag{3.5}$$

Equation (3.5) represents a pulse soliton centered at point x_0. The energy of the soliton is

$$E_{sol} = E - 2J - \frac{\chi^4}{3K^2 J}\,. \tag{3.6}$$

If the chain of peptide groups were absolutely rigid, that means, $K = \infty$, then $\kappa = 0$ and equation (3.2) would contain only linear terms. The solution of this linear equation is a plane wave which means that the energy of the C=O vibration would become uniformly distributed along the whole chain, *i.e.*, it would no longer be localized. The energy of the plane wave is equal to $E_{plane} = E - 2J$ which is larger than the energy of the soliton. This implies that it is more favourable for

the chain of peptide groups along the α-helix to localize its energy, *i.e.*, to take into account the nonlinear coupling between the amide-I vibration and the displacement of a peptide group.

Some indications that C=O vibrational energy may be localized on an α-helix comes from the experiments with the crystalline polymer acetanilide or ACN ($(CH_3C\text{-}ONHC_6H_5)_x$). The molecule of ACN is arranged in a hydrogen-bonded chain that is similar to the polypeptide chains in the proteins with α helical structure. The ACN spectrum contains an anomalous line which is very close to that corresponding to the amide-I vibration in the spectra of proteins. Theoretical calculations show that this line may be due to the soliton-like excitation described above, however, other explanations of its origin can not be excluded [9]. The possibility of the existence of solitons on an α-helix is also supported by the estimated values of the coupling parameter χ in real proteins. According to these estimates the coupling between the C=O vibration and elastic displacement in these molecules may be sufficiently strong for the solitons to arise.

3.3 Kink-Like Solitary Waves in Microtubules

By means of the Monte Carlo simulations performed with a lattice of dipoles in the previous chapter it was shown that depending on the conditions in the cell a MT can be in ferroelectric or paraelectric phase. It is suggested here that in the process of the MT assembly the low-temperature ferroelectric phase can support propagation of the free portion of the energy released in the GTP hydrolysis along a MT in the form of kink-like solitary waves of tubulin dipole states coupled to its conformational states.

In the ferroelectric phase, all dipole moments on the tubulin dimers in the MT are oriented in the same direction. It will be assumed here that this direction corresponds either to the α or to the β state of the tubulin dimer. Further, let us assume that when a free tubulin dimer attaches itself to the MT its dipole moment flips into the opposite state. The work needed for the flip is done using the free portion of the energy released in the GTP hydrolysis. The amount of this energy can be comparable to $0.9\,\text{kcal/mol} = 6.25 \times 10^{-21}\,\text{J}$ (see section 1.4.3 in Chapter 1). Due to the dipole-dipole coupling flipping one dipole induces flipping of one or more neighbouring dipoles and so on along the most energetically favourable path.

In this way the free energy released in the GTP hydrolysis can propagate in the MT wall.

To illustrate the above described process, a situation can be assumed when at the assembling end of a MT with the A lattice all dipoles are in the same state, say α. A free tubulin dimer that also happens to be in the α state is attached to one of the protofilaments of the assembling end. Using the values of the interaction constants calculated in Chapter 2 for the case when the dipoles in the β state are nontilted, the energy of the just attached dimer is $E_{initial} = -4.81 \times 10^{-21}$ J. After the flip of the dipole into the β state its energy would be $E_{final} = 3.04 \times 10^{-21}$ J. The difference of the two energies is $\Delta E = 7.85 \times 10^{-21}$ J and this is the energy needed to flip the dipole from the α to the β state. ΔE is indeed comparable with 6.25×10^{-21} J which suggests that the propagation of the free portion of the energy of the GTP hydrolysis in the way described above is quite feasible. It can be noted that the energy needed to flip the dipole of the just attached dimer depends on the configuration of dimers at the assembling end.

However, just as in Davydov's model the dipole-dipole interaction would lead to the dispersion of the portion of the energy freed in the GTP hydrolysis along a MT. But, if the interaction between two neighbouring dipoles is nonlinearly coupled to the elastic distortion along the chain of dimers, the energy may become localized and it can travel along a MT as a solitary wave. If all dipoles in the MT are initially in the same state, then this wave represents a domain wall between two subchains of dipoles in each of which all dipoles are in the α and in the β state, respectively. Hence, the possible excitations of tubulin dipole states in MTs can be described as kink-like solitary waves.

In the rest of this chapter, a simplified situation is assumed in which the lateral interactions between the tubulin dimers in a MT are neglected. Due to that the free energy released in the GTP hydrolysis propagates along MT protofilaments. In the following section a model is studied which was originally proposed in [10]. This model is based on the assumption that the dipole state (polarization) of the tubulin dimer and the distortion (displacement) of the dimer are linearly proportional, for example, due to a strong coupling between them. In such a case, the dipole dynamics in the chain of tubulin dimers can be described by only one equation, *e.g.*, for the distortion and the polarization follows exactly the distortion of the dimer.

In the last section, two other models of propagation of kinks in ferroelectric systems are described. In these models polarization is nonlinearly coupled to displace-

ment or stress. The equations of motions are represented by two coupled equations.

3.4 Model with Strong Coupling between Polarization and Displacement

3.4.1 Equation of Motion

The Hamiltonian associated with the dynamics of a dipole placed at site n in a MT protofilament with N tubulin dimers can be represented by the following equation [10]

$$H = \sum_{n=1}^{N} [\frac{1}{2} M (\frac{du_n}{dt})^2 + \frac{1}{2} K (u_{n+1} - u_n)^2 - (\frac{\alpha_2}{2} u_n^2 - \frac{\alpha_4}{4} u_n^4) - c u_n]. \tag{3.7}$$

In (3.7) the variable u_n represents the projection on the protofilament axis of the distortion of the dimer which is in the β state with respect to the α state [16], $\frac{1}{2} M (du_n/dt)^2$ is the kinetic energy of the tubulin molecule of mass M, $\frac{1}{2} K (u_{n+1} - u_n)^2$ represents the elastic energy that originates from the restoring elastic forces characterized by a constant K that act between each two dimers. The quartic double-well potential energy $V(u_n) = -\frac{\alpha_2}{2} u_n^2 + \frac{\alpha_4}{4} u_n^4$ approximates the average effect of the surrounding dipoles on the dipole at site n. $V(u_n)$ can be viewed as the Landau free energy expansion where u_n corresponds to the order parameter and the coefficients α_2 and α_4 are characteristics of the physical system. Assuming that the phase transition from a ferroelectric to a paraelectric phase in a MT is a second order phase transition, α_4 is a positive constant and $\alpha_2 = a_2 (T_c - T)$, where $a_2 > 0$ (see section 2.1 in Chapter 2).

A plot of the potential energy $V(u_n)$ when $a_2 > 0$ and $T < T_c$ is shown in Figure 3.3a. The potential energy $V(u_n)$ has two symmetric local minima such that $V(\pm(\alpha_2/\alpha_4)^{1/2}) = -\alpha_2^2/(4\alpha_4)$ and a maximum at $V(0) = 0$. The two symmetric local minima correspond to the two states of the tubulin dimer α and β. The approximation of the effect of the environment by the double-well quartic potential assumes that all dipoles are in their equilibrium positions and they can be either in the α or in the β state.

The last term, $-cu_n$, in (3.7) accounts for the effect of the electric fields to which the chain of dipoles can be exposed. The total electric field E at a site n along a MT protofilament produces potential energy $V_E = -cu_n = -q_{eff}Eu_n$, where q_{eff} is the effective charge of the n'th tubulin dimer. The addition of V_E to the quartic double-well potential energy $V(u_n)$ results in an asymmetric function with two local minima and one local maximum that is plotted in Figure 3.3b. To one of the minima corresponds a lower value of the potential energy than to the other. This means that the two dipole states of the system are not equivalent but the state that is oriented in the same direction as the electric field is energetically favoured.

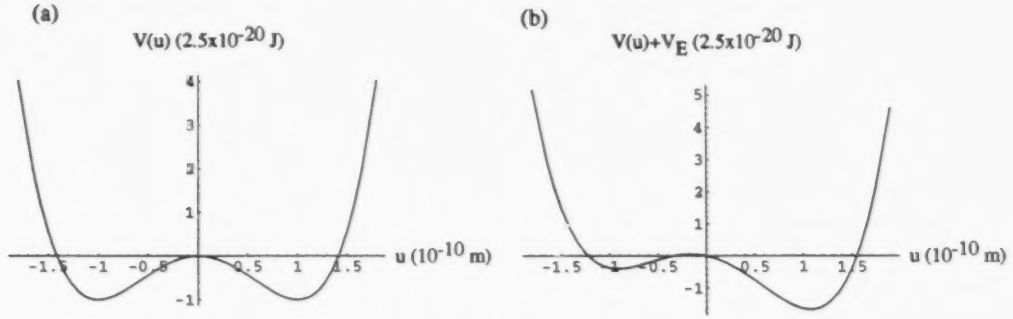

Figure 3.3: The local potential energy at a site n in a MT protofilament when the MT is in the ferroelectric phase. (a) $V(u_n)$, (b) $V(u_n) + V_E$.

In order to derive a realistic equation of motion the effect of the medium surrounding the MT has to be taken into account. As has been mentioned several times, cellular MTs are embedded in cytosol which is a water solution of various ions. Ions and polar water molecules can affect the electrostatic interaction between the dipoles on the dimers and they can also act as a viscous medium and damp the motion of the dimers [10]. The damping effect can be represented by a viscous force

$$F_v = -\gamma \frac{\partial u_n}{\partial t}, \tag{3.8}$$

where γ is the damping coefficient.

If the displacements of the neighbouring dimers are assumed to be small and gradual, the equation of motion can be derived using the continuum approximation [10]. The discrete variable $u_n(t)$ is replaced by the continuum variable $u(x,t)$ and $u_{n+1}(t)$ is expanded in a Taylor series about the point x, *i.e.*,

$$u_{n+1}(t) \rightarrow u(x,t) + R_0 \frac{\partial u(x,t)}{\partial x} + \frac{1}{2} R_0^2 \frac{\partial^2 u(x,t)}{\partial x^2} + ... \tag{3.9}$$

In (3.9), R_0 is the equilibrium distance between two neighbouring tubulin dimers. When only the first two terms in (3.9) are considered, the equation of motion that corresponds to the Hamiltonian (3.7) and the dissipative force (3.8) is the following

$$M\frac{\partial^2 u(x,t)}{\partial t^2} - KR_0^2\frac{\partial^2 u(x,t)}{\partial x^2} - \alpha_2 u(x,t) + \alpha_4 u(x,t)^3 + \gamma\frac{\partial u(x,t)}{\partial t} - q_{eff}E(x) = 0. \tag{3.10}$$

The values of the constants in (3.10) can be determined as follows [10]: The mass of the tubulin dimer was calculated as $M = 2 \times 55000 \times 1.66 \times 10^{-27}\,\mathrm{kg} = 1.83 \times 10^{-22}\,\mathrm{kg}$. The constants K and R_0 are related to the velocity of longitudinal sound waves through the formula $KR_0^2 = Mv_0^2$, where v_0 is the sound velocity. Since no value for the velocity of sound in a MT has been known to the author of this work so far, the value found for DNA, $v_0 = 1700\,\mathrm{ms}^{-1}$ [11], has been used here. The coefficients $\alpha_2 = a_2(T_c - T)$ and α_4 for a MT are also not known. However, inorganic crystals exist in which ferrodistortive domain walls can be formed. For example, for the crystal $Pb_5Ge_3O_{11}$ below the critical temperature, $\alpha_4 = 1.6 \times 10^{24}\,\mathrm{Jm}^{-4}$ and $a_2 = 10\,\mathrm{Jm}^{-2}\mathrm{K}^{-1}$. If the MT is in the ferroelectric phase then the critical temperature T_c can be approximately taken as $350\,K$ and T is body temperature 310 K. This gives for the coefficient α_2

$$\alpha_2 = 10 \times (350 - 310) = 400\,\mathrm{Jm}^{-2}. \tag{3.11}$$

To estimate the damping coefficient γ, the tubulin dimer can be considered a sphere of radius $R = 4 \times 10^{-9}\,\mathrm{m}$ and mass M that is moving in a fluid of viscosity η. The drag force exerted by the fluid on the sphere is

$$F_v = -6\pi R\eta\frac{du}{dt} = -\gamma\frac{du}{dt}. \tag{3.12}$$

Assuming that a MT is mainly surrounded by water molecules, η can be taken as the viscosity of water. At body temperature, $\eta = \eta_{water} = 6.9 \times 10^{-4}\,\mathrm{kgm}^{-1}\mathrm{s}^{-1}$. Consequently, $\gamma = 6\pi R\eta = 5.2 \times 10^{-11}\,\mathrm{kgs}^{-1}$.

3.4.2 Electric Fields in Microtubules

The total electric field E on each site in a MT is due to the external electric fields of other MTs and cell membranes and the electric field of the MT itself. The intrinsic electric field of a MT is caused by the distribution of positive and negative

charges and ions within the tubulin molecules which produce electronegative fields on the MT surface.

An indication of the presence of the electronegative fields in MTs is the existence of the so-called "clear zone" [12]. This is a space in the shape of a tube that surrounds a MT and is 5-10 nm wide. According to experiments organelles, the cytoplasmic ground substance or any other material normally seen throughout the cell are very seldom present in this zone.

Further indications about the electromagnetic nature of MTs are *in vitro* experiments in which a pool of assembling tubulin was subjected to electric and magnetic fields. In [13] electric fields of the order $1\,\mathrm{Vm}^{-1}$ and a magnetic field of intensity $0.02\,\mathrm{T}$ were used. After 10 minutes the assembled MTs ordered along the direction of the field. Applying higher electric fields resulted in larger amounts of assembled MT polymer.

Ordering of MTs is observed in many cellular structures. Regularly aligned MTs exist in axons, cilia, and mitotic spindles (see Chapter 1). These and other cellular elements that contain parallel arrays of MTs perform important functions in the cell. Control of these functions may be also related to the electromagnetic fields in MTs and in the cell. According to [14] electric fields inside the cell are in the range $2 - 50\,\mathrm{Vm}^{-1}$.

The exact distribution of charges in the tubulin molecules bound in a MT is not known. In the calculations presented here an approximation has been chosen according to which the charge distribution was represented by the net point charge $+q_{eff}$ at one end and the net point charge $-q_{eff}$ at the other end of each MT protofilament. It will be assumed that the protofilament on which the dipoles change their states due to the travelling free portion of the energy of the GTP hydrolysis is subjected to the electric field produced by the remaining protofilaments. In a MT composed of 13 protofilaments, the number of remaining protofilaments is 12.

The longitudinal component of the electric field produced by 12 protofilaments at a point x along the axis of the 13-th protofilament can be calculated using the expression

$$E(x) = \sum_{i=1}^{12} \frac{q_{eff}}{4\pi\epsilon_0\epsilon_r}\{\frac{L/2+x}{[d_i^2+(L/2+x)^2]^{3/2}} + \frac{L/2-x}{[d_i^2+(L/2-x)^2]^{3/2}}\}\,. \qquad (3.13)$$

In (3.13) the sum over i adds up the electric fields from each of the 12 protofilaments surrounding the 13-th protofilament, the permittivity of vacuum $\epsilon_0 = 8.85 \times 10^{-12}\,\mathrm{Fm}^{-1}$, ϵ_r is the relative permittivity, L is the length of the MT and d_i is the

distance between the axes of the i-th protofilament and the 13-th protofilament (Figure 3.4). d_i can be found from the formula

$$d_i = 2R \sin \frac{i\alpha}{2}, \tag{3.14}$$

where $R = 10.4 \times 10^{-9}\,\mathrm{m}$ is the distance of the charges from the center of the MT and $\alpha = 2\pi/13$ is the angle subtended by a tubulin dimer. Each protofilament is assumed to have a circular cross-section of radius $r = 2.5 \times 10^{-9}\,\mathrm{m}$. The charges are placed in the centers of the cross-section (on the axes of the protofilaments).

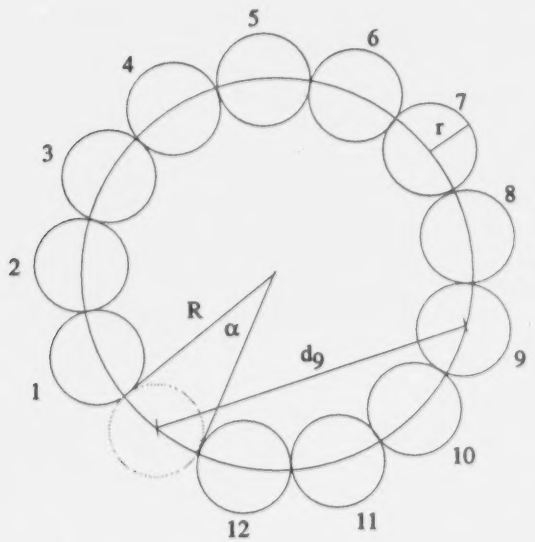

Figure 3.4: The cross-section of a MT with 13 protofilaments. The 13-th protofilament is subjected to the electric field of the surrounding 12 protofilaments.

The electric field calculated according to formula (3.13) for a MT with length $10^{-6}\,\mathrm{m}$, which corresponds to protofilaments composed of 125 dimers, is plotted in Figure 3.5a. The field has the lowest value in the center of the MT and increases towards the ends. The charge q_{eff} was chosen to be $1.602 \times 10^{-19}\,\mathrm{C}$ and $\epsilon_r = 1$. This gives $E(0) = 2.3 \times 10^4\,\mathrm{Vm}^{-1}$ and at the maxima $E_{max} = 2.62 \times 10^6\,\mathrm{Vm}^{-1}$. These values are considerably higher than $2 - 50\,\mathrm{Vm}^{-1}$. By choosing a different value of ϵ_r the values of $E(x)$ can be decreased. As in previous chapter, ϵ_r can be taken as the relative permittivity of free water whose value at body temperature ranges from about 4 to about 70. Setting $\epsilon_r = 10$ would decrease $E(x)$ by one order of

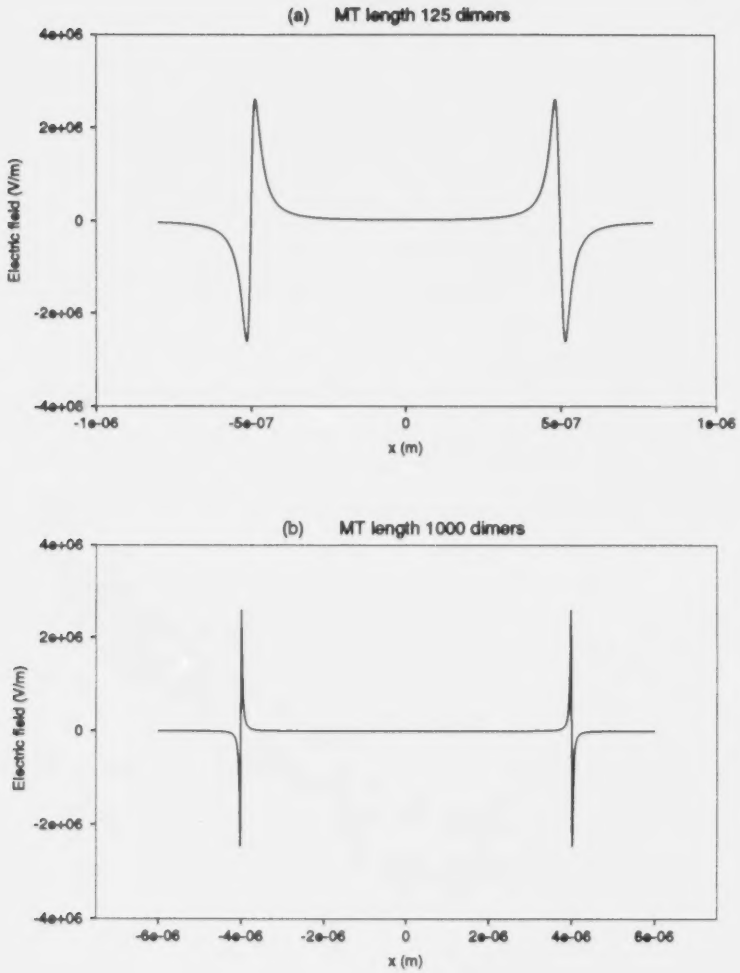

Figure 3.5: The electric field generated by 12 protofilaments on the axis of the 13-th protofilament of a MT whose protofilaments consist of (a) 125 and (b) 1000 dimers.

magnitude. Due to screening caused by other charges within the tubulin molecule, the value of the electric field in the MT can be also substantially lowered.

Furthermore, it can be noticed that the electric field is different for MTs of different lengths. In Figure 3.5b is plotted the electric field for a MT in which the protofilaments consist of 1000 dimers, *i.e.*, $L = 8\times10^{-6}\,\mathrm{m}$. For $q_{eff} = 1.602\times10^{-19}\,\mathrm{C}$ and $\epsilon_r = 1$, in the center of the MT $E(0) = 360\,\mathrm{Vm}^{-1}$ and at the maxima $E_{max} = 2.62 \times 10^6\,\mathrm{Vm}^{-1}$. This implies that longer MTs produce lower fields which is the natural feature of the charge distribution (3.13).

3.4.3 Analytical Solution

For a constant electric field E, equation (3.10) can be solved analytically. In order to find a solution in the form of a wave that travels at a constant velocity v [10], a moving coordinate $\xi = \xi(x - vt)$ can be introduced as follows

$$\xi = [\frac{|\alpha_2|}{M(v_0^2 - v^2)}]^{1/2}(x - vt)\,. \tag{3.15}$$

The partial differential equation (3.10) then reduces to an ordinary differential equation

$$\frac{d^2\psi}{d\xi^2} + \rho\frac{d\psi}{d\xi} - \psi^3 + \psi + \sigma = 0\,, \tag{3.16}$$

where

$$\rho = \frac{v\gamma}{[M\alpha_2(v_0^2 - v^2)]^{1/2}}\,, \qquad \sigma = \frac{qE}{\alpha_2}(\frac{\alpha_4}{\alpha_2})^{1/2} \tag{3.17}$$

and

$$\psi(\xi) = \frac{u(\xi)}{u_0}\,, \qquad u_0 = (\frac{\alpha_2}{\alpha_4})^{1/2}\,. \tag{3.18}$$

The travelling kink wave solution of (3.16) is listed in [15]. The solution that corresponds to the kink wave moving with the velocity $v > 0$ is

$$\psi(\xi) = \psi_2 + \frac{\psi_1 - \psi_2}{1 + e^{\xi(\psi_1 - \psi_2)/\sqrt{2}}}\,, \tag{3.19}$$

where ψ_1 and ψ_2 satisfy the cubic equation

$$(\psi - \psi_1)(\psi - \psi_2)(\psi - \psi_3) = \psi^3 - \psi - \sigma\,. \tag{3.20}$$

Equation (3.19) is a solution of (3.16) for $v > 0$ when

$$\rho = \frac{\psi_1 + \psi_2 - 2\psi_3}{\sqrt{2}}\,. \tag{3.21}$$

Equating the coefficients at the second power of ψ in (3.20) gives another equality for $\psi_1,\ \psi_2,\ \psi_3$

$$\psi_1 + \psi_2 + \psi_3 = 0\,. \tag{3.22}$$

$\psi_1,\ \psi_2,\ \psi_3$ can be found as the roots of the cubic polynomial $\psi^3 - \psi - \sigma$. A straightforward algebraic calculation gives the following expressions for $\psi_1,\ \psi_2,\ \psi_3$

$$\psi_1 = \frac{2}{\sqrt{3}}\cos\{\frac{1}{3}\arccos[\frac{3qE}{2\alpha_2}(\frac{3\alpha_4}{\alpha_2})^{1/2}]\}\,, \tag{3.23}$$

$$\psi_2 = \frac{2}{\sqrt{3}}\cos\{\frac{2\pi}{3} + \frac{1}{3}\arccos[\frac{3qE}{2\alpha_2}(\frac{3\alpha_4}{\alpha_2})^{1/2}]\}\,, \tag{3.24}$$

$$\psi_3 = \frac{2}{\sqrt{3}}\cos\{\frac{4\pi}{3} + \frac{1}{3}\arccos[\frac{3qE}{2\alpha_2}(\frac{3\alpha_4}{\alpha_2})^{1/2}]\}\,. \tag{3.25}$$

The argument $\delta = 3qE/(2\alpha_2) \times (3\alpha_4/\alpha_2)^{1/2}$ in the above three equations is small for the values of the electric field $E(x)$ calculated in the previous section. For the maximum value of the electric field $E_{max} = 2.62 \times 10^6\,\mathrm{Vm}^{-1}$, $\delta = 0.000115$. Hence $\psi_1 - \psi_2$ is positive and the kink (3.19) is a domain wall between two states $\psi = \psi_1$ when $\xi \to -\infty$ and $\psi = \psi_2$ when $\xi \to \infty$, travelling to the right as illustrated in Figure 3.6. This solution is consistent with the potential $V(u)$ plotted in Figure 3.3b. The state of the variable $u = u_0\psi$ changes from a negative to a positive value as the domain wall moves towards the right boundary. Because the parameter δ is small for the electric fields considered here, ψ_1 and ψ_2 can be safely expanded with respect to δ around 0 which gives the following approximate expressions

$$\psi_1 \simeq 1 + \frac{\delta}{3^{3/2}} + O(\delta^2)\,, \tag{3.26}$$

and

$$\psi_2 \simeq -1 + \frac{\delta}{3^{3/2}} + O(\delta^2)\,. \tag{3.27}$$

Using the two expansions in equation (3.23) and (3.24) and substituting the result into (3.19) yields for the continuous displacement $u(\xi)$

$$u(\xi) = (\frac{\alpha_2}{\alpha_4})^{1/2}[-1 + \frac{\delta}{3^{3/2}} + \frac{2}{1 + \mathrm{e}^{\sqrt{2}\xi}}]\,. \tag{3.28}$$

This approximate solution was used in the numerical simulations below.

From equations (3.21) and (3.22) follows that $\rho = -3\psi_3/\sqrt{2}$. After substituting for ρ and ψ_3 from (3.17) and (3.25), the equation for the velocity of the kink wave v is obtained

$$\frac{v\gamma}{[\alpha_2 M(v_0^2 - v^2)]^{1/2}} = -\sqrt{6}cos\{\frac{4\pi}{3} + \frac{1}{3}\arccos[\frac{3qE}{2\alpha_2}(\frac{3\alpha_4}{\alpha_2})^{1/2}]\}\,. \tag{3.29}$$

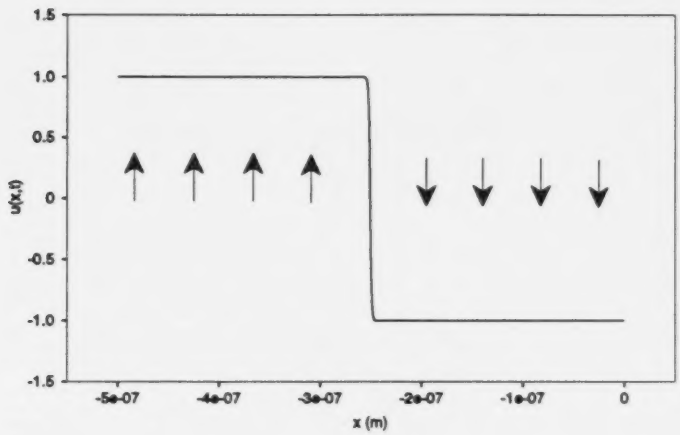

Figure 3.6: A domain wall between two subchains of a MT protofilament in which the tubulin dimers are in two different states.

The equation above is a quadratic equation for velocity v. The velocity depends on the values of the constants α_2, α_4, γ, M, q and on the value of the electric field E. If the electric field is a function of the distance from the MT ends, then v changes as a function of E along the MT.

Equation (3.29) can be expanded if it is assumed that the velocity of the kink wave travelling along a MT is very small compared to the speed of sound, *i.e.*, $v \ll v_0$. Solving the quadratic equation (3.29) for the values of the parameters α_2, α_4, γ, M and q that were given in section 3.2.2 and maximum electric field along the MT $E_{max} = 2.62 \times 10^6\,\mathrm{Vm}^{-1}$ gives the value of the velocity $v = 1.24\,\mathrm{ms}^{-1}$. This number is much smaller than the velocity of phonons $v_0 = 1700\,\mathrm{ms}^{-1}$. Thus in the numerator of the right hand side of equation (3.29), v^2 can be neglected and ψ_3 can be expanded with respect to the small argument δ as follows

$$\psi_3 \simeq -\frac{\delta}{3^{3/2}} + O(\delta^2)\,. \tag{3.30}$$

The resulting approximate formula for v is

$$v = \frac{3v_0}{\gamma\alpha_2}\left(\frac{M\alpha_4}{2}\right)^{1/2} qE = \frac{3v_0}{\gamma a_2(T_c - T)}\left(\frac{M\alpha_4}{2}\right)^{1/2} qE\,. \tag{3.31}$$

The approximate expression (3.31) shows in an instructive way how the velocity of the kink depends on the parameters of the modelled system and on the critical

temperature T_c. Since the MT is assumed to be in the ferroelectric phase, $a_2 > 0$ and $T = T_{body} < T_c$. Then equation (3.31) implies that if the conditions in the cell cause T_c to increase, the kinks moving along the MTs will have a greater velocity. Decreasing T_c will cause the kink domain walls to move slower. The values of the parameters a_2, α_4, γ, q and ϵ_r used here were approximated or estimated but they are not known precisely for a MT. More precise knowledge of these parameters would help to determine the value of the velocities of the kink waves more accurately.

The velocity v depends linearly on the electric field E. This means that larger electric fields on MTs will generate kinks moving at larger velocities and *vice versa*. The magnitude of the intrinsic electric field of a MT can be altered if the MT is subjected to an external electric field generated, for example, by a membrane or by other MTs [16]. If the external electric field is oriented in the same direction as the intrinsic electric field of the MT, this will result in a faster propagation of kinks. If the external and intrinsic electric fields are oriented in the opposite directions, the propagation of kinks will be slowed down or reoriented when the magnitude of the external field is larger than the magnitude of the intrinsic field of the MT. In the previous chapter it was shown that sufficiently strong external fields can alter the direction in which the dipoles are aligned when the MT is in the ferroelectric phase. Then the external field and the intrinsic MT field would be oriented in the same direction. This would change the direction of propagation and increase the velocity of the kink waves. When the total electric field to which the dipoles on the tubulin dimers are subjected is zero the kinks won't propagate at all. According to the approximation of the charge distribution in a MT chosen here the magnitude of the intrinsic field of a MT also depends on its length. This means that MTs with different sizes may support kink waves travelling at different velocities.

The kinks moving along MTs represent quanta of energy that can also be viewed alternatively as bits of information moving on an information string [16]. This information can signal other events taking place in MTs, for example, attachment of MAPs, detachment of a tubulin dimer from the MT in the process of disassembly, coordinated behaviour of cilia and flagella, *etc.*, (see Chapter 4). Thus the mechanisms which control the propagation of information along MTs in the form of the kink-like waves of the tubulin dipole states can govern the various MT functions in the cell.

3.4.4 Numerical Solution

For the electric field (3.13) that is a function of the position along the MT axis, equation (3.10) had to be solved numerically. As an initial condition the approximate solution (3.28) was chosen for the value of E set equal to $E(x_0)$, where x_0 is the point at which the kink is centered at $t = 0$.

Figure 3.7a shows a numerically obtained kink wave travelling in a section of a MT protofilament along which the electric field decreases. The length of the protofilament is $L = 10^{-6}\,\mathrm{m}$ (125 dimers). The kink starts moving towards the right end of the MT at $x_0 = -4 \times 10^{-7}\,\mathrm{m}$ where $E(x_0) = 274000\,\mathrm{Vm}^{-1}$ and the corresponding velocity is $v_0 = 0.13\,\mathrm{ms}^{-1}$. The time interval between two successive plotted waves is $\Delta t = 3.38 \times 10^{-7}\,\mathrm{s}$. The total distance $D = 1.41 \times 10^{-7}\,\mathrm{m}$, which corresponds to about 16.5 dimers, was travelled by the kink in time $T = 2.7 \times 10^{-6}\,\mathrm{s}$.

According to the plots with the decreasing value of the electric field along the MT the motion of the kink is slowed down. The last plotted wave moves at a velocity of about $v = \Delta d_{end}/\Delta t = 0.026\,\mathrm{ms}^{-1}$ where $\Delta d_{end} = 8.79 \times 10^{-9}\,\mathrm{m}$ is a distance over which the kink moves in time Δt at the end of the simulation. In the center of the interval Δd_{end} the value of the electric field $E = 55900\,\mathrm{Vm}^{-1}$. According to (3.31), the corresponding velocity is $v(E) = 0.027\,\mathrm{ms}^{-1}$. This shows that the analytical and numerical solutions are in a good agreement.

Figure 3.7b shows the travelling kink wave if the electric field is assumed to have the same value $E = 274000\,\mathrm{Vm}^{-1}$ over the entire length of the MT. The numerical calculation reproduces the analytical solution which is a kink moving with constant velocity $v = 0.13\,\mathrm{ms}^{-1}$. In time $T = 2.7 \times 10^{-6}\,\mathrm{s}$ the kink travels over the distance $D = 4 \times 10^{-7}\,\mathrm{m}$ which corresponds to 44 dimers. This is almost three times further than in the previous case.

Figure 3.8 depicts the situation when the kink wave moves in a section of the protofilament along which the electric field increases. The kink starts moving at $x_0 = 2.5 \times 10^{-7}\,\mathrm{ms}^{-1}$, where $E(x_0) = 50700\,\mathrm{Vm}^{-1}$ and $v_0 = 0.0241\,\mathrm{ms}^{-1}$ towards the right boundary. The time interval between two successive waves is the same as before, $\Delta t = 3.38 \times 10^{-7}\,\mathrm{s}$. Corresponding to the increasing electric field, the velocity of the kink increases as well and at the end of the simulation $v = 0.121\,\mathrm{ms}^{-1}$. The velocity calculated according to (3.31) for the last plotted wave is about $v = 0.12\,\mathrm{ms}^{-1}$. Over the total time of simulation $T = 3.38 \times 10^{-6}\,\mathrm{s}$ the kink travelled the total distance $D = 1.45 \times 10^{-7}\,\mathrm{m}$, which corresponds to 18 tubulin dimers. The

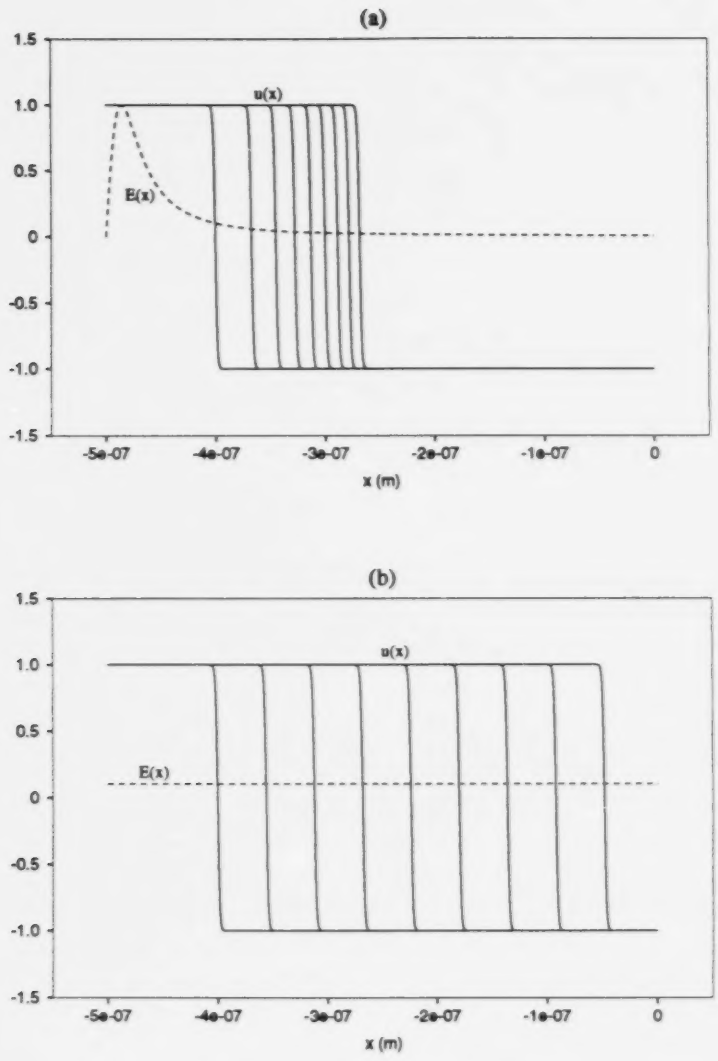

Figure 3.7: A kink wave moving on a section of a MT which is 125 dimers long. The time interval between two successive waves is $\Delta t = 3.38 \times 10^{-7}$ s. Figure (a) shows the time evolution of a kink wave exposed to a decreasing electric field of the MT. Figure (b) shows the kink moving in a constant electric field of value equal to that at the beginning of the kink motion in figure (a). The electric field is in units of $2.62 \times 10^{6}\,\mathrm{Vm}^{-1}$ and the displacement $u(x)$ is in units of 1.58×10^{-11} m.

dotted line shows how far the kink would travel if it moved at the constant velocity $0.0241\,\mathrm{ms}^{-1}$ over the same total time. The total distance travelled in the constant field is $D = 8.15 \times 10^{-8}\,\mathrm{m}$ which corresponds to 10 dimers.

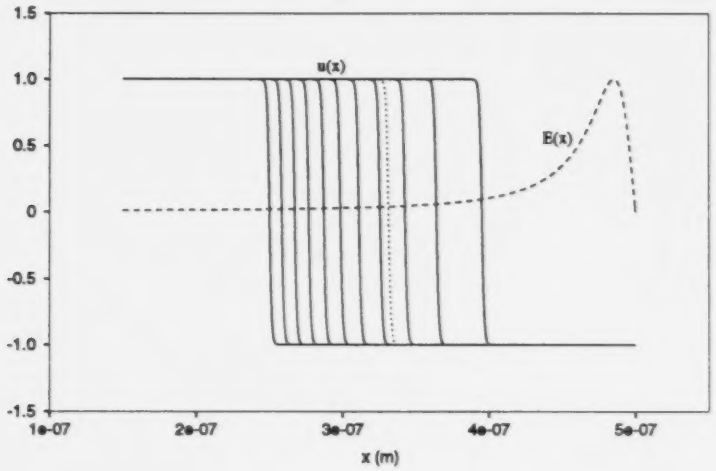

Figure 3.8: A kink wave moving on the background of an increasing electric field along a MT which is 125 dimers long. The time interval between two successive waves is $\Delta t = 3.38 \times 10^{-7}\,\mathrm{s}$. As the electric field increases the kink moves faster. The dashed line shows how far the kink would travel if the electric field was constant and equal to the value at the starting point. The units of the plots are the same as in Figure 3.7.

It should be pointed out that according to the analytical solution for a constant electric field E given by equations (3.19), (3.23), (3.24), (3.25), the form of the kink changes every time the value of E changes. However, the values of E along a MT are such that the approximate solution (3.28) is valid with good accuracy and the change in the form of the wave is negligible.

3.4.5 Numerical Solution in the Presence of an Impurity

In this section the collision of a travelling kink wave with a defect in the MT is studied. The defect can be an attached MAP or a structural discontinuity [extra

seams, protofilaments or even point dislocations (extra tubulin or missing tubulin) have all been seen in experiments]. The defect is represented by a localized potential energy of the Gaussian form

$$V(x) = V_0 \sum_{n=1}^{N} e^{-\beta\{x-[x_d+(n-1)a_n]\}^2} . \tag{3.32}$$

In (3.32), N is the number of defects along the MT protofilament, x_d is the location of the first defect, a_n is the distance between two impurities, β is a constant that determines the steepness of the Gaussian bump or well and V_0 is the amplitude of the potential energy.

The derivative of the potential energy (3.32) is the additional local force $-\frac{dV(x)}{dx}$ which acts at the travelling kink. The effect of this force is included on the left hand side of the equation of motion (3.10) as a term

$$\frac{dV(x)}{dx} = -2V_0\beta \sum_{n=1}^{N} \{x - [x_d + (n-1)a_n]\} e^{-\beta\{x-[x_d+(n-1)a_n]\}^2} . \tag{3.33}$$

The amplitude V_0 is positive for a bump and negative for a well. An example of local potential energies and the corresponding local forces that could be due to the impurities placed at regular distances on a section of a MT protofilament are plotted in Figure 3.9. The parameters of the local forces are $a_n = const. = 8 \times 10^{-8}\,\mathrm{m}$ (10 tubulin dimers), $V_0 = 10^{-21}\,\mathrm{J}$, $\beta = 10^{17}\,\mathrm{m}^{-2}$ and $x_d = -1.2 \times 10^{-7}\,\mathrm{m}$.

Hence, a kink moving down a MT protofilament is exposed to a smoothly changing electric field $E(x)$ and local fields such as those shown in Figure 3.9. It can be expected that the effect of the localized potential energy will be similar to that caused by the electric field. Where the force due to the local defect increases, the velocity of the kink will increase as well, and *vice versa*.

Figure 3.10a shows the motion of a kink wave in a section of the MT protofilament along which the background electric field $E(x)$ from the surrounding 12 protofilaments decreases and at time $t = 0\,\mathrm{s}$, a localized potential energy $V(x)$ centered at $x_d = -3.7 \times 10^{-7}\,\mathrm{m}$ is switched on. The time interval between two successive waves is $\Delta t = 1.35 \times 10^{-7}\,\mathrm{s}$. The kink starts moving at a point $x_0 = -4.0 \times 10^{-7}\,\mathrm{m}$ with a velocity $v_0 = 0.13\,\mathrm{ms}^{-1}$. The potential energy function is a bump with parameters $\beta = 10^{17}\,\mathrm{m}^{-2}$ and the amplitude $V_0 = 1.00 \times 10^{-22}\,\mathrm{J}$ which corresponds to the maximum amplitude of the local force $\pm 2.71 \times 10^{-14}\,\mathrm{N}$.

As can be seen, in the presence of the localized potential energy $V(x)$ the velocity of the kink wave changes more rapidly compared to the case when only the electric

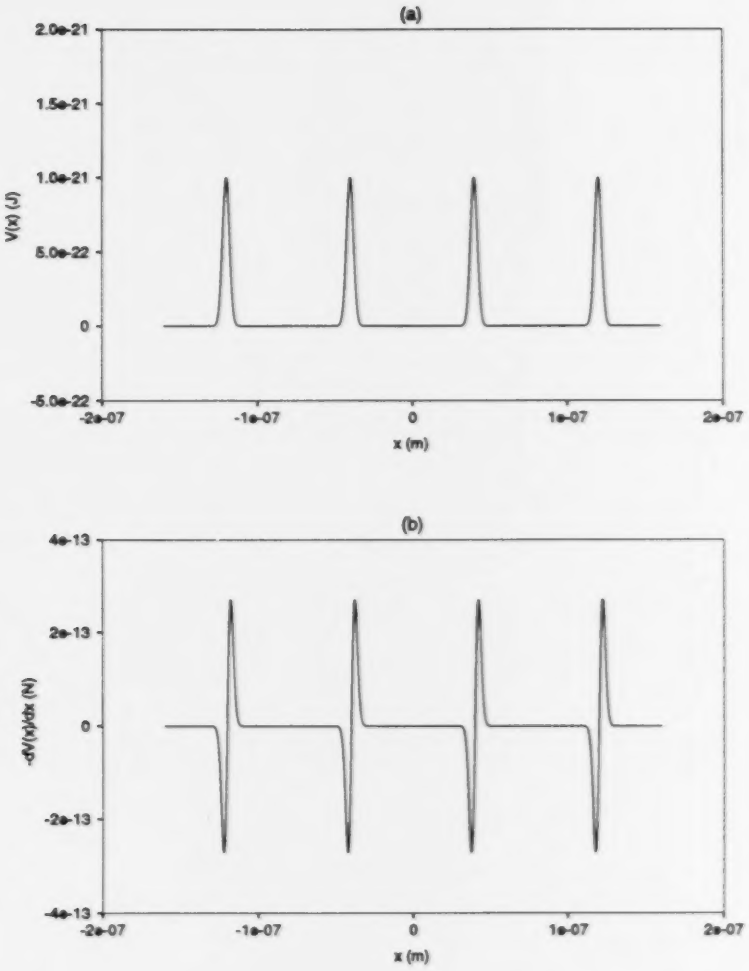

Figure 3.9: Local potential energy (a) and the corresponding local force (b) produced by local defects placed at each 10-th dimer along a MT protofilament.

field is present. When the kink approaches the defect, its velocity decreases because the local force produced by the impurity is negative. When the kink moves away from the center of the defect, its velocity increases since the defect generates a positive force. Eventually the wave moves with a steadily decreasing speed due to the smoothly decreasing electric field $E(x)$. The overall distance travelled by the wave when the local potential energy is switched on is smaller than the distance the kink moves in the same amount of time only on the background of the electric field. This is indicated by the difference between the position of the last solid line and the dotted line which represents a kink travelling only on the background of the changing electric field.

The situation when the impurity is placed in the section of the MT protofilament along which the electric field increases is depicted in Figure 3.10b. At time $t = 0\,\mathrm{s}$, a localized potential energy is switched on at $x_d = 4.3 \times 10^{-7}\,\mathrm{m}$. The time interval between two successive waves and the parameters of the localized force are the same as in Figure 3.10a.

The kink starts moving at a velocity $v = 0.13\,\mathrm{ms}^{-1}$. When the wave approaches the impurity, its velocity decreases and when it passes the center of the local potential energy its motion is accelerated. Sufficiently far from the local defect the kink wave accelerates only due to the electric field of the MT. The total distance travelled by the kink is shorter compared to the case when there is no defect. This is indicated by the difference between the last solid line and the dotted line which show the position of the kink reached in the same amount of time with and without the presence of the local defect, respectively. It can be noticed that the effect of the local defect shown in Figure 3.10b is not as large as in Figure 3.10a. The reason for this is that in Figure 3.10b the magnitude of the electric field at the site at which the local defect is placed, is larger than the magnitude of the local force while in Figure 3.10a the situation is opposite.

The motion of the kink would be affected in a similar way if the local impurity were a Gaussian well since the well differs from a bump only by a minus sign. This means that the local force due to a well will cause a travelling kink to accelerate before it reaches the centre of the local force and decelerate after it passes through the centre of the local force.

Increasing the amplitude of the local potential barrier results in a greater delay of the kink and when the amplitude reaches a critical value the kink will come to a complete stop. This is illustrated in Figure 3.11 that shows a kink wave stopped by

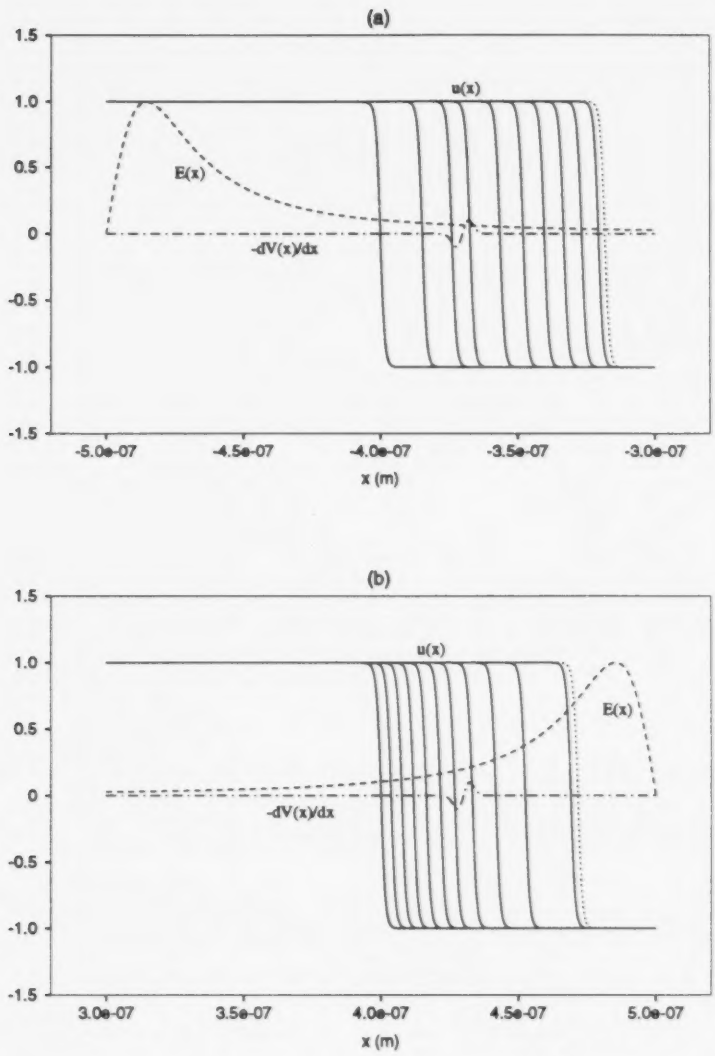

Figure 3.10: A kink wave traveling along the section of a MT protofilament in which the electric field decreases (a) and increases (b) and a defect represented by a localized potential energy is placed at a point $x_0 = -3.7 \times 10^{-7}\,\mathrm{m}$ (a) and at a point $x_0 = 4.3 \times 10^{-7}\,\mathrm{m}$ (b). The amplitude of the local potential energy is $1.00 \times 10^{-22}\,\mathrm{J}$ and the length of the MT protofilaments is 125 dimers. The solid line shows how far the kink would travel if there was no defect. The electric field is plotted in units $2.62 \times 10^{6}\,\mathrm{Vm}^{-1}$, the local force is in units $2.71 \times 10^{-13}\,\mathrm{N}$ and the kink wave is in units $1.58 \times 10^{-11}\,\mathrm{m}$.

a bump located at $x_d = -3.7 \times 10^{-7}$ m. The amplitude of the bump is 1.00×10^{-21} J and the corresponding maximum amplitude of the local force is $\pm 2.71 \times 10^{-13}$ N (10 times larger than in the previous case).

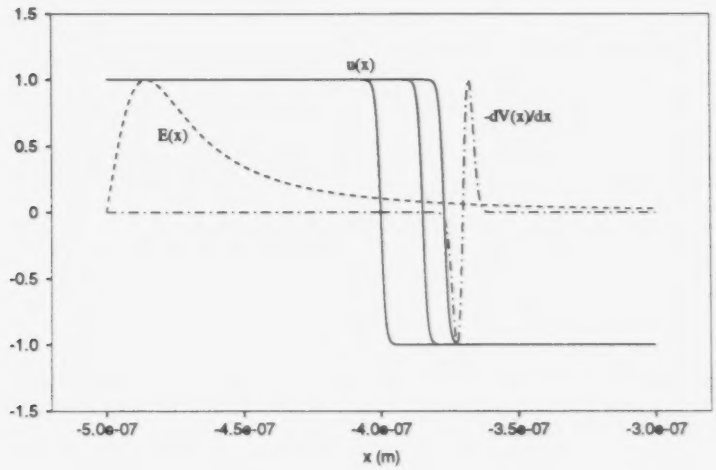

Figure 3.11: When the defect on the MT produces a sufficiently large potential barrier, the kink wave is stopped. In this case the amplitude of the potential energy due to the defect is 1.00×10^{-21} J and it is located at $x_d = -3.7 \times 10^{-7}$ m in the MT which is 125 dimers long. The units for all the curves are the same as in Figure 3.10.

The force produced by the local defect can be compared to the force due to the electric field. When the MT is 125 dimers long, the electric force ranges from $q_{eff}E_{max} = 1.602 \times 10^{-19} \times 2.62 \times 10^{6}\,\mathrm{N} = 4.18 \times 10^{-13}\,\mathrm{N}$ down to $q_{eff}E(0) = 1.602 \times 10^{-19} \times 2.3 \times 10^{4}\,\mathrm{N} = 3.68 \times 10^{-15}\,\mathrm{N}$. The minima of the local forces shown in Figure 3.10a and 3.11 have the values -2.71×10^{-14} N and -2.71×10^{-13} N, respectively, at the point $x_{min} = -3.72 \times 10^{-7}$ m. At this point the value of the electric force is $1.602 \times 10^{-19} \times 1.74 \times 10^{6}\,\mathrm{N} = +2.78 \times 10^{-14}\,\mathrm{N}$. Thus, in the case plotted in Figure 3.10a, the kink wave passes through the potential energy barrier since the positive electric force is larger than the magnitude of the negative local force at the point at which the local force has its minimum. In the case shown in Figure 3.11, the kink wave is stopped by the local defect because the magnitude of the negative local force at the point of its minimum is larger than the force due

to the electric field. The plots of both local forces (with opposite sign) and the electric force are shown in Figure 3.12. It can also be noted that the amplitude $V_0 = 1.00 \times 10^{-21}$ J is of the order of the interaction constants calculated for the MT lattice of dipoles in Chapter 2.

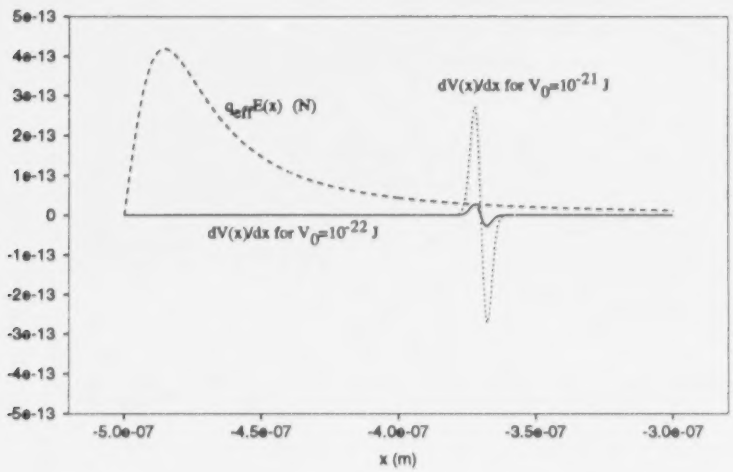

Figure 3.12: The electric force $q_{eff}E(x)$ for a MT which is 125 dimers long and the local forces $-dV(x)/dx$ that correspond to the amplitudes of the localized potential energy $V_0 = 1.00 \times 10^{-22}$ J and $V_0 = 1.00 \times 10^{-21}$ J. The local forces are plotted with the opposite sign to see the difference between the electric force and the local forces at the point of their minimum $x_{min} = -3.72 \times 10^{-7}$ m.

3.5 Two Other Models of Propagation of Kinks in Ferroelectric Systems

3.5.1 Coupled Polarization and Displacement

If polarization and displacement of the tubulin dimers are nonlinearly coupled then the dynamics of the chain of tubulins has to be described by means of two

equations, one for each of the two variables. The model equations in this case of coupled elastic and dielectric degrees of freedom can be derived in the continuum approximation from the energy density which takes the standard form [16]

$$H = \frac{1}{R_0}[\frac{M}{2}(\frac{\partial u}{\partial t})^2 + \frac{KR_0^2}{2}(\frac{\partial u}{\partial x})^2 + \frac{D}{2}(\frac{\partial P}{\partial x})^2 - \alpha_2\frac{u^2}{2} + \alpha_4\frac{u^4}{4} - A_2\frac{P^2}{2} + A_4\frac{P^4}{4} + \gamma_c uP]\,. \tag{3.34}$$

In (3.34), $u(x,t)$ is the displacement at a point x at time t and $P(x,t)$ is the dipole moment at a point x at time t. As can be noticed that $P(x,t)$ depends on time only through its coupling to $u(x,t)$.

The term $\frac{M}{2}(\frac{\partial u}{\partial t})^2$ in (3.34) represents the kinetic energy with M being the mass of one tubulin dimer. The second term $\frac{KR_0^2}{2}(\frac{\partial u}{\partial x})^2$ describes the interaction between points $u(x)$ and $u(x+dx)$ that is due to the elastic restoring forces, where K is the elastic constant and R_0 is the equilibrium distance between two tubulin dimers. The product $\gamma_c uP$ represents coupling between u and P where γ_c is the coupling constant. The quartic double-well potential energies $\alpha_2\frac{u^2}{2} + \alpha_4\frac{u^4}{4}$ and $A_2\frac{P^2}{2} + A_4\frac{P^4}{4}$ originate from the Landau free energy expansions. The coefficients α_2 and α_4 are the same as in the previous model and for a second order phase transition below the critical temperature, α_2, α_4, A_2 and A_4 are positive.

Finally, the term $\frac{D}{2}(\frac{\partial P}{\partial x})^2$ is the non-uniformity energy [17]. This energy exists in the transition regions between domains in which the direction of polarization is different. In these regions, the dipole moments change their direction continuously and their width is given by the conditions of thermodynamic equilibrium. The largest contribution to this energy comes from the exchange interaction [18].

The non-uniformity energy can be expressed by means of spatial derivatives if the gradient of direction of polarization is relatively small, that means, if the polarization changes its direction over distances that are large compared to the distances between two neighbouring dipoles. This condition is fulfilled because if the directions of neighbouring dipole moments were considerably different, this would lead to a large increase of the exchange energy, which is thermodynamically unfavourable.

Applying Langrangian formalism to the energy density (3.34) gives two following coupled equations for P and u

$$M\frac{\partial^2 u}{\partial t^2} = KR_0^2\frac{\partial^2 u}{\partial x^2} + \alpha_2 u - \alpha_4 u^3 - \gamma_c P \tag{3.35}$$

$$0 = D\frac{\partial^2 P}{\partial x^2} + A_2 P - A_4 P^3 - \gamma_c u\,. \tag{3.36}$$

When $\gamma_c = 0$, equations (3.35) and (3.36) have an analytical solution [19] that can be obtained by reducing the partial differential equations to ordinary differential equations. This can be achieved by making the substitution $\xi = x - vt$ which gives the solutions in the travelling wave form. Since K is related to the speed of sound v_0 through $KR_0^2 = Mv_0^2$, then under the assumption that $v_0^2 > v^2$ and after performing the above substitution, both (3.35) and (3.36) can be written in the standard elliptic form

$$c\frac{d^2y(\xi)}{d\xi^2} = -c_2y(\xi) + c_4y(\xi)^3\,, \tag{3.37}$$

where y can be either u or P. For $y = u$, $c = (v_0^2 - v^2)M$, $c_2 = \alpha_2$ and $c_4 = \alpha_4$. For $y = P$, $c = D$, $c_2 = A_2$ and $c_4 = A_4$. The solution of (3.37) is in the form of a kink

$$y(\xi) = \pm(\frac{c_2}{2c_4})^{1/2}\tanh(\frac{c_2}{2c}\xi)\,. \tag{3.38}$$

The system of equations (3.35) and (3.36) can be solved numerically with the initial condition (3.38) at $t = 0$. However, the values of the coefficients D, A_2, A_4 and γ_c for a MT are not known at the present time. In this work A_2 and A_4 could be estimated by fitting the polarization curves calculated in Chapter 2 and D was estimated on the basis of the interaction energies between two dipoles. These estimates are given in Appendix A.

To demonstrate the properties of the coupled system (3.35) and (3.36) the numerical solution is presented here for parameters chosen arbitrarily. Figure 3.13 depicts the numerical solution when $\alpha_2 = \alpha_4 = A_2 = A_4 = 1$, $\gamma_c = 0.1$, $v = 1$, $M = 1$, $v_0 = 3$ and $D = 2$. Polarization and displacement are two coupled kink waves travelling with the same velocity. The velocity is slightly less than the velocity given by the initial condition (3.38). It can be noticed that the amplitude of the u wave fluctuates which is due to the coupling between u and P. The amplitude of P is slightly larger than the amplitude of the initial P kink and it is stable over the course of time.

The effect of an impurity can be included in the coupled system by adding a local force of the form (3.33) to the right hand side of equation (3.35). The numerical results are shown in Figure 3.14a and Figure 3.14b for the parameters of the local force $\beta = 0.5$, $x_d = 15$, $V_0 = 0.2$ and $V_0 = 0.4$. In both pictures u is shown at regular time intervals. The P wave is coupled to the u wave exactly as in Figure 3.13 and it is plotted only at the end of the last interval.

Figure 3.14a illustrates a situation when the local force is small. In this case both waves pass through the potential energy barrier and their velocity is altered.

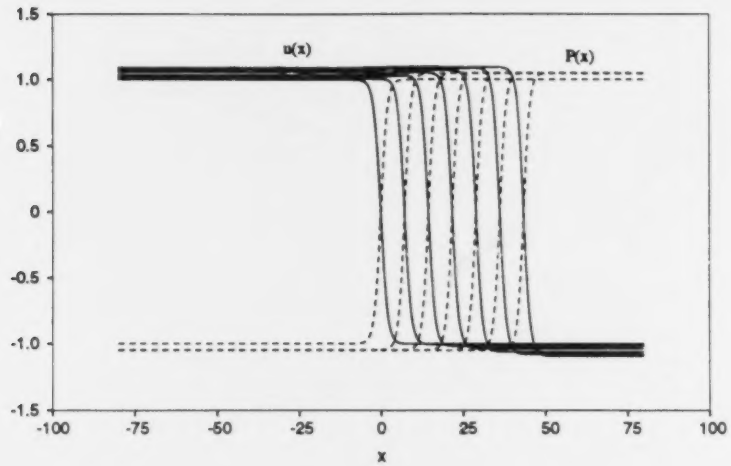

Figure 3.13: Numerical solution of the coupled system of equations (3.35) and (3.36) for parameters $\gamma_c = 0.1$, $v = 1$, $M = 1$, $v_0 = 3$, $\alpha_2 = \alpha_4 = A_2 = A_4 = 1$ and $D = 2$.

The overall distance travelled in the presence of the local defect is smaller than the distance which the two coupled waves would travel in the same time but without the presence of the defect which is indicated by the dotted line. Figure 3.14b shows the case when the local force is large. Both coupled waves reflect from the potential barrier and propagate in the opposite direction.

The results described above are similar to the results obtained by means of the model represented by equation (3.10). However, the kink solutions of (3.10) are more stable, and they preserve their shape and velocity. Since equation (3.10) also includes the force of friction, a large potential energy barrier causes the kink to come to a stop rather than to reflect from it.

The spatial and time scales over which u and P change are determined by the parameters of the model (see Appendix A). According to the two models described above the elastic state of the tubulin dimer changes within a length of about one tubulin dimer and the relative distortion of the dimer is about $1.58 \times 10^{-11}/8 \times 10^{-9} = 0.002$. For the estimated values of the parameters D, A_2, A_4 the width of the P-kink is about three tubulin dimers when it is assumed that the maximum change of P is the magnitude of the dipole moment on the tubulin dimer. However, a trial simulation using the estimated parameters showed that the possibility of using the

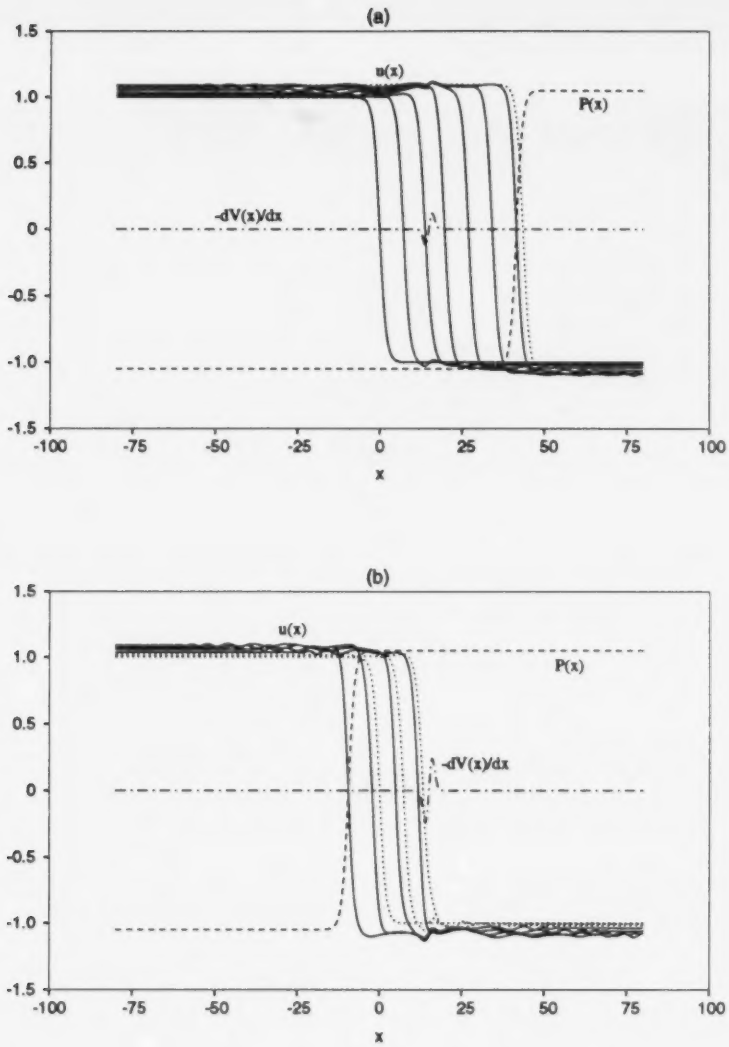

Figure 3.14: Numerical solution of the coupled system of equations (3.35) and (3.36) when a local force $-dV(x)/dx$ is added to the right hand side of equation (3.35). The parameters in the equations are the same as for the solution drawn in Figure 3.13. The parameters of the local force are $\beta = 0.5$, $x_d = 15$ and (a) $V_0 = 0.2$, (b) $V_0 = 0.4$. The solution for u is plotted in regular time intervals and the solution for P is plotted only at the end of the simulation. In Figure 3.14b the dotted line shows u before it is reflected and the solid line is the solution for u after it is reflected from the local potential energy barrier.

model suggested in this section to describe the energy propagation along MTs may require more extensive numerical investigation.

It can be pointed out here that another group of authors found solitary wave solutions of an equation of motion set up for a chain of tubulin dimers in a MT protofilament [20]. They considered only the elastic degrees of freedom. Their solutions were kinks and pulses whose propagation along a MT could be driven, for example, by the energy of the GTP hydrolysis. The width of the kink solution was about 7 to 10 tubulin dimers.

3.5.2 Coupled Polarization and Stress

Another possible approach to the interface motion in ferroelectric systems is presented in works [21], [22]. In [21] the Landau-Ginzburg type free energy expansion is postulated in the following form

$$F = F_0 + \frac{1}{2}AP^2 - \frac{1}{4}BP^4 + \frac{1}{6}CP^6 - \frac{1}{2}e\sigma P^2 - \frac{1}{2}s_0\sigma^2 + \frac{D}{2}(\frac{\partial P}{\partial x})^2 , \qquad (3.39)$$

where P is polarization and σ is the mechanical stress that couples to P due to the piezoelectric effect. Coupling between P and σ is expressed by the term $\frac{1}{2}e\sigma P^2$ where e is the elastic constant. The parameter s_0 is related to the velocity of sound v_0 and the density ρ of the elastic medium through $v_0 = (\rho s_0)^{-1/2}$.

Without the terms containing σ, the free energy (3.39) describes a first order phase transition in uniaxial proper ferroelectrics. The coefficient A is defined as $A = a(T_0 - T)$, where T_0 is the transition temperature at which the paraelectric phase loses its stability [23], B and C are positive constants, $\frac{D}{2}(\partial P/\partial x)^2$ is the non-uniformity energy where $D > 0$.

The time evolution of the order parameter P can be derived using the time dependent Landau-Ginzburg equation [24]

$$\frac{\partial P}{\partial t} = -\Gamma\frac{\delta F}{\delta P} , \qquad (3.40)$$

where Γ is the Landau-Khalatnikov damping coefficient. Substituting (3.39) into (3.40) and performing the variational derivative $\delta F/\delta P$ gives the following equation

$$\frac{\partial P}{\partial t} + \Gamma(AP - BP^3 + CP^5 - e\sigma P) - \Gamma D\frac{\partial^2 P}{\partial x^2} = 0 . \qquad (3.41)$$

The second equation for σ and P can be found from the coupling of σ and P to the mechanical deformation ϵ which is equal to

$$\epsilon = -\frac{\partial F}{\partial \sigma} = \frac{1}{2} e P^2 + s_0 \sigma \,. \tag{3.42}$$

Here, $\epsilon = \partial u / \partial x$ is the strain tensor component corresponding to σ. Hence, it satisfies the wave equation of an elastic medium with density ρ

$$\rho \frac{\partial^2 \epsilon}{\partial t^2} = \frac{\partial^2 \sigma}{\partial x^2} \,. \tag{3.43}$$

After substituting (3.42) into (3.43) the second equation for coupled polarization and mechanical stress is obtained

$$\frac{\rho e}{2} \frac{\partial^2}{\partial t^2} P^2 = (\frac{\partial^2}{\partial x^2} - \rho s_0 \frac{\partial^2}{\partial t^2}) \sigma \,. \tag{3.44}$$

To find the solutions of the system of coupled equations (3.41) and (3.44) in the travelling wave form the standard substitution can be made $\xi = x - vt$. Then equation (3.44) can be integrated which yields

$$\frac{\rho e}{2} v^2 P^2 - (1 - \rho s_0 v^2) \sigma = c_1 \xi + c_0 \,. \tag{3.45}$$

In (3.45), c_1 and c_0 are integration constants. If it is assumed that $c_1 = c_0 = 0$[2] and (3.45) is substituted into (3.41), the following ordinary differential equation results for P

$$\Gamma D \frac{d^2 P}{d\xi^2} + v \frac{dP}{d\xi} - \Gamma (AP - \tilde{B} P^3 + C P^5) = 0 \,, \tag{3.46}$$

where

$$\tilde{B} = B + \frac{\rho e^2 v^2}{2(1 - \rho s_0 v^2)} \,. \tag{3.47}$$

The solution of (3.46) is a travelling kink wave

$$P = \frac{P_f}{\sqrt{2}} [1 + \tanh (\frac{\xi}{2\Delta})]^{1/2} \,, \tag{3.48}$$

where

$$P_f^2 = \frac{\tilde{B}}{2C} [1 + (1 - \frac{4AC}{\tilde{B}^2})^{1/2}] \,, \tag{3.49}$$

$$\Delta = [\frac{3D}{4(\tilde{B} P_f^2 - A)}]^{1/2} \,, \tag{3.50}$$

[2]The solutions for c_1 and c_0 nonzero were studied, *e.g.*, in [25].

and

$$v = \frac{2}{3}\Gamma\Delta(4A - \tilde{B}P_f^2). \tag{3.51}$$

An impurity in a ferroelectric medium described by the two coupled equations (3.41) and (3.44) can be included into this system of equations as a local fluctuation of the density of the medium ρ. The model function that represents the fluctuation was again chosen to have a form of a Gaussian. Hence, the density changes as a function of the position along a MT as

$$\rho(x) = \rho_0(1 + \rho_r \sum_{n=1}^{N} e^{-\beta\{x-[x_d+(n-1)a_n]\}^2}), \tag{3.52}$$

where ρ_0=const. is the density in the medium when no impurity is present, ρ_r is the dimensionless amplitude of the inhomogeneity function and the rest of the variables are the same as in (3.32).

The system of partial differential equations (3.41) and (3.44) in which the parameter ρ changes as a function of x according to (3.52) was solved numerically. As initial conditions were chosen the solutions obtained for a constant density ($\rho_r = 0$) from (3.48) for P and by combining (3.48) and (3.45) for σ. The values of the parameters A, B, C, D, Γ and e for a MT are not known. Here they were chosen as follows: $A = B = C = \Gamma = 1$ and $D = 2$. For the choice $\tilde{B} = 2$, $e = -1$ and $s_0 = 1$, the velocity v obtained from (3.51) was $\sqrt{\frac{8}{3}}$ and ρ_0 from (3.47) was 0.25. The solutions obtained were found to have interesting properties which could be relevant for MTs. However, this model should be examined with proper MT parameters some of which are estimated in Appendix A.

The numerical calculations were performed for two cases. In one case the elastic constant s_0 was kept constant so that the speed of sound v_0 was changing due to the change in ρ. In the second case the speed of sound was assumed to be constant, *i.e.*, the change in ρ was compensated for by the change in s_0 .

The sequence of pictures in Figures 3.15 and 3.16 shows the results of a numerical calculation assuming that s_0 is constant and a local density fluctuation of the form (3.52) is switched on at time $t = 0$. The center of the inhomogeneity is located at $x_d = 10$ and $\beta = 0.2$. The amplitude of the fluctuation is $\rho_r = 0.5$, *i.e.*, there is a maximum 50% increase in density. Initially, both polarization and stress are kink waves obtained from (3.48) and (3.45). After the density fluctuation is introduced into the medium both waves significantly change their shape. When the polarization wave passes through the inhomogeneity, it partially recovers and eventually disappears approximately after time t=90. The stress wave, however,

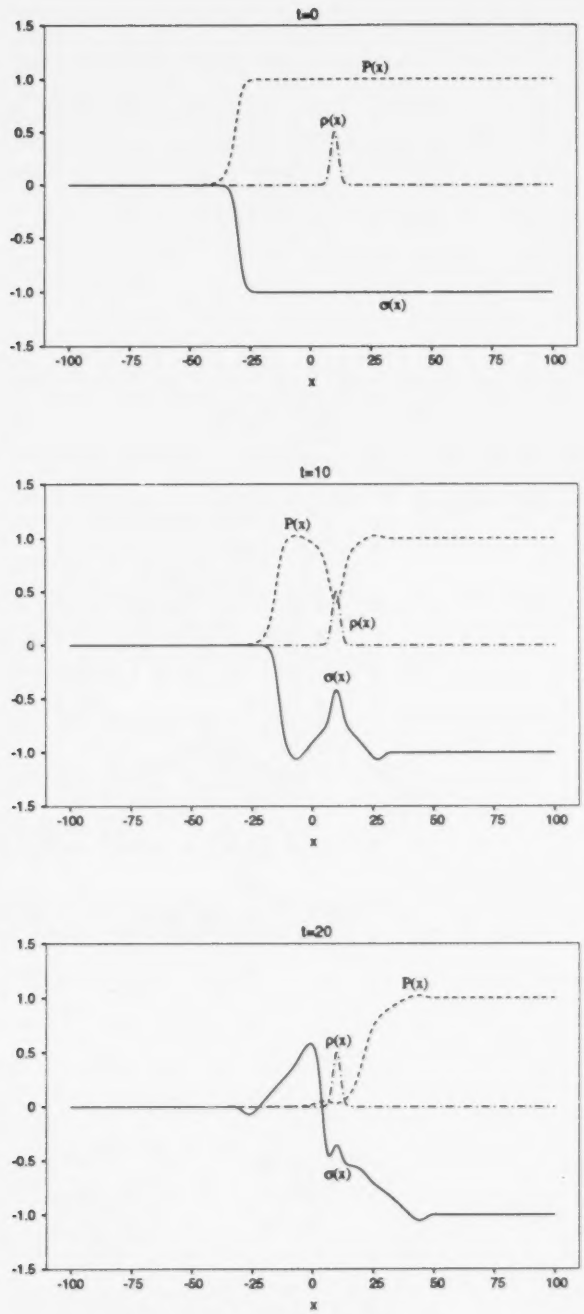

Figure 3.15: Numerical solution of (3.41) , (3.44) and (3.52) at times $t = 0$, $t = 10$ and $t = 20$ when the amplitude of the density fluctuation is $\rho_r = 0.5$.

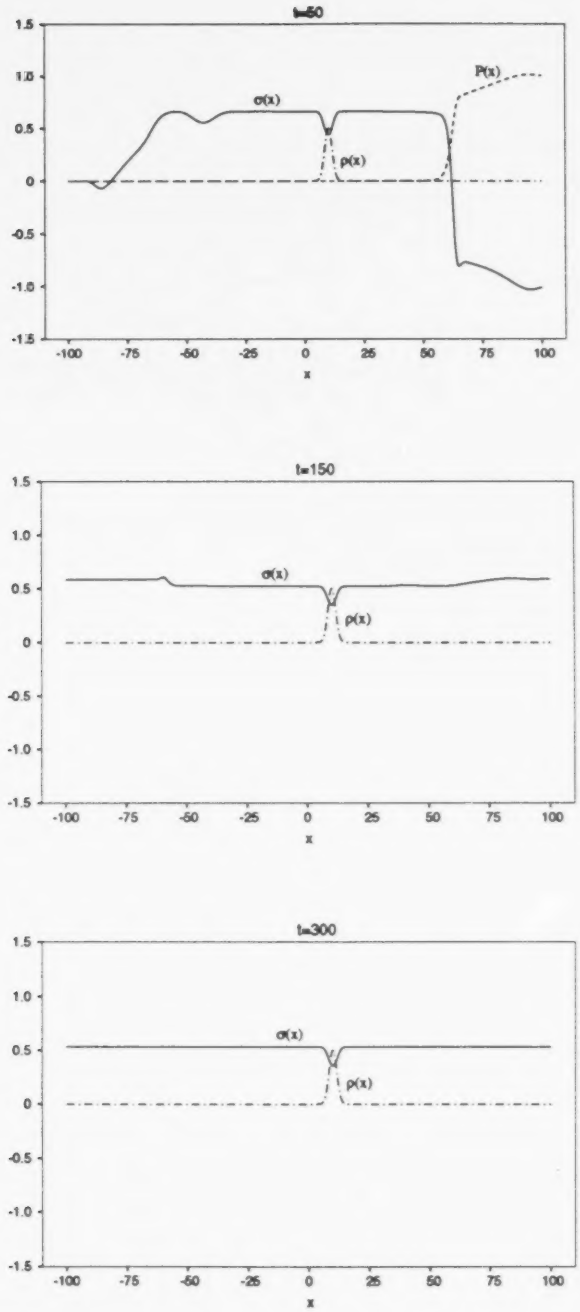

Figure 3.16: Numerical solution of (3.41) , (3.44) and (3.52) at times $t = 50$, $t = 150$ and $t = 300$ when the amplitude of the density fluctuation is $\rho_r = 0.5$.

becomes trapped by the density fluctuation and approximately after time $t = 300$ a stationary solution forms which is characterized by a constant value along the whole MT except for a local bump centered at the center of the inhomogeneity. It is shown in Figures 3.17, 3.18 and 3.19 that the amplitudes that characterize the stationary solution for stress in case of constant s_0 increase with the increasing ρ_r and with the increasing number of inhomogeneities along a MT as well.

Figure 3.17 depicts the initial and final stationary solutions of (3.41), (3.44) and (3.52) when the density fluctuation has an amplitude $\rho_r = 1$ and the same x_d and β as previously. Figures 3.18 and 3.19 show the evolution of the solutions in the case

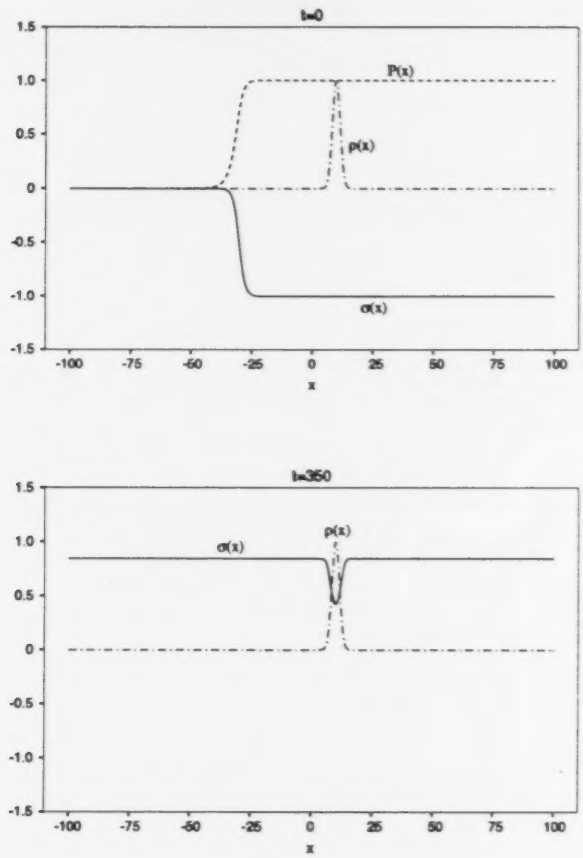

Figure 3.17: Numerical solution of (3.41) , (3.44) and (3.52) at times $t = 0$ and $t = 350$ when the amplitude of the density fluctuation is $\rho_r = 1$.

when two inhomogeneities with the same parameters as in Figures 3.15 and 3.16 are placed in the MT and they are centered at $x = x_d = 10$ and $x = x_d + a_1 = 40$. It can be noticed in this sequence of pictures that the polarization wave is significantly destructed and recovers after it passes through the density fluctuations. The latter observation suggests that fluctuations of density located along the whole MT (for example, due to MAPs attached at regular intervals along the protofilaments) may cause a complete destruction of the polarization wave. At the same time one or more local density inhomogeneities may create a permanent stress that is constant along the MT with the exception of the sections where the inhomogeneities are placed at which the permanent stress is smaller. Such a mechanism may play a role in the MT destabilization and overall destruction.

The solutions obtained for the case when the speed of sound is constant were found to have similar properties to those described above. They differed only by the form of the stationary stress which was constant along the whole MT.

On the basis of the calculations above it can be suggested that local fluctuations of density which could be caused, for example, by an attached MAP or a structural discontinuity in a MT, may impose permanent stress in the MT. When the stress is sufficiently large, for example, due to large impurity or a large number of impurities, the whole MT could become unstable and, as a result, might rapidly disassemble.

The investigation presented in this chapter has shown that coupling between elastic and dielectric degrees of freedom may give rise to kink-like solitary waves travelling along MT protofilaments that could be driven by the energy freed in the GTP hydrolysis.

In the first model studied, polarization and displacement of the tubulin dimer were assumed to be strongly coupled so that the relationship between both quantities can be assumed to be linear. The solutions of this model are travelling kinks represented by domain walls with a width of about one tubulin dimer. The velocity the kink waves depends linearly on the value of the electric field on the MT surface. A collision with an impurity placed in the MT causes the kink to travel a shorter distance compared to the case when the impurity was not present. When the local force produced by the impurity is sufficiently large the kink wave stops propagating.

Another model was suggested in which the coupling between the distortion of the tubulin dimer and its dipole state is assumed to be nonlinear. Polarization depends on time only implicitly through its coupling to the displacement of the tubulin dimer. This model was studied with parameters chosen arbitrarily. One

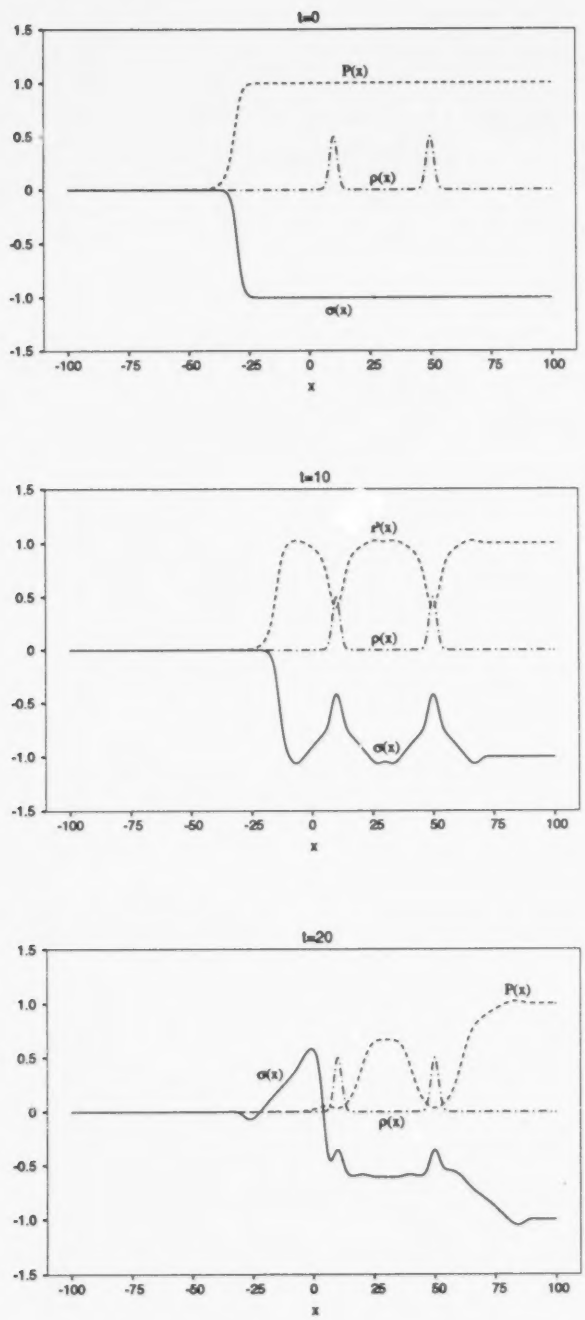

Figure 3.18: Numerical solution of (3.41) , (3.44) and (3.52) at times $t = 0$, $t = 10$ and $t = 20$ when the amplitude of the density fluctuations is $\rho_r = 0.5$.

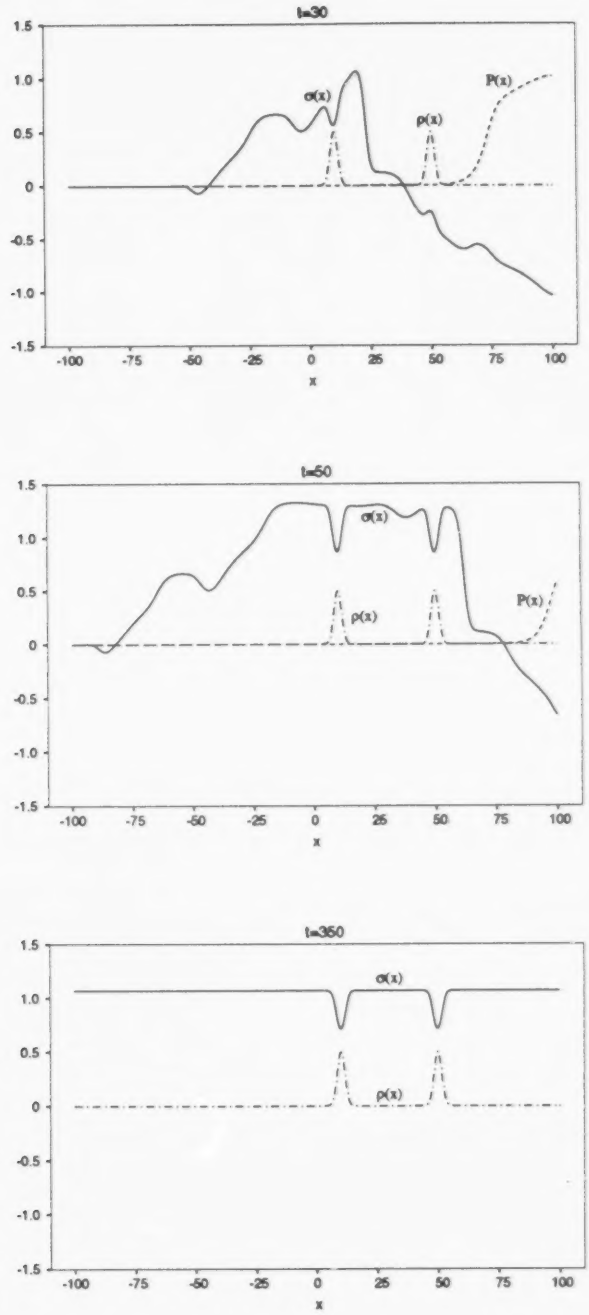

Figure 3.19: Numerical solution of (3.41) , (3.44) and (3.52) at times $t = 30$, $t = 50$ and $t = 350$ when the amplitudes when the amplitude of the density fluctuations is $\rho_r = 0.5$.

class of the solutions of this model are travelling kink-like waves for both polarization and displacement. Both waves travelled with the same velocity. A local impurity caused slower motion of the kinks and when the impurity was large both coupled waves reflected from it and continued to propagate in the opposite direction. The travelling kink waves studied by means of the first two models, could be signals for other important cellular events.

The last model studied here is represented by equations that describe a ferroelectric system in which polarization is coupled to mechanical stress. The calculations were performed for an arbitrary choice of parameters. The system of equations has, under special circumstances, travelling kink wave solutions. When a local impurity represented by a fluctuation of the density of the medium is included in the system the numerical solution is a stationary stress constant along the whole MT. Depending on the way the density of the medium affects the other parameters in the system, a local bump placed at the center of the impurity may form on the background of the constant stress. The amplitudes that characterize the stationary solutions increase when the amplitude and the number of the inhomogeneities increase. The permanent stress imposed in the MT in this way could be a means of destabilizing the MT and hence a factor in the MT disassembly. This model and the second model, however, should be studied with parameters proper for MTs.

References

[1] A. L. Lehninger, *Principles of Biochemistry* (Worth, New York, 1982)

[2] H. Bilz, H. Büttner, H. Fröhlich, Electret Model for the Collective Behaviour of Biological Systems, *Zeitschrift für Naturforschung* **36b**, p. 208-212 (1981)

[3] A. S. Davydov, The Theory of Contraction of Proteins under Their Excitation, *Journal of Theoretical Biology* **38**, p. 559-569 (1973)

[4] P. S. Lomdahl, Solitons in Biology? *Los Alamos Science*, No. 10, p. 2-31 (1984)

[5] A. C. Scott, F. Y. F. Chu, and D. W. McLaughlin, The Soliton: A New Concept in Applied Science, *Proceedings of the IEEE* **61**, p.1443-1483 (1973)

[6] R. K. Bullough and R. K. Dodd, Solitons: I. Basic Concepts, *Synergetics. A Workshop*, editor H. Haken, Springer, Berlin, 1977, p. 92-119

[7] N. Flytzanis, St. Pnevmatikos and M. Remoissenet, Kink, breather and assymetric envelope or dark solitons in nonlinear chains: I. Monatomic chain, *Journal of Physics C: Solid State Physics*, p. 4603-4629 (1985)

[8] P. Das and W. H. Schwartz, Solitons in Cell Membranes, *Physical Review E*, **51**, p. 3588-3612 (1995)

[9] A. C. Scott, Davydov's Soliton, *Physics Reports* **217**, p. 1-67 (1992)

[10] M. V. Satarić, R. B. Žakula, J. A. Tuszyński, A model of the energy transfer mechanism in microtubules involving domain-wall-type solitons, *Physical Review E* **48**, p. 589-597 (1993)

[11] M. B. Hakim, S. M. Lindsay, and J. Powell, The Speed of Sound in DNA, *Biopolymers* **23**, p. 1185-1192 (1984)

[12] S. Hameroff, *Ultimate Computing* (North-Holland, Amsterdam, 1987)

[13] P. M. Vassilev, R. T. Dronzine, M. P. Vassileva, and G. A. Georgiev, Parallel Arrays of Microtubules Formed in Electric and Magnetic Fields, *Bioscience Reports* **2**, p. 1025-1029 (1982)

[14] L. F. Jaffe and R. Nuccitelli, Electrical Controls of Development, *Annual Review of Biophysics and Bioengineering* **6**, p. 445-476 (1977)

[15] J. M. Dixon, J. A. Tuszyński and M. Otwinowski, Special analytical solutions of the damped-anharmonic-oscillator equation, *Physical Review A* **44**, p. 3484-3491 (1991)

[16] J. A. Tuszyński, B. Trpišová, D. Sept, M. V. Satarić, S. Hameroff, The Cell's Microtubules: Self-Organization and Information Processing Properties, proceedings of the conference *Nonlinear Excitations in Biomolecules*, Les Houches School, May 30 to June 4, 1994, editor M. Peyrard, Springer, p. 387-404

[17] L. D. Landau and E. M. Lifshitz, *Electrodynamics of Continuous Media* (Pergamon Press, Oxford, 1960)

[18] P. W. Anderson, *Basic Notions of Condensed Matter Physics* (The Benjamin-Cummings Publishing Company, 1984)

[19] M. L. A. Nip and J. A. Tuszyński, Statistical Properties of the Exact-Solutions of the One-Dimensional ϕ^4-Model, *Il Nuovo Cimento* **109 B**, p. 507-521 (1994)

[20] Kuo-Chen Chou, Chun-Ting Zhang, and G. M. Maggiora, Solitary Wave Dynamics as a Mechanism for Explaining the Internal Motion During Microtubule Growth, *Biopolymers* **34**, p. 143-153 (1994)

[21] A. Gordon, Propagation of solitary stress waves at first-order ferroelectric phase transitions, *Physics Letters A* **154**, p. 79-80 (1991)

[22] A. Gordon, Interface motion in ferroelectrics, *Physica B* **138**, p. 239-243 (1986)

[23] A. Gordon, S. Dorfman, Pressure-induced kinetics of ferroelectric phase transitions, *Physical Review B* **50**, p. 132-137 (1994)

[24] L. D. Landau and I. M. Khalatnikov, On the anomalous absorption of sound near a second order phase transition point, *Doklady Akademii Nauk SSSR* **96**, p. 469 (1954) [English translation in Collected papers of Landau, editor D. ter Haar (Pergamon Press, Gordon and Breach, London, New York, 1965)]

[25] J. A. Tuszyński and D. Sept, Comments on phase-front propagation in ferroelectrics, *Journal of Physics, Condensed Matter* **6**, p. 3583-3591 (1994)

4 Information in Microtubules

The many functions that MTs perform in the cell are a result of the interactions within MTs and with the external environment. The internal and external interactions are represented by biophysical and biochemical processes that take place at a molecular level. These processes can be viewed as information received, processed and transferred by MTs.

The exact ways through which MTs communicate within themselves and with their surroundings have been the subject of the present investigation. The research presented in this work gave rise to a few suggestions and questions about the communication pathways in MTs on the basis of their physical properties. In this chapter, an attempt is made to qualitatively estimate the information capacity of a MT on the basis of patterns formed by the tubulin dipole states. Before the results are presented, a well-known model of information processing in MTs called **MT automata** is described. Its features are compared to those of **neural networks** models and **cell signalling**.

4.1 Models of Communication in Biological Systems

The basic assumption in the MT automata models is that a tubulin molecule can be in several different conformational states and that it can switch between those states at discrete time steps. The MT automaton described here is presented in [1]. The authors assumed that a tubulin molecule in a MT can be in two electrostatic states due to the presence of a mobile electron that is located in one of the hydrophobic pockets either closer to the α or closer to the β monomer (section 2.4 in Chapter 2). Due to the coupling between the electrostatic and conformational states of the tubulin dimer, the electrostatic events in MTs can be coupled to the mechanical and chemical events.

The automaton was modelled on a MT with the A-lattice and with 13 protofilaments. At discrete time steps determined by a clocking frequency, a dimer can switch from the α to the β state or *vice versa*. The switching takes place if the sum of electrostatic forces acting on the free electron in the dimer, due to the electrons from the six nearest dimers, reaches a prescribed threshold value. The clocking

frequency was assumed to be a frequency at which a coherent sound wave travels across the MT diameter.

The above rules applied to a MT lattice result in different patterns of tubulin electrostatic states that blink or form travelling waves along MTs. The type of pattern is determined by the value of the threshold force. Thus the threshold value is a parameter by means of which different information flow pathways in a MT can be selected. A different threshold can be chosen for switching from α to β and from β to α state. The threshold force can also be viewed as a parameter that includes the influence of such biological factors as the GTP hydrolysis, binding of MAPs and other molecules and ions, genetic variations, *etc.*, on the tubulin conformation. All these factors can alter the propagating information patterns represented by the electrostatic interactions.

The communication between MTs interconnected with other protein filaments and MAPs can be modelled in the MT automata by placing connections between MTs. The sites of the connections are chosen randomly or by some other considerations. The task is to find a connection which will generate a desired output pattern in response to some input pattern. This is achieved by parallel testing of several automata. In this way connections can be found which are associated with a certain input-output map.

How well a connection can perform a certain task depends on its position but also on the values of the threshold parameters and the background of tubulin conformational states. For example, α gliders on the β background always travel in the opposite direction to the β gliders on the α background. This means that MT automata allow for back propagation of information. By varying the parameters of the MT automata, that is, the threshold values, the connections and the background, the MT network can be adapted to performing different tasks.

The functioning of MT automata is similar to the well-known models of neural networks which were originally designed in order to simulate the behaviour of neurons and on the basis of that to study the principles of intelligent behaviour.

A neural network consists of a net of units connected with each other [2]. To each connection a certain weight is assigned. The output from each unit is created according to mathematical rules that sum up the inputs from other units connected with it. The goal is to obtain a certain output from the network in response to some input signal. For example, the input can be a series of letters and the output the correct identification of each of them. This is achieved in a similar way as in MT

automata. The weights in the network are chosen randomly and the combination of weights which produces the best result is maintained and further trained until the output from the neural network is close enough to the one that is wanted. In this way the network of units has learned which configuration of parameters can perform a certain task. At this level of learning, the network is able to give the right response to an input that wasn't originally used in the learning process.

In neural networks that have accomplished the process of learning, specific units of the net are strongly connected to specific inputs. For example, in the network used for recognizing letters, a certain subset of units can be connected to recognizing right angles or curves. The information from different subsets is then integrated into an overall output which is recognizing letters. If some elements of the input are missing, the network will still be able to recognize it, just its ability will be somewhat lessened.

In the same way as the nets of neurons, neural networks could model extra- and intracellular signalling that goes on by means of molecules and ions [2]. A certain event in the cell happens as a response to the combination of several signals. This event can be, for example, a chemical reaction induced by an enzyme that in the course of evolution has learned which signals are associated with this reaction, and the whole process then became encoded in the genes. Through random mutation in the genetic code the enzyme can learn a new function in response to some combination of signals which can result in the development of a more intelligent and thus more viable organism.

The signalling pathways even in simple organisms are often very complex. An event happens as a response to many previous events or to a combination of appropriate signals. But complexity seems to be inevitable for survival. Even when one element of the signalling pathway is removed, the cell can still function nearly normally.

The features of neural networks or MT automata are reminiscent of the principles of evolution that takes place by random mutation and natural selection when only the individual species that can best adapt to the environment can survive. They are found in biological organisms and they can be quite successfully modeled by means of artificial networks of units as well.

4.2 Calculation of Information Capacity in Microtubules

The numerous biological functions of MTs have been described in Chapter 1. The dynamic instability of MTs is a major tool of cell division and polarization. MTs serve as tracks along which organelles and neuronal vesicles are transported to the proper place in the cell. They are the main components of cilia and flagella that exhibit coordinated motions in cell motility. On the basis of the numerical studies presented in the previous two chapters of this work some suggestions about the physical processes that underlie these activities can be made.

As was shown in Chapter 2, a MT may exist at least in two dielectric phases, ferroelectric and paraelectric phase. According to the investigation presented in Chapter 3, ferroelectric phase may be suitable for propagation of kink-like excitations of tubulin dipole states which are coupled to the tubulin conformational states. Kinks propagating along MT protofilaments or another (more energetically favourable) path could serve as information bits or information waves. At the sites of attached MAPs the information may be transferred to other MTs or cytoskeletal components. Hence, the travelling localized energy would be a means of the intercytoskeletal communication.

By means of the kink-like excitations, the transport of organelles or beat-like motions in cilia and flagella could be coordinated. The common wall shared by the A and B tubules of cilia and flagella could be the place where the information is integrated. Kink-like waves travelling to the end of a MT could cause its detachment from the centrosome or attachment to a kinetochore in the metaphase of cell division.

At higher temperatures a MT ceases to be in the ferroelectric phase due to the formation of domains (or clusters) with different orientation of dipoles. The configuration of the domains in a MT may serve for storage of information. This assumption is the subject of investigation in the following sections of this chapter.

The calculations of information capacity in a MT were based on Shannon's definition of information [3]

$$I = -\sum_{i=1}^{K} p_i \ln p_i \,, \qquad \sum_{i=1}^{K} p_i = 1 \,, \tag{4.1}$$

where p_i is probability of state i. The probability p_i at a temperature T is proportional to the factor [4]

$$\exp\left[-\frac{E_i}{k_B T}\right], \tag{4.2}$$

where k_B is the Boltzmann constant and E_i is the energy of a domain i in which the individual dipoles are oriented in the same direction.

Two approaches were used to find the probabilities p_i and the corresponding information (4.1). In the first case the energy of a domain with N dipoles (sites) was approximated by the Landau free energy expansion for the order parameter polarization per site P (in units Cm). Because P is a continuous variable the sum (4.1) for the discrete variable p_i is replaced by an integral over P. In the second method the energies E_i at each temperature were calculated exactly by summing up the interaction energies J_n between the neighbouring dipoles in each domain.

4.2.1 Continuous Probability Distribution

If it is assumed that the mean polarization per site in the MT lattice of dipoles changes continuously, the energy of each cluster can be expressed in the Landau form

$$E(P,N) = (\frac{A}{2}P^2 + \frac{B}{4}P^4)N\,. \tag{4.3}$$

In (4.3), P is the mean polarization per site, N is the number of tubulin molecules in the cluster, $A = a(T/T_c - 1)$ and B is a temperature independent constant. For a second order phase transition $a > 0$ and $B > 0$ (see section 2.1 in Chapter 2). The minima of the energy function (4.3) are obtained by taking its derivative with respect to P and setting it equal to zero. This yields the following equation of state

$$0 = a(\frac{T}{T_c} - 1)P + BP^3\,. \tag{4.4}$$

Above the critical temperature T_c the only solution of (4.4) is $P = 0$, which corresponds to the paraelectric phase. For $T < T_c$ equation (4.4) has two symmetric nonzero roots $P_\pm = \pm\sqrt{-a(T/T_c - 1)/B}$.

Using (4.3) in (4.2) gives the following probability associated with a value of mean polarization per site P in a cluster with N members at each temperature

$$f(P,N)) = f_0 \exp[-\frac{E(P,N)}{k_B T}] = f_0 \exp(\alpha P^2 - \beta P^4)\,, \tag{4.5}$$

where $\alpha = -a(T/T_c - 1)N/2k_BT$, $\beta = BN/4k_BT$ and $f_0 = Z^{-1}$ is a normalization constant. The above continuous probability distribution is an example of the

Boltzmann distribution. For $T > T_c$ the distribution function $f(P,N))$ has a single maximum at $P = 0$. Below T_c the probability distribution has two maxima at $P = P_\pm$ corresponding to the two branches of polarization in the ferroelectric phase.

For a system characterized by the continuous probability distribution (4.5) the information capacity can be derived as follows [5]. In a continuous case the sum over all states of the system in the formula (4.1) becomes an integral, *i.e.*, the information capacity of a cluster with N members can be expressed as

$$I(N) = -\int_{-\infty}^{\infty} f(P,N) \ln f(P,N) dP \,. \tag{4.6}$$

Similarly as in the discrete case the integral over all states P is equal to unity

$$\int_{-\infty}^{\infty} f(P,N) dP = 1 \,. \tag{4.7}$$

Substituting (4.5) into equation (4.6) and using the latter equality gives

$$I(N) = \ln Z - \alpha \int_{-\infty}^{\infty} P^2 f(P,N) dP + \beta \int_{-\infty}^{\infty} P^4 f(P,N) dP \,. \tag{4.8}$$

The normalization constant Z and the two integrals in (4.8) can be evaluated by means of the formula [6]

$$\int_0^{\infty} x^{2\nu-1} \exp\left(-\gamma x^2 - \delta x^4\right) dx = \frac{(2\delta)^{\frac{-\nu}{2}}}{2} \Gamma(\nu) D_{-\nu}(\lambda) \exp\left(\frac{\lambda^2}{4}\right), \tag{4.9}$$

where $\lambda = \gamma/\sqrt{2\delta}$, $Re\,\gamma > 0$, $Re\,\nu > 0$, Γ is the gamma function and D is the parabolic cylinder function. The final expression for the information of a cluster with N members has the following form

$$I(N) = \frac{1}{2}\ln\pi - \frac{1}{4}\ln 2 - \frac{1}{4}\ln\delta + \frac{\lambda^2}{4}\ln D_{-\frac{1}{2}}(\lambda) + [\frac{\lambda}{2} D_{-\frac{3}{2}}(\lambda) + \frac{3}{8} D_{-\frac{5}{2}}(\lambda)]/D_{-\frac{1}{2}}(\lambda) \,, \tag{4.10}$$

where

$$\lambda = \frac{-a(T/T_c - 1)\sqrt{N}}{\sqrt{2Bk_BT}} \,, \qquad \delta = \frac{BN}{4k_BT} \,. \tag{4.11}$$

The parabolic cylinder functions in (4.10) were evaluated with Mathematica using the identity

$$D_p(\lambda) = 2^{\frac{p}{2}} \exp(-\frac{\lambda^2}{4}) \Psi(-\frac{p}{2}, \frac{1}{2}; \frac{\lambda^2}{2}) \,, \tag{4.12}$$

where $\Psi(a,b;x)$ is the degenerate hypergeometric function.

Since equation (4.10) was derived on the basis of the distribution (4.5) and the energy (4.3), the information of each cluster depends on the mean polarization per site in the cluster and on the size of the cluster N.

The information capacity of the lattice with n clusters can be obtained in a straightforward manner. The probability distribution of the whole lattice can be written as a product of the probability distributions for each cluster k with N_k members, which is characterized by a local polarization per site P_k

$$f_{lattice} = \prod_{k=1}^{n} f_{0k} \exp\left(\alpha_k P_k^2 - \beta_k P_k^4\right). \tag{4.13}$$

Using $f_{lattice}$ instead of $f(N,P)$ in the integral (4.6) gives for the total information capacity

$$I = \sum_{k=1}^{n} I_k(N_k), \tag{4.14}$$

where $I_k(N_k)$ is the information of the k-th cluster that has N_k members and can be calculated according to (4.10).

The actual calculation of the information capacity of a MT was performed in a simplified way. At each temperature the information of an average cluster was found from (4.8). The size of the average cluster was obtained by dividing the total number of sites in the MT lattice by the number of clusters n found in the lattice at temperature T. To obtain the information capacity of the MT the information capacity of the average cluster was calculated and then multiplied by the number of clusters n. The number of clusters was determined by means of the Monte Carlo procedure described in Chapter 2. The number and size of clusters was found from the configuration of dipoles in the MT lattice after the last Monte Carlo step at each temperature.

Examples of calculations are shown in Figure 4.1 and Figure 4.2. The values of the constants a and B were chosen such that $a/k_B = 1\,\mathrm{KC^2m^2}$ and $B/k_B = 1\,\mathrm{KC^{-4}m^{-4}}$. The calculations were performed using both the tilted and nontilted model. In the case of the tilted model the value of $\bar{Q}$ was $4.5 \times 10^{-56}\,\mathrm{C^2m^2}$ and for the nontilted model $12 \times 10^{-56}\,\mathrm{C^2m^2}$. The dipoles were assumed to be tilted by 29° to the left with respect to the MT axis.

Figure 4.1 shows the number of clusters and the information capacity of a MT with the A lattice of size 13 protofilaments and 100 rows. The critical temperatures of the lattices are $T_c = 300\,\mathrm{K}$ in the case of the tilted model and $T_c = 253\,\mathrm{K}$ in the case of the nontilted.

It can be seen from the above pictures that the information capacity changes in the same way as the number of clusters. With an increasing temperature both the number of clusters and the information capacity increase. In the lattice with tilted

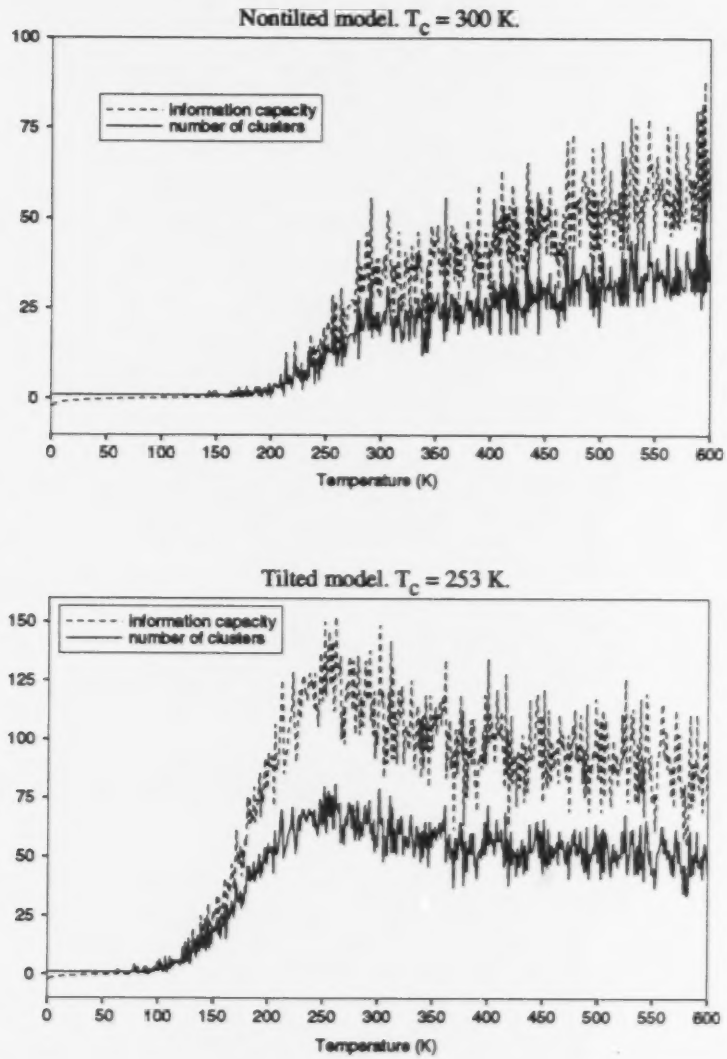

Figure 4.1: Number of clusters and information capacity of a MT with the A lattice for both tilted and nontilted model. The MT consists of 13 columns and 100 rows.

dipoles, the number of clusters is the largest at $T = 251\,\mathrm{K}$ and the information capacity peaks at the critical temperature $T_c = 253\,\mathrm{K}$. At temperatures higher than the critical temperature both the number of clusters and the information capacity decrease. In the lattice in which the dipoles are nontilted, the number of clusters and the information capacity exhibit a local peak at temperature $T = 291\,\mathrm{K}$, and at higher temperatures both quantities increase but with a smaller slope than in the critical region. It can be noted that the value of the information capacity in the lattice with tilted dipoles is almost three times larger at the critical temperature than in the lattice with the nontilted dipoles.

Figure 4.2 shows the number of clusters and the information capacity for a MT with the A lattice which consists of 13 columns and 3000 rows. The critical temperatures of the lattices in which the dipoles are nontilted is $T_c = 311\,\mathrm{K}$ and the critical temperatures of the lattices in which the dipoles are tilted is $T_c = 271\,\mathrm{K}$. The character of the number of clusters and the information capacity is similar to that shown in Figure 4.1. Both quantities in the nontilted case have a local peak at $T = 303\,\mathrm{K}$. The curves obtained for the tilted model have a maximum at $T = 274\,\mathrm{K}$. Since the lattice is 30 times larger than in the former case, the number of clusters is larger and the information capacity is larger as well.

It can be seen in Figures 4.1 and 4.2, that at low temperatures the information capacity is negative. This could be due to the integration over all states of P in the infinite range while the values of the mean polarization per site are in the range from -1 to 1. To improve the calculation, the integrals in (4.8) could be evaluated numerically in the interval (-1,1). It should also be pointed out that the polarization per site in a cluster is not a continuous but a discrete variable since the dipole states of the tubulin dimer change in a discrete rather than in a continuous way.

4.2.2 Discrete Probability Distribution

For the case of a discrete probability distribution, the energies $E_k(N_k)$ of all n clusters in the lattice were found at each temperature by summing up the interaction energies between each two tubulin dimers in a cluster that consists of N_k dipoles. At the borders between two clusters half of the interaction energy between two dipoles was allocated into each of the two clusters. To each cluster was assigned the

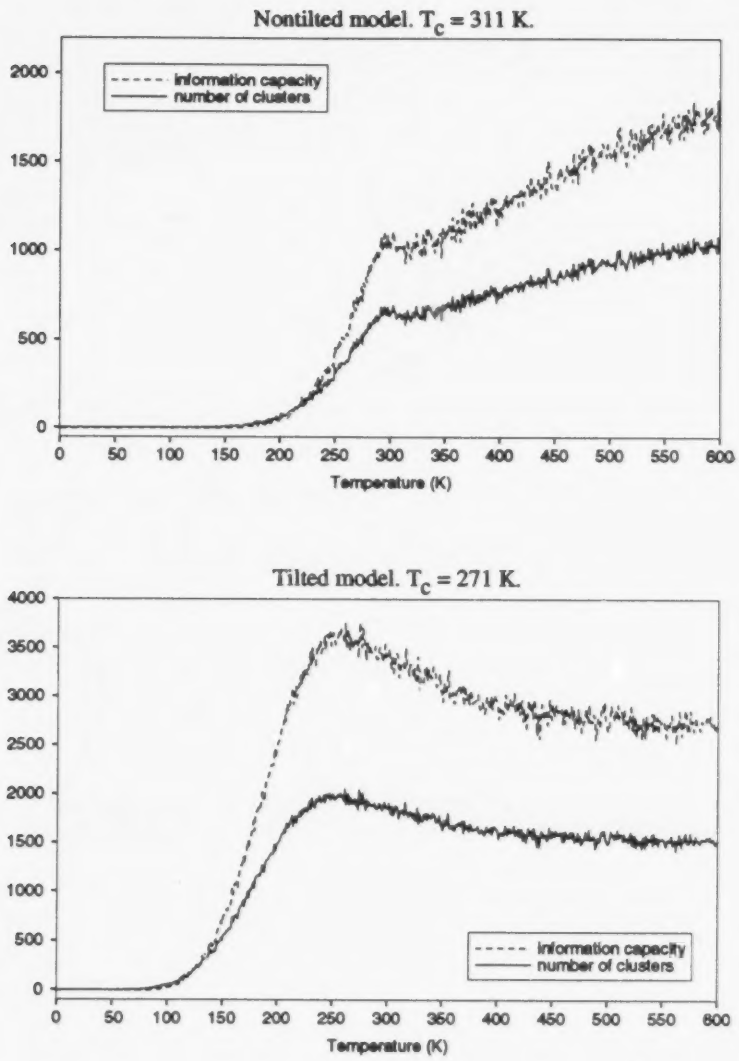

Figure 4.2: Number of clusters and information capacity of a MT with the A lattice for both tilted and nontilted model. The size of the MT is 13 columns and 3000 rows.

canonical probability given below [4]

$$p_k(N_k) = \frac{\exp\left[-\frac{1}{k_B T} E_k(N_k)\right]}{\sum_{k=1}^{n} \exp\left[-\frac{1}{k_B T} E_k(N_k)\right]} . \tag{4.15}$$

Substituting the equation above into (4.14) gives for the information capacity of a MT at a temperature T

$$I = \frac{\sum_{k=1}^{n} \frac{E_k(N_k)}{k_B T} \exp\left[-\frac{1}{k_B T} E_k(N_k)\right]}{\sum_{k=1}^{n} \exp\left[-\frac{1}{k_B T} E_k(N_k)\right]} + \ln \sum_{k=1}^{n} \exp\left[-\frac{1}{k_B T} E_k(N_k)\right] . \tag{4.16}$$

From (4.16) follows that if there is only one cluster in the lattice, *i.e.*, when all dipoles are oriented in one direction (ferroelectric phase) the information is zero.

According to statistical mechanics the sum in (4.16) should go over all possible states of the system. Due to the computational limitations it was impossible to count all possible configurations of dipoles of the MT lattice. To evaluate (4.16), only one of the configurations of the clusters with the largest weight was used. This configuration was determined by means of the Monte Carlo procedure similarly as in the previous section.

Figure 4.3 is a plot of the information capacity of a MT with the A lattice and with 13 protofilaments and 3000 rows. In this calculation the model with nontilted dipoles was used and the critical temperature of this lattice is $T_c = 311\,\mathrm{K}$. Calculations for lattices with 100 and 500 rows were performed as well. The result was similar to that plotted in Figure 4.3.

As the figure shows, at temperatures below the critical temperature the information capacity is zero. Above T_c at some temperatures the information has nonzero values which are larger at higher temperatures. The regions of nonzero information are separated with numerous regions where the information is zero or almost zero. This result is overall similar to that presented in the previous section. The information capacity doesn't exhibit the expected peak at the critical temperature, it is zero below T_c and increases for $T > T_c$.

The quite unusual shape of the information curve in Figure 4.3 is due to the character of the function (4.16). Since it is composed of exponential functions then when only one cluster has energy larger by one order than the rest of the clusters, the resulting sum is very small. In the dielectric phase transition in the MT lattice of dipoles there is usually one cluster which is much larger then the rest of the clusters. This is the cluster that corresponds to the orientation of dipoles in the ferroelectric phase. The clusters of dipoles which are oriented in the opposite

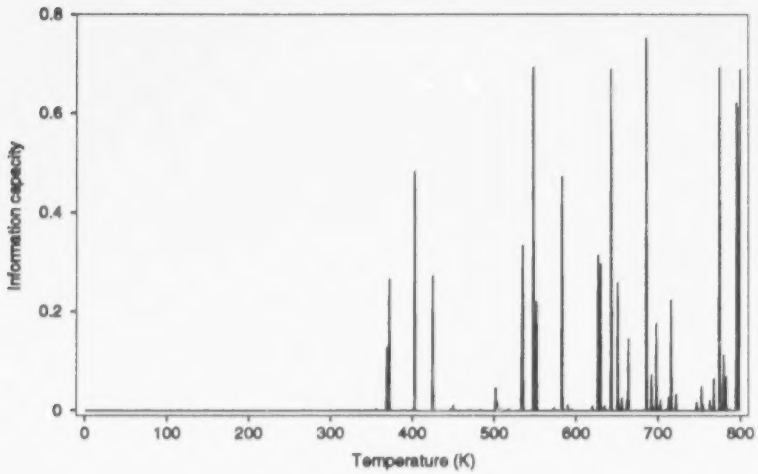

Figure 4.3: Information capacity of a MT with the A lattice that consists of 13 columns and 3000 rows. The calculation was performed using the tilted model. The critical temperature is $T_c = 311\,\mathrm{K}$.

direction are immersed in the background of this large cluster. The size of this cluster decreases with increasing temperature when more clusters with the opposite direction of polarization form and so the sum (4.16) becomes larger. An example of the MT lattice composed of clusters is Figure 4.4 where the configuration of dipoles on a section of the MT A lattice with 13 columns and 3000 rows is shown for the nontilted model at temperatures $T = T_c = 311\,\mathrm{K}$ and $T = 400\,\mathrm{K}$.

The occurrence of regions with zero information capacity between the regions with nonzero information capacity means that some states with the highest weight weren't included in the sum (4.16) [7]. To include only one state at the end of the Monte Carlo importance sampling at each temperature is not sufficient to evaluate the sum (4.16).

Another factor that wasn't taken into account in the evaluation of information according to the probability (4.15) is the degeneracy of the states of the MT lattice of dipoles. In case of the nontilted model each configuration of dipoles in the MT is at least double degenerate because the two orientations of polarization in the lattice are equivalent. Degeneracy should be also considered in each cluster with N_k members. That means, that it should be found how many different configurations

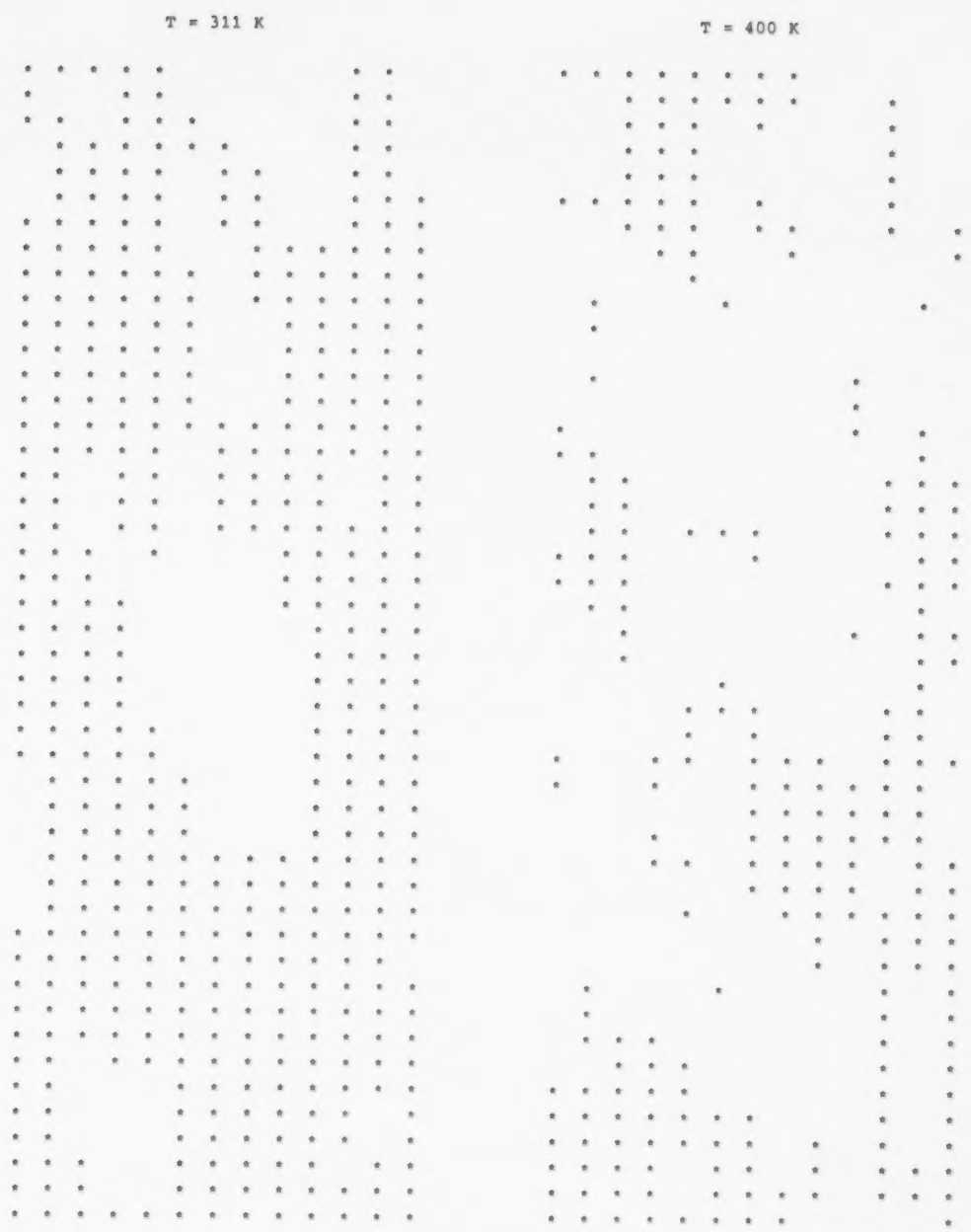

Figure 4.4: The configuration of dipoles on a section of a MT with the A lattice of size 13x3000 at $T = 311\,\mathrm{K}$ and $T = 400\,\mathrm{K}$. The empty sites represent the dipoles in the down states, the sites with a star represent the up states. The configuration was obtained for the nontilted model.

of N_k dipoles in the cluster give the same energy $E_k(N_k)$. It is also very likely to find clusters of different sizes N_k that have the same energy. This is not taken into consideration here because the formula (4.16) depends only on the energy $E_k(N_k)$, but not explicitly on N_k. The information capabilities of MTs should also depend on the location of the clusters in the MT.

The objective of the model calculations presented here was to show that the amount of information stored in a MT is connected with the patterns of dipole states formed on the MT at different temperatures. Two models were suggested in which the information capacity in a MT is assumed to be a function of the number of domains in the MT that differ by the orientation of dipoles. More consistent results were obtained in the case when the probability distribution associated with different clusters was assumed to be continuous. To obtain a more reliable estimate when a discrete probability distribution is used will require more extensive investigations.

The calculations were performed for a MT with the A lattice. According to the results the information capacity of a MT is zero or very small when the MT is in the ferroelectric phase and starts increasing in the region where the phase transition into the paraelectric phase takes place. The calculations using the continuous probability distribution showed that in the case of the model with dipoles tilted in the β state the information has a maximum at the critical temperature of the dielectric transition and decreases at temperatures larger than T_c. The information capacity of the lattice with nontilted dipoles exhibits a local peak at the critical temperature and then keeps increasing but with a smaller slope than below T_c. This difference between the results obtained for the tilted and nontilted model indicates that the information capacity doesn't depend only on the configuration of dipoles but on their orientation as well.

Using both discrete and continuous probability distribution it was found that at high temperatures the information capacity is nonzero. This is because at high temperatures the dipoles are not distributed randomly but rather form quite large clusters as is illustrated in Figure 4.4. However, due to the thermal energy the relaxation time of a particular pattern of dipoles is proportional to $\exp(\Delta E/k_B T)$, where ΔE is the difference between energies of two different patterns due to the dipole-dipole interaction. This means that at higher temperatures, the patterns of clusters will decay very quickly. Consequently, the MT won't be capable of storing information for a sufficiently long time and its information capacity will decrease.

References

[1] S. Rasmussen, H. Karampurwala, R. Vaidyanath, K. S. Jensen and S. Hameroff, Computational Connectionism within Neurons: A Model of Cytoskeletal Automata Subserving Neural Networks, *Physica D* **42**, p. 428-449 (1990)

[2] B. Alberts, D. Bray, J. Lewis, M. Raff, K. Roberts, and J. D. Watson, *Molecular Biology of the Cell*, 3-rd edition (Garland Publishing, New York and London, 1994)

[3] C. E. Shannon, A Mathematical Theory of Communication, *Bell System Technical Journal*, **27**, p. 379-423 and 623-656 (1948)

[4] F. Reif, *Fundamentals of statistical mechanics and thermal physics* (McGraw-Hill, 1965)

[5] J. A. Tuszyński, Comments on the Information Gain and Efficiency of Self-Organizing Systems, *Zeitschrift für Physik B, Condensed Matter* **65**, p. 375-379 (1987)

[6] I. S. Gradshteyn and I. M. Ryzhik, *Table of Integrals, Series, and Products*, editor Alan Jeffrey (Academic Press, 1980)

[7] J. M. Yeomans, *Statistical Mechanics of Phase Transitions* (Clarendon Press, Oxford, 1992)

Conclusions

The object of the research presented in this thesis was to suggest how dielectric and elastic properties of MTs could be related to their biological functions.

As is known, tubulin molecules which are the subunits of MTs carry permanent dipole moments. This implies that a MT may have properties similar to ferroelectric crystals. Based on this assumption, in Chapter 2 the possibility of a transition from a ferroelectric to a paraelectric phase in a MT was studied. It was speculated that a certain mode of operation of a MT may be associated with its dielectric phase.

In the model suggested, a MT was viewed as a two-dimensional lattice of dipoles and each dipole was assumed to possess only two dipole states termed α and β state. To find the dielectric transition, the polarization per site was calculated using the Monte Carlo procedure by means of which the states with the highest statistical weight can be selected. Both A and B type lattices were examined for a MT with 13 protofilaments. Two possible orientations of the dipole on the tubulin dimer in the β state were considered, parallel or tilted with respect to the MT axis. In the α state the dipole is always parallel to the MT axis and points in the direction opposite to the projection of the dipole in the β state on the MT axis.

When the dipoles in the β state were assumed to be nontilted, a dielectric transition was found in a MT with the A lattice but not in a MT with the B lattice. In the case when the dipoles in the β state were tilted the transition from a ferroelectric to a paraelectric phase exists also in the B lattice. The B lattice has been observed in a great majority of MTs. However, the A lattice has not been observed yet. This may mean that the A lattice either doesn't exist in MTs or that MTs with this lattice are very rare.

According to the obtained polarization curves, the value of the transition temperature in a specified type of the MT lattice with a specified orientation of dipole moments on the tubulin dimers depends on the magnitude of the dipole moments and the permittivity of the medium surrounding a MT. A moderate change in these parameters can considerably affect the transition temperature and, consequently, the dielectric phase of the MT at body temperature. However, it should be pointed out that the exact values of the dipole moment of tubulin and the relative permittivity of cytosol are not known and they should be measured experimentally.

Further, the Monte Carlo calculations demonstrated that the states of dipoles on the tubulin dimers can be affected by external electric fields. This effect is observable

if the external electric field is so large that the energy due to the interaction of the dipoles with the field is a significant fraction of the interaction energy between the nearest dipoles in the MT lattice. When the electric fields are oriented in the same direction as is the direction of dipoles in the ferroelectric phase, the transition moves towards higher temperatures, and when the electric field is sufficiently large, the system of dipoles in the MT is in the ferroelectric phase at all temperatures. Electric fields applied in the direction opposite to the alignment of dipoles in the ferroelectric phase cause switching of the assembly of dipoles into the state with the opposite sign of polarization.

The effect of MAPs attached to a MT at sites which formed regular patterns was also studied. The results showed that the higher is the ratio of attached MAPs to a MT the higher is the degree of alignment of dipoles. Hence, MAPs promote the existence of the ferroelectric phase in MTs.

It can be pointed out that MTs with the B lattice may be frustrated. That means, the assemblies of dipoles in such MTs may possess a multitude of energetically equivalent ground states. A transition between these states can happen either at no or very little energy cost. Such a phase may be very suitable for information processing in MTs.

The results summarized above imply that MTs may exist in a variety of dielectric states depending on the configuration of such parameters as the geometrical structure of the MT lattice, the magnitude and orientation of the dipolar states on the tubulin dimers, the presence or absence of MAPs, and the magnitude and direction of external electric fields which can be generated by other cell structures or other MTs.

In Chapter 3, the possibility of propagation of localized quanta of energy along MTs in the form of kink-like solitary waves of tubulin dipole states coupled to its elastic (conformational) states was investigated. The existence of such excitations could be a possible answer of the question how the free portion of the energy released in the GTP hydrolysis is utilized in MTs.

The propagation of kink-like solitary waves along MTs was studied by means of three models that describe the interface motion in ferroelectric systems. In the first model, the dipole state of tubulin and its elastic state were assumed to be strongly coupled. The model was represented by one equation of motion for the elastic distortion of the tubulin dimer. The travelling solutions of the model equation were kinks with a width of about one tubulin dimer. The velocity of the kinks depended

on the parameters of the ferroelectric system (MT), on the critical temperature of the transition from the ferroelectric to the paraelectric phase and on the value of the electric field on the MT surface. Changing the values of the critical temperature and the electric field could control the velocity of kinks.

The calculations showed that the velocity of kinks also changes in a collision with a local defect in a MT. When the defect is large, the kink domain wall ceases to propagate. Thus the question arises as to what happens to the energy that arrives at the potential energy barrier created by the local defect. If the local defect is an attached MAP, it can serve for transfer of the signal in the form of the solitary wave to other parts of the cytoskeleton. If the travelling kink wave doesn't encounter any local defects, it moves along the MT to its other end where it can be used for destabilizing the lateral bonds between the neighbouring protofilaments which may cause detachment of the tubulin dimers from the MT end. Since the velocity of kinks depends linearly on the value of the electric field on the MT surface, this process may be coordinated in the assembly of MTs by means of intrinsic electric fields of MTs. Such a mechanism could be a factor in the regular oscillations observed in populations of MTs.

In the second model, two nonlinear equations for coupled polarization and displacement of the tubulin dimer were studied. In the numerical calculations with arbitrarily chosen parameters, kink-like solutions were found for both variables. They were coupled travelling waves that were affected by a local potential energy barrier in a way similar as in the case described above.

The last model used to describe the travelling quanta of energy in MTs was based on Gordon's model of stress wave propagation in ferroelectrics. The model equations were two coupled equations for polarization and mechanical stress. The solutions of this system of equations under certain conditions were travelling kinks. In the numerical simulations it was found that the interaction of these waves with a local defect imposes a stationary stress along the MT. These results could have interesting implications for MTs. Permanent stress in a MT could be a way of destabilization of the MT and thus a factor in MT disassembly. However, to find out whether the latter two models are applicable to a MT, more numerical investigation should be done using proper MT parameters that are still to be determined. Some of these model parameters are estimated in Appendix A.

In Chapter 4, an estimate of the information capacity of a MT was presented. The basic assumption was that information is represented by different configurations

of the tubulin dipole states in the MT. In the low-temperature ferroelectric phase the information capacity of a MT is zero because all dipoles are oriented in one direction. When the temperature approaches the critical temperature of the transition from the ferroelectric to the paraelectric phase, domains of dipoles with the opposite orientation of polarization start to form due to which the information capacity is expected to have nonzero values.

Two models were suggested according to which the information capacity depends on the number of the domains with a different orientation of dipoles and on the size of each domain. In both cases, the evaluation of the information capacity was based on Shannon's definition of information $I = -\sum_{i=1}^{K} p_i \ln p_i$, where p_i is the probability of state i. According to equilibrium statistical mechanics, the probability p_i is proportional to the Boltzmann factor $\exp[-E_i/k_BT]$, where E_i is the energy in state i.

In the first approach, the energy of a domain with N dipoles was approximated by the Landau free energy expansion for mean polarization per site in the domain. This results in a continuous probability distribution of energies E_i in one domain. Using this distribution, the information capacity of a domain with an average size was determined and then multiplied by the total number of domains in order to find the total information capacity of a MT. The number of domains and their size were found using the Monte Carlo procedure.

The computations were performed for a MT with the A lattice for both the tilted and nontilted model. According to expectations, the information capacity strongly depended on the number of domains or clusters in a MT. When the number of domains increased, the information capacity increased and *vice versa*. At low temperatures when the MT was in the ferroelectric phase, the information capacity was zero. For the tilted model, the information capacity and the number of clusters had a maximum at a temperature close to the critical temperature, and then decreased. In case of the model with nontilted states, both quantities had a local peak in the critical region but then increased even at higher temperatures. These results imply that the information capacity also depends on the orientation of dipolar states of the tubulin dimers.

In the second approach, the energy E_i of each cluster in the MT was calculated exactly using the values of the interaction energies between the dipoles in the MT lattice. The corresponding probability p_i was assigned to each cluster and the total information was calculated using Shannon's definition. According to the calculations

performed, the information was zero below T_c. Above T_c at some temperatures, the information was nonzero. The intervals in which the information is nonzero were separated by regions with an essentially zero information. Such a result is due to the character of the probability distribution $\exp[-E_i/k_BT]$. Usually the energies of the clusters E_i are distributed in such a way that one of them is larger then the rest, which will result in a very small value of I. The energies E_i were determined only for one state of the system with the highest weight, which was selected in the same way as for the previous model using Monte Carlo. An estimate based on only one state of a statistical system is not a very reliable estimate, and this was actually demonstrated in the calculations presented here. In evaluating I, the degeneracy of the configuration of dipoles could also be an important factor. This means that a cluster with energy E_i could be formed in many ways. Thus a more reliable application of this method to the evaluation of the information capacity of a MT would require a more complex analysis.

Finally, the author of this thesis concludes that MTs viewed as physical systems open a number of possibilities for interesting theoretical research. This work was focused mainly on the possibility of propagation of kink-like solitary waves of tubulin dipole states along MTs and the possible existence of different dielectric phases in MTs. These physical phenomena may underlie important biological activities in the cell that involve MTs. Even though not all the questions put forward here have been completely resolved, this work is hoped to lead to new ideas and further theoretical investigations in the future.

Appendix A

The coefficients A_2 and A_4 in equation (3.36) and A, B, C in equation (3.41) can be estimated by fitting plots of polarization calculated in Chapter 2. In order to calculate the fitting curve the following expression for the free energy has been utilized

$$F = \frac{A_2^t}{2}P_t^2 + \frac{A_4^t}{4}P_t^4 + \frac{A_6^t}{6}P_t^6 - EP_t - Nk_BTS_{1/2}\,, \tag{A.1}$$

where P_t is the total polarization (sum of all dipole moments) of a MT. In (A.1), E is an electric field which points in the direction of orientation of dipoles in the ferroelectric phase, $S_{1/2}$ is entropy of the ensemble of spins whose projections on the z-axis can have two values $\pm\frac{1}{2}$, N is the number of spins and k_B is Boltzmann constant. $S_{1/2}$ is given by the formula [1]

$$S_{1/2} = Nk_B[\ln N - \frac{1+2m}{2}\ln\frac{N}{2}(1+2m) - \frac{1-2m}{2}\ln\frac{N}{2}(1-2m)]\,, \tag{A.2}$$

where m is one half of the relative polarization, *i.e.*,

$$m = \frac{N_+ - N_-}{2N}\,. \tag{A.3}$$

In the equation above N_+ is the number of spins up and N_- is the number of spins down.

The minima of the free energy (A.1) at a temperature T can be found by taking the derivative of F with respect to P_t which yields

$$0 = a_2^t(T-T_c)P_t + A_4^tP_t^3 + A_6^tP_t^5 - E - Nk_BT\frac{\partial S_{1/2}}{\partial P_t}\,. \tag{A.4}$$

In the latter equation the coefficient A_2 has been replaced by $a_2^t(T-T_c)$. From (A.2), $S_{1/2}$ is in terms of m. To express the rest of equation (A.4) in terms of m as well, P_t can be replaced by

$$P_t = 2Nqsm\,, \tag{A.5}$$

where q is the charge on each dipole and s is the dipole length. After substituting (A.5) into (A.4), the following equation for the variable m is obtained

$$0 = a_2^t(T-T_c)(2Nqs)m + A_4^t(2Nqs)^3m^3 + A_6^t(2Nqs)^5m^5 - E - \frac{Nk_BT}{2Nqs}\ln\frac{1-2m}{1+2m}\,. \tag{A.6}$$

Multiplying (A.6) by $2Nqs$ gives the final equation

$$0 = a_2^t(T-T_c)(2Nqs)^2 m + A_4^t(2Nqs)^4 m^3 + A_6^t(2Nqs)^6 m^5 - 2NqsE - Nk_BT \ln\frac{1-2m}{1+2m}, \tag{A.7}$$

or

$$0 = a_2'(T-T_c)m + A_4' m^3 + A_6' m^5 - 2NqsE - Nk_BT \ln\frac{1-2m}{1+2m}. \tag{A.8}$$

Equation (A.8) was solved numerically (using the bisection method) to find the equilibrium values of m such that m as a function of T fits the calculated polarization curve for a MT with the A lattice and 13 columns and 3000 rows for which $\bar{Q} = 12 \times 10^{-56}\,\mathrm{C^2m^2}$. The critical temperature corresponding to this curve is 311 K and its plot is shown in Figure 2.11. For $\bar{Q} = 12\times10^{-56}\,\mathrm{C^2m^2}$ and $\epsilon_r = 70$, the magnitude of the dipole moment qs is $2.90 \times 10^{-27}\,\mathrm{Cm}$.

The calculated fit is shown in Figure A.1. The plot corresponds to the coefficients

$$a_2' = 1.5 \times 10^{-16}\,\mathrm{JK^{-1}}, \qquad A_4' = 1.5 \times 10^{-15}\,\mathrm{J}, \qquad A_6' = 1.2 \times 10^{-13}\,\mathrm{J}, \tag{A.9}$$

and electric field

$$E = 3.5 \times 10^5\,\mathrm{Vm^{-1}}. \tag{A.10}$$

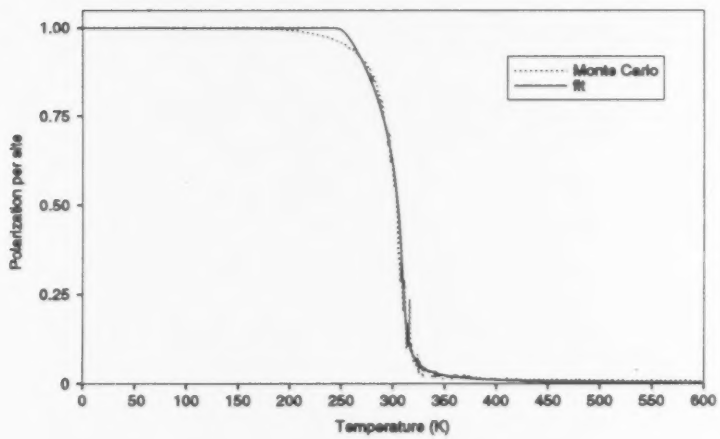

Figure A.1: Relative polarization in a MT with the A lattice and size 13x3000 for $\bar{Q} = 12 \times 10^{-56}\,\mathrm{C^2m^2}$ (dotted line), and the curve calculated by finding the roots of equation (A.8) (solid line).

It can be noted that the potential energy of a dipole due to its interaction with an electric field which points in the same direction as the dipole and has a magnitude $3.5 \times 10^5\,\mathrm{Vm}^{-1}$ is $-qsE = -1.0143 \times 10^{-21}\,\mathrm{J}$. The latter number is of the order of the interaction energies between the dipoles in a MT.

A_2^t, A_4^t and A_6^t can be easily obtained by comparing the coefficients at the same powers of m in equations (A.7) and (A.8). In order to calculate A_2^t it will be assumed that the temperature T is body temperature 310 K and the critical temperature is $T_c = 350\,\mathrm{K}$ which corresponds to the ferroelectric phase. Hence, using the magnitude of the dipole moment $2.90 \times 10^{-27}\,\mathrm{Cm}$ and $N = 39000$, the coefficients which correspond to the total polarization P_t are

$$\begin{aligned} A_2^t &= 1.74 \times 10^{29}\,\mathrm{NC}^{-2}\mathrm{m}^{-1}, \\ A_4^t &= 5.75 \times 10^{71}\,\mathrm{NC}^{-4}\mathrm{m}^{-3}, \\ A_6^t &= 9.00 \times 10^{116}\,\mathrm{NC}^{-6}\mathrm{m}^{-5}. \end{aligned} \tag{A.11}$$

Finally, to find the coefficients which correspond to the variable dipole moment per site the constants (A.11) have to be transformed according to the identity

$$A_k^t P_t^{k-1} = (\frac{P_t}{N})^{k-1} N^{k-1} A_k^t, \tag{A.12}$$

where $P = P_t/N$ is the dipole moment per site and $A_k = N^{k-1}A_k^t$ are the corresponding coefficients. Their values are

$$\begin{aligned} A_2 &= 4.58 \times 10^{33}\,\mathrm{NC}^{-2}\mathrm{m}^{-1}, \\ A_4 &= 3.41 \times 10^{85}\,\mathrm{NC}^{-4}\mathrm{m}^{-3}, \\ A_6 &= 8.12 \times 10^{139}\,\mathrm{NC}^{-6}\mathrm{m}^{-5}. \end{aligned} \tag{A.13}$$

The parameter D can be estimated on the basis of the interaction energy between two dipoles. Assume that at the interface between two subchains of a protofilament which differ by the orientation of dipoles, two neighbouring dipoles are tilted by angles $\theta_n = 0$ and $\theta_{n+1} = \Delta\theta$ with respect to the protofilament axis and the difference $\theta_{n+1} - \theta_n = \Delta\theta$ is small. The interaction energy between these two dipoles is

$$W = \frac{1}{4\pi\epsilon_0\epsilon_r} \frac{\vec{p}_{n+1}.\vec{p}_n - 3(\vec{p}_{n+1}.\vec{u})(\vec{p}_n.\vec{u})}{R_0^3} = -\frac{q^2 s^2}{2\pi\epsilon_0\epsilon_r R_0^3} \cos(\Delta\theta). \tag{A.14}$$

In (A.14), $p_{n+1} = p_n = qs$ is the magnitude of the dipole moment of each dipole, $\vec{u}$ is a unit vector oriented along a line that connects the centers of the dipoles and $R_0 = 8 \times 10^{-9}\,\mathrm{m}$ is the equilibrium distance between two tubulin dimers along a MT protofilament. Since $\Delta\theta$ is small the cosine in (A.14) can be expanded, *i.e.*,

$$\cos(\Delta\theta) = 1 - \frac{(\Delta\theta)^2}{2} + \ldots. \tag{A.15}$$

Keeping only the first two terms in the expansion above gives an approximate expression for the energy (A.14)

$$W \simeq -\frac{q^2 s^2}{2\pi\epsilon_0\epsilon_r R_0^3} + \frac{q^2 s^2}{2\pi\epsilon_0\epsilon_r R_0^3}\frac{(\Delta\theta)^2}{2}. \tag{A.16}$$

The first term in (A.16) is a constant which means that it doesn't appear in the equations of motion. In the continuum limit $(\Delta\theta)^2$ in the second term becomes $R_0^2(\partial\theta/\partial x)^2$ and the variable dipole moment per site becomes polarization at a point x. Polarization changes only due to change in θ, *i.e.*, $\partial P = P(\theta)\partial\theta$. Using this and taking approximately $P \simeq qs$, equation (A.16) becomes

$$W \simeq const. + \frac{1}{4\pi\epsilon_0\epsilon_r R_0}(\frac{\partial P}{\partial x})^2. \tag{A.17}$$

From (A.17) the coefficient D is

$$D = \frac{1}{2\pi\epsilon_0\epsilon_r R_0} = 3.21 \times 10^{16}\,\mathrm{NC^{-2}m}. \tag{A.18}$$

The coefficients (A.13) and (A.18) can be now substituted into equations (3.35) and (3.36). The resulting equations are

$$\frac{\partial^2\bar{u}}{\partial\bar{t}^2} = \frac{\partial^2\bar{u}}{\partial\bar{x}^2} + \bar{u} - \bar{u}^3 - 4.58 \times 10^{-19}\gamma_c\bar{P}, \tag{A.19}$$

$$0 = 5.32\frac{\partial^2\bar{P}}{\partial\bar{x}^2} + \bar{P} - 0.0625\bar{P}^3 - 1.19 \times 10^{-18}\gamma_c\bar{u}. \tag{A.20}$$

In the system of two coupled partial differential equations above the variables are scaled as follows

$$\begin{aligned} u &= (\alpha_2/\alpha_4)^{1/2}\bar{u} = 1.58 \times 10^{-11}\bar{u}, \quad & P &= qs\bar{P} = 2.90 \times 10^{-27}\bar{P}, \\ x &= v_0(M/\alpha_2)^{1/2}\bar{x} = 1.15 \times 10^{-9}\bar{x}, \quad & t &= (M/\alpha_2)^{1/2}\bar{t} = 6.76 \times 10^{-13}\bar{t}. \end{aligned} \tag{A.21}$$

The solution for the case when $\gamma_c = 0$ are kinks for both displacement and polarization. The width of the u-kink is about one tubulin dimer while the width of the P-kink is about three tubulin dimers if both waves are moving at a velocity $17\,\mathrm{ms^{-1}}$. It should be noted that the system of equations (A.19) and (A.20) for $\gamma_c = 0$ doesn't give any equation for the velocity of the solitary waves. The only condition is that in the case of a kink solution the velocity v has to be smaller than the speed of sound v_0.

The parameters (A.13) and (A.18) may also be useful in solving the coupled system of equations (3.41), (3.44) and (3.52).

References

[1] J. A. Tuszyński and W. Wierzbicki, The mean field entropy for an ensemble of identical spins with arbitrary magnitude, *American Journal of Physics* **59**, p. 555-561 (1991)

[2] P. A. Janmey, U. Euteneuer, P. Traub, and M. Schliwa, Viscoelastic Properties of Vimentin Compared with Other Filamentous Biopolymer Networks, *Journal of Cell Biology* **113**, p. 155-160 (1991)

Appendix B

The Fortran program CLUSTER described in this section finds all clusters in a hexagonal MT lattice of dipoles. The clusters are regions which differ by the direction along which the dipoles are aligned. Each dipole is represented by a dipole variable which can have two values +1 or -1 corresponding to the up and down state, respectively. The program also counts the number of dipoles in each cluster to find the size of the cluster.

Description of the variables:

NR - number of rows in the lattice
NC - number of columns in the lattice
D(I,J) - the value of the dipole variable at a site (i,j)
DN(1,K), DN(2,K) - number of -1 and +1 dipoles, respectively, in a cluster K
IC(L), JC(L) - These arrays record the position of a new found cluster member
IL(N), IE(N), IR(N) - The lattice is searched for clusters in which the state of each dipole is represented by a number IL(N) and the background consists of dipoles which are in states represented by a number IE(N). A new found cluster member is replaced by a number IR(N) so that it is not counted again
NCL - total number of -1 and +1 clusters in the lattice

Description of the algorithm:

STEP 1 The program reads the values of the dipole variables D(I,J) at each lattice site (i,j) of the lattice.

STEP 2 The boundary conditions for a MT are set up so that the end of the first row matches with the beginning of the 9th row, *etc.*, and the first row is adjacent to the last row (see also section 2.3 in Chapter 2).

STEP 3 The configuration of the dipole variables in the lattice including the boundary conditions is printed.

STEP 4 Definition of the arrays IL(N), IE(N) and IR(N). The values of N and NCL are initiated.

When N=1, the program first searches the lattice for clusters that consist of -1's on the background of +1's. If D(I,J)=-1 is found, it is replaced by a 0 so that it is not counted again. After all clusters of -1's are found, the program returns to the

statement number 1 and increases the value of N to 2. Now the program is looking for clusters which consist of 1's on the background of 0's and when D(I,J)=1 is found it is replaced by a 5. Thus at the end of the counting the lattice of -1's and 1's is a lattice of 0's and 5's in which 0's correspond to -1's and 5's correspond to 1's (see Figure B.2).

STEP 5 The values K, I, J are initiated. The program starts searching the lattice row by row to find a site at which D(I,J)=IL(N). When such a site is found the value of D(I,J) is replaced by IR(N) so that this cluster member is not counted again.

STEP 6 A site at which D(I,J)=IL(N) is found. This is the first member of a found cluster K and the program remembers the position of this site in variables IS and JS. After the number of members of this cluster is counted the program returns to this position and starts searching for another cluster.

STEP 7 The program examines the nearest neighbours of a cluster member placed at site (i,j). Here the user of the program defines the type of the lattice, for example, square, hexagonal, *etc.*, and the nearest neighbours to the site (i,j). In this example the hexagonal lattice is defined in such a way that the nearest neighbours to the site (i,j) are sites (i,j+1), (i,j-1), (i-1,j), (i+1,j), (i-1,j+1) and (i+1,j-1) as shown in Figure B.1. This means that the sites (i-1,j-1) and (i+1,j+1) are not the nearest neighbours to the site (i,j).

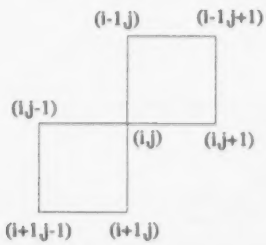

Figure B.1 Nearest neighbours to a site (i,j) in a hexagonal lattice.

If the dipole variables of some of the nearest neighbours to the cluster member (i,j) are equal to IL(N), they are counted into the cluster, replaced by IR(N) and their position is remembered in arrays IC(L) and JC(L). The sites at the boundaries, *i.e.*, when I=1 or I=NR or J=1 or J=NC have to be examined differently from the sites inside the lattice.

STEP 8 After all nearest neighbours of the site (i,j) are examined, the program

returns to the sites whose positions are stored in the arrays IC(L) and JC(L) and examines their nearest neighbours in the same way as described in STEP 7. After all members of the cluster K have been counted, the program prints the position (IS,JS) of the site at which the cluster K started, the cluster number K and the number of dipoles in the cluster DN(N,K). Then the program starts to look for another cluster from the position (IS,JS).

STEP 9 After the whole lattice has been searched for clusters of one type, the value of NCL is updated. Then the program continues searching for clusters of another type. After all cluster in the lattice have been counted the program ends the search by printing the total number of clusters and the configuration of 0's and 5's that replaced -1's and 1's, respectively.

Example:

An example of the output of the program CLUSTER for a corresponding input lattice is shown in Figure B.2. The input lattice consists of 13 columns and 20 rows and the boundary conditions are set up according to STEP 2. Row 20 which is adjacent to row 1 is also row 0 and row 1 is also row 21. Column 13 is column 0 shifted with respect to column 1 by 8 rows down. Column 1 is column 14 shifted with respect to column 13 by 8 rows up. The output lattice is a lattice in which all -1's have been replaced by 0's and all +1's have been replaced by 5's.

The first cluster of -1's which consists of 26 members starts at site (1,1). Site (1,1) is neighbouring to sites (20,1) and (13,13). Due to this the first cluster consists of three parts - site (1,1) and two other subclusters which start at sites (18,20) and (12,13) and contain 5 and 20 members, respectively. These two subclusters form also one cluster since sites (19,1) and (20,1) are nearest neighbours of site (12,13). It can be noticed that the dipole placed at site (1,1) is not a member of the cluster with 12 dipoles which starts at site (2,2) since it is not a nearest neighbour of the site (2,2) in the hexagonal MT lattice as was explained in STEP 7. Third cluster of -1's starts at site (3,5) and has 2 members and the last cluster of -1's starts at site (13,6) and contains 8 members. There is only one cluster of +1's in the lattice which fills out the space between the clusters of -1's. Hence, the total number of clusters in the lattice is 5 and the sum of the numbers of dipoles in each cluster is 260 which is the total number of sites in the lattice.

It is not difficult to modify the procedure described above so that it could be applied to a lattice with more types of constituent particles than 2. Any kind of

```
     0  1  2  3  4  5  6  7  8  9 10 11 12 13 14

 0   0 -1 -1  1  1  1  1  1  1  1  1  1 -1  1  1
 1  -1 -1  1  1  1  1  1  1  1  1  1  1  1  1  1
 2  -1  1 -1  1  1  1  1  1  1  1  1  1  1  1  1
 3  -1  1 -1  1  1 -1  1  1  1  1  1  1  1  1  1
 4  -1  1 -1  1  1 -1  1  1  1  1  1  1  1  1  1
 5  -1  1 -1  1  1  1  1  1  1  1  1  1  1  1  1
 6  -1  1 -1  1  1  1  1  1  1  1  1  1  1  1  1
 7  -1  1 -1  1  1  1  1  1  1  1  1  1  1  1  1
 8   1  1 -1 -1  1  1  1  1  1  1  1  1  1  1  1
 9   1  1 -1 -1  1  1  1  1  1  1  1  1  1  1  1
10   1  1  1 -1 -1  1  1  1  1  1  1  1  1  1  1
11   1  1  1  1  1  1  1  1  1  1  1  1  1  1 -1
12   1  1  1  1  1  1  1  1  1  1  1  1  1 -1 -1
13   1  1  1  1  1  1 -1  1  1  1  1 -1  1 -1 -1
14   1  1  1  1  1  1 -1 -1  1  1 -1 -1 -1 -1  1
15   1  1  1  1  1  1 -1 -1  1  1  1 -1 -1 -1  1
16   1  1  1  1  1  1 -1 -1  1  1  1 -1 -1 -1  1
17   1  1  1  1  1  1 -1  1  1  1  1  1 -1 -1  1
18   1  1 -1  1  1  1  1  1  1  1  1  1 -1 -1  1
19   1 -1 -1  1  1  1  1  1  1  1  1  1 -1 -1  1
20  -1 -1 -1  1  1  1  1  1  1  1  1  1 -1  1  1
21  -1 -1  1  1  1  1  1  1  1  1  1  1  1  1  0

-1 clusters:
IS  JS      K  DN
 1   1      1  26
 2   2      2  12
 3   5      3   2
13   6      4   8

 1 clusters:
IS  JS      K  DN
 1   2      1 212

Number of clusters NCL =  5

     1  2  3  4  5  6  7  8  9 10 11 12 13

 1   0  5  5  5  5  5  5  5  5  5  5  5  5
 2   5  0  5  5  5  5  5  5  5  5  5  5  5
 3   5  0  5  5  0  5  5  5  5  5  5  5  5
 4   5  0  5  5  0  5  5  5  5  5  5  5  5
 5   5  0  5  5  5  5  5  5  5  5  5  5  5
 6   5  0  5  5  5  5  5  5  5  5  5  5  5
 7   5  0  5  5  5  5  5  5  5  5  5  5  5
 8   5  0  0  5  5  5  5  5  5  5  5  5  5
 9   5  0  0  5  5  5  5  5  5  5  5  5  5
10   5  5  0  0  5  5  5  5  5  5  5  5  5
11   5  5  5  5  5  5  5  5  5  5  5  5  5
12   5  5  5  5  5  5  5  5  5  5  5  5  0
13   5  5  5  5  5  0  5  5  5  5  0  5  0
14   5  5  5  5  5  0  0  5  5  0  0  0  0
15   5  5  5  5  5  0  0  5  5  5  0  0  0
16   5  5  5  5  5  0  0  5  5  5  0  0  0
17   5  5  5  5  5  0  5  5  5  5  5  0  0
18   5  0  5  5  5  5  5  5  5  5  5  0  0
19   0  0  5  5  5  5  5  5  5  5  5  0  0
20   0  0  5  5  5  5  5  5  5  5  5  0  5
```

Figure B.2: An example of an input and corresponding output for the program CLUSTER. The A lattice that consists of 13 columns and 20 rows contains 4 clusters of -1's and one cluster of +1's. After the lattice is examined by the program CLUSTER, -1's are replaced with 0's and +1's are replaced with 5's.

clusters can be counted by defining what are the particles in these clusters and what are the background particles.

```
                PROGRAM CLUSTER

      INTEGER*4 D(0:3001,0:14),DN(2,13000)
      INTEGER*4 IC(13000),JC(13000),IL(2),IE(2),IR(2),NCL

      OPEN(UNIT=8,FILE='clusterin.d',STATUS='old')

*     STEP 1

      READ(8,*) NC,NR
      DO I=1,NR
        READ(8,400) I,(D(I,J),J=1,NC)
  400 FORMAT(14I3)
      ENDDO
      CLOSE(UNIT=8)

*     STEP 2

      DO I = 1 , NR
        DO J = 1 ,NC
         IF(I.EQ.1) D(NR+1,J)=D(I,J)
         IF(I.EQ.NR) D(0,J)=D(I,J)

         IF(J.EQ.1) THEN
          IF(I.LT.8) THEN
           D(NR-8+I,NC+1)=D(I,J)
          ELSE IF (I.EQ.8) THEN
           D(0,NC+1)=D(I,J)
           D(NR,NC+1)=D(I,J)
          ELSE IF (I.GT.8) THEN
           D(I-8,NC+1)=D(I,J)
          ENDIF
         ENDIF

         IF(J.EQ.NC) THEN
          IF(I.LT.(NR-7)) THEN
           D(I+8,0)=D(I,J)
          ELSE IF (I.EQ.(NR-7)) THEN
           D(NR+1,0)=D(I,J)
           D(1,0)=D(I,J)
          ELSE IF (I.GT.(NR-7)) THEN
           D(-NR+8+I,0)=D(I,J)
          ENDIF
         ENDIF
        ENDDO
      ENDDO

*     STEP 3

      WRITE(*,101) (J,J=0,NC+1)
  101 FORMAT(5X,15I3)

      PRINT*,'     '
```

```
      DO I=0,NR+1
        WRITE(*,100) I,(D(I,J),J=0,NC+1)
  100 FORMAT(I4,X,15I3)
      ENDDO

*     STEP 4

      IL(1)=-1
      IE(1)=1
      IR(1)=0

      IL(2)=1
      IE(2)=0
      IR(2)=5

      N=0
      NCL=0

    1 N=N+1

*     STEP 5

      K=0
      I=1
      J=1

    5 IF(I.LT.NR) THEN

   10 IF((D(I,J).EQ.IE(N).OR.D(I,J).EQ.IR(N)).AND.J.LT.NC) THEN
        J=J+1
        GO TO 10
      ENDIF

      IF((D(I,J).EQ.IE(N).OR.D(I,J).EQ.IR(N))
     &.AND.J.EQ.NC.AND.I.LT.NR) THEN
        J=1
        I=I+1
        GO TO 10
      ENDIF

      IF((D(I,J).EQ.IE(N).OR.D(I,J).EQ.IR(N))
     &.AND.J.EQ.NC.AND.I.EQ.NR) GO TO 30

*     STEP 6 - You found a cluster!!

      IF(D(I,J).EQ.IL(N)) THEN

      JS=J
      IS=I
      K=K+1
      DN(N,K)=1
      D(I,J)=IR(N)
```

```
      L=0

*     STEP 7

   20 IF(I.GT.1.AND.I.LT.NR.AND.J.GT.1.AND.J.LT.NC) THEN

         IF(D(I,J+1).EQ.IL(N)) THEN
            D(I,J+1)=IR(N)
            L=L+1
            IC(L)=I
            JC(L)=J+1
            DN(N,K)=DN(N,K)+1
         ENDIF

         IF(D(I-1,J+1).EQ.IL(N)) THEN
            D(I-1,J+1)=IR(N)
            L=L+1
            IC(L)=I-1
            JC(L)=J+1
            DN(N,K)=DN(N,K)+1
         ENDIF

         IF(D(I-1,J).EQ.IL(N)) THEN
            D(I-1,J)=IR(N)
            L=L+1
            IC(L)=I-1
            JC(L)=J
            DN(N,K)=DN(N,K)+1
         ENDIF

         IF(D(I,J-1).EQ.IL(N)) THEN
            D(I,J-1)=IR(N)
            L=L+1
            IC(L)=I
            JC(L)=J-1
            DN(N,K)=DN(N,K)+1
         ENDIF

         IF(D(I+1,J-1).EQ.IL(N)) THEN
            D(I+1,J-1)=IR(N)
            L=L+1
            IC(L)=I+1
            JC(L)=J-1
            DN(N,K)=DN(N,K)+1
         ENDIF

         IF(D(I+1,J).EQ.IL(N)) THEN
            D(I+1,J)=IR(N)
            L=L+1
            IC(L)=I+1
            JC(L)=J
            DN(N,K)=DN(N,K)+1
         ENDIF
```

```
            GO TO 24

         ENDIF

* * *       upper left corner

         IF(I.EQ.1.AND.J.EQ.1) THEN

            IF(D(NR-7,NC).EQ.IL(N)) THEN
               D(NR-7,NC)=IR(N)
               L=L+1
               IC(L)=NR-7
               JC(L)=NC
               DN(N,K)=DN(N,K)+1
            ENDIF

            IF(D(NR-6,NC).EQ.IL(N)) THEN
               D(NR-6,NC)=IR(N)
               L=L+1
               IC(L)=NR-6
               JC(L)=NC
               DN(N,K)=DN(N,K)+1
            ENDIF

            IF(D(NR,1).EQ.IL(N)) THEN
               D(NR,1)=IR(N)
               L=L+1
               IC(L)=NR
               JC(L)=1
               DN(N,K)=DN(N,K)+1
            ENDIF

            IF(D(NR,2).EQ.IL(N)) THEN
               D(NR,2)=IR(N)
               L=L+1
               IC(L)=NR
               JC(L)=2
               DN(N,K)=DN(N,K)+1
            ENDIF

            IF(D(1,2).EQ.IL(N)) THEN
               D(1,2)=IR(N)
               L=L+1
               IC(L)=1
               JC(L)=2
               DN(N,K)=DN(N,K)+1
            ENDIF

            IF(D(2,1).EQ.IL(N)) THEN
               D(2,1)=IR(N)
               L=L+1
               IC(L)=2
```

```
            JC(L)=1
            DN(N,K)=DN(N,K)+1
         ENDIF

         GO TO 24

      ENDIF

* * *       upper right corner

      IF(I.EQ.1.AND.J.EQ.NC) THEN

         IF(D(8,1).EQ.IL(N)) THEN
            D(8,1)=IR(N)
            L=L+1
            IC(L)=8
            JC(L)=1
            DN(N,K)=DN(N,K)+1
         ENDIF

         IF(D(9,1).EQ.IL(N)) THEN
            D(9,1)=IR(N)
            L=L+1
            IC(L)=9
            JC(L)=1
            DN(N,K)=DN(N,K)+1
         ENDIF

         IF(D(NR,NC).EQ.IL(N)) THEN
            D(NR,NC)=IR(N)
            L=L+1
            IC(L)=NR
            JC(L)=NC
            DN(N,K)=DN(N,K)+1
         ENDIF

         IF(D(1,NC-1).EQ.IL(N)) THEN
            D(1,NC-1)=IR(N)
            L=L+1
            IC(L)=1
            JC(L)=NC-1
            DN(N,K)=DN(N,K)+1
         ENDIF

         IF(D(2,NC).EQ.IL(N)) THEN
            D(2,NC)=IR(N)
            L=L+1
            IC(L)=2
            JC(L)=NC
            DN(N,K)=DN(N,K)+1
         ENDIF

         IF(D(2,NC-1).EQ.IL(N)) THEN
```

```
            D(2,NC-1)=IR(N)
            L=L+1
            IC(L)=2
            JC(L)=NC-1
            DN(N,K)=DN(N,K)+1
         ENDIF

         GO TO 24

      ENDIF

* * *       lower left corner

      IF(I.EQ.NR.AND.J.EQ.1) THEN

         IF(D(NR-8,NC).EQ.IL(N)) THEN
            D(NR-8,NC)=IR(N)
            L=L+1
            IC(L)=NR-8
            JC(L)=NC
            DN(N,K)=DN(N,K)+1
         ENDIF

         IF(D(NR-7,NC).EQ.IL(N)) THEN
            D(NR-7,NC)=IR(N)
            L=L+1
            IC(L)=NR-7
            JC(L)=NC
            DN(N,K)=DN(N,K)+1
         ENDIF

         IF(D(1,1).EQ.IL(N)) THEN
            D(1,1)=IR(N)
            L=L+1
            IC(L)=1
            JC(L)=1
            DN(N,K)=DN(N,K)+1
         ENDIF

         IF(D(NR-1,1).EQ.IL(N)) THEN
            D(NR-1,1)=IR(N)
            L=L+1
            IC(L)=NR-1
            JC(L)=1
            DN(N,K)=DN(N,K)+1
         ENDIF

         IF(D(NR,2).EQ.IL(N)) THEN
            D(NR,2)=IR(N)
            L=L+1
            IC(L)=NR
            JC(L)=2
            DN(N,K)=DN(N,K)+1
```

```
            ENDIF

            IF(D(NR-1,2).EQ.IL(N)) THEN
               D(NR-1,2)=IR(N)
               L=L+1
               IC(L)=NR-1
               JC(L)=2
               DN(N,K)=DN(N,K)+1
            ENDIF

            GO TO 24

         ENDIF

* * *       lower right corner

         IF(I.EQ.NR.AND.J.EQ.NC) THEN

            IF(D(8,1).EQ.IL(N)) THEN
               D(8,1)=IR(N)
               L=L+1
               IC(L)=8
               JC(L)=1
               DN(N,K)=DN(N,K)+1
            ENDIF

            IF(D(7,1).EQ.IL(N)) THEN
               D(7,1)=IR(N)
               L=L+1
               IC(L)=7
               JC(L)=1
               DN(N,K)=DN(N,K)+1
            ENDIF

            IF(D(1,NC).EQ.IL(N)) THEN
               D(1,NC)=IR(N)
               L=L+1
               IC(L)=1
               JC(L)=NC
               DN(N,K)=DN(N,K)+1
            ENDIF

            IF(D(1,NC-1).EQ.IL(N)) THEN
               D(1,NC-1)=IR(N)
               L=L+1
               IC(L)=1
               JC(L)=NC-1
               DN(N,K)=DN(N,K)+1
            ENDIF

            IF(D(NR,NC-1).EQ.IL(N)) THEN
               D(NR,NC-1)=IR(N)
               L=L+1
```

```
            IC(L)=NR
            JC(L)=NC-1
            DN(N,K)=DN(N,K)+1
         ENDIF

         IF(D(NR-1,NC).EQ.IL(N)) THEN
            D(NR-1,NC)=IR(N)
            L=L+1
            IC(L)=NR-1
            JC(L)=NC
            DN(N,K)=DN(N,K)+1
         ENDIF

         GO TO 24

      ENDIF

* * *       upper boundary

      IF(I.EQ.1.AND.J.GT.1.AND.J.LT.NC) THEN

         IF(D(NR,J).EQ.IL(N)) THEN
            D(NR,J)=IR(N)
            L=L+1
            IC(L)=NR
            JC(L)=J
            DN(N,K)=DN(N,K)+1
         ENDIF

         IF(D(NR,J+1).EQ.IL(N)) THEN
            D(NR,J+1)=IR(N)
            L=L+1
            IC(L)=NR
            JC(L)=J+1
            DN(N,K)=DN(N,K)+1
         ENDIF

         IF(D(1,J+1).EQ.IL(N)) THEN
            D(1,J+1)=IR(N)
            L=L+1
            IC(L)=1
            JC(L)=J+1
            DN(N,K)=DN(N,K)+1
         ENDIF

         IF(D(1,J-1).EQ.IL(N)) THEN
            D(1,J-1)=IR(N)
            L=L+1
            IC(L)=1
            JC(L)=J-1
            DN(N,K)=DN(N,K)+1
         ENDIF
```

```
            IF(D(2,J-1).EQ.IL(N)) THEN
               D(2,J-1)=IR(N)
               L=L+1
               IC(L)=2
               JC(L)=J-1
               DN(N,K)=DN(N,K)+1
            ENDIF

            IF(D(2,J).EQ.IL(N)) THEN
               D(2,J)=IR(N)
               L=L+1
               IC(L)=2
               JC(L)=J
               DN(N,K)=DN(N,K)+1
            ENDIF

            GO TO 24

         ENDIF

* * *       lower boundary

         IF(I.EQ.NR.AND.J.GT.1.AND.J.LT.NC) THEN

            IF(D(1,J).EQ.IL(N)) THEN
               D(1,J)=IR(N)
                 L=L+1
               IC(L)=1
               JC(L)=J
               DN(N,K)=DN(N,K)+1
            ENDIF

            IF(D(1,J-1).EQ.IL(N)) THEN
               D(1,J-1)=IR(N)
               L=L+1
               IC(L)=1
               JC(L)=J-1
               DN(N,K)=DN(N,K)+1
            ENDIF

            IF(D(NR,J-1).EQ.IL(N)) THEN
               D(NR,J-1)=IR(N)
               L=L+1
               IC(L)=NR
               JC(L)=J-1
               DN(N,K)=DN(N,K)+1
            ENDIF

            IF(D(NR,J+1).EQ.IL(N)) THEN
               D(NR,J+1)=IR(N)
               L=L+1
               IC(L)=NR
               JC(L)=J+1
```

```
            DN(N,K)=DN(N,K)+1
         ENDIF

         IF(D(NR-1,J).EQ.IL(N)) THEN
            D(NR-1,J)=IR(N)
            L=L+1
            IC(L)=NR-1
            JC(L)=J
            DN(N,K)=DN(N,K)+1
         ENDIF

         IF(D(NR-1,J+1).EQ.IL(N)) THEN
            D(NR-1,J+1)=IR(N)
            L=L+1
            IC(L)=NR-1
            JC(L)=J+1
            DN(N,K)=DN(N,K)+1
         ENDIF

         GO TO 24

      ENDIF

* * *      left boundary

      IF(I.GT.1.AND.I.LT.NR.AND.J.EQ.1) THEN

         IF(I.LE.7) THEN
            IF(D(NR-8+I,NC).EQ.IL(N)) THEN
               D(NR-8+I,NC)=IR(N)
               L=L+1
               IC(L)=NR-8+I
               JC(L)=NC
               DN(N,K)=DN(N,K)+1
            ENDIF

            IF(D(NR-7+I,NC).EQ.IL(N)) THEN
               D(NR-7+I,NC)=IR(N)
               L=L+1
               IC(L)=NR-7+I
               JC(L)=NC
               DN(N,K)=DN(N,K)+1
            ENDIF
         ENDIF

         IF(I.EQ.8) THEN
            IF(D(NR,NC).EQ.IL(N)) THEN
               D(NR,NC)=IR(N)
               L=L+1
               IC(L)=NR
               JC(L)=NC
               DN(N,K)=DN(N,K)+1
            ENDIF
```

```
      IF(D(1,NC).EQ.IL(N)) THEN
         D(1,NC)=IR(N)
         L=L+1
         IC(L)=1
         JC(L)=NC
         DN(N,K)=DN(N,K)+1
      ENDIF
   ENDIF

   IF(I.GT.8) THEN
      IF(D(I-8,NC).EQ.IL(N)) THEN
         D(I-8,NC)=IR(N)
         L=L+1
         IC(L)=I-8
         JC(L)=NC
         DN(N,K)=DN(N,K)+1
      ENDIF

      IF(D(I-7,NC).EQ.IL(N)) THEN
         D(I-7,NC)=IR(N)
         L=L+1
         IC(L)=I-7
         JC(L)=NC
         DN(N,K)=DN(N,K)+1
      ENDIF
   ENDIF

   IF(D(I-1,1).EQ.IL(N)) THEN
      D(I-1,1)=IR(N)
      L=L+1
      IC(L)=I-1
      JC(L)=1
      DN(N,K)=DN(N,K)+1
   ENDIF

   IF(D(I+1,1).EQ.IL(N)) THEN
      D(I+1,1)=IR(N)
      L=L+1
      IC(L)=I+1
      JC(L)=1
      DN(N,K)=DN(N,K)+1
   ENDIF

   IF(D(I,2).EQ.IL(N)) THEN
      D(I,2)=IR(N)
      L=L+1
      IC(L)=I
      JC(L)=2
      DN(N,K)=DN(N,K)+1
   ENDIF

   IF(D(I-1,2).EQ.IL(N)) THEN
```

```
            D(I-1,2)=IR(N)
            L=L+1
            IC(L)=I-1
            JC(L)=2
            DN(N,K)=DN(N,K)+1
         ENDIF

         GO TO 24

      ENDIF

* * *       right boundary

      IF(I.GT.1.AND.I.LT.NR.AND.J.EQ.NC) THEN

         IF(I.LT.(NR-7)) THEN
            IF(D(I+7,1).EQ.IL(N)) THEN
               D(I+7,1)=IR(N)
               L=L+1
               IC(L)=I+7
               JC(L)=1
               DN(N,K)=DN(N,K)+1
            ENDIF

            IF(D(I+8,1).EQ.IL(N)) THEN
               D(I+8,1)=IR(N)
               L=L+1
               IC(L)=I+8
               JC(L)=1
               DN(N,K)=DN(N,K)+1
            ENDIF
         ENDIF

         IF(I.EQ.(NR-7)) THEN
            IF(D(NR,1).EQ.IL(N)) THEN
               D(NR,1)=IR(N)
               L=L+1
               IC(L)=NR
               JC(L)=1
               DN(N,K)=DN(N,K)+1
            ENDIF

            IF(D(1,1).EQ.IL(N)) THEN
               D(1,1)=IR(N)
               L=L+1
               IC(L)=1
               JC(L)=1
               DN(N,K)=DN(N,K)+1
            ENDIF
         ENDIF

         IF(I.GE.(NR-6)) THEN
            IF(D(I+8-NR,1).EQ.IL(N)) THEN
```

```
            D(I+8-NR,1)=IR(N)
            L=L+1
            IC(L)=I+8-NR
            JC(L)=1
            DN(N,K)=DN(N,K)+1
         ENDIF

         IF(D(I+7-NR,1).EQ.IL(N)) THEN
            D(I+7-NR,1)=IR(N)
            L=L+1
            IC(L)=I+7-NR
            JC(L)=1
            DN(N,K)=DN(N,K)+1
         ENDIF
      ENDIF

      IF(D(I-1,NC).EQ.IL(N)) THEN
         D(I-1,NC)=IR(N)
         L=L+1
         IC(L)=I-1
         JC(L)=NC
         DN(N,K)=DN(N,K)+1
      ENDIF

      IF(D(I+1,NC).EQ.IL(N)) THEN
         D(I+1,NC)=IR(N)
         L=L+1
         IC(L)=I+1
         JC(L)=NC
         DN(N,K)=DN(N,K)+1
      ENDIF

      IF(D(I+1,NC-1).EQ.IL(N)) THEN
         D(I+1,NC-1)=IR(N)
         L=L+1
         IC(L)=I+1
         JC(L)=NC-1
         DN(N,K)=DN(N,K)+1
      ENDIF

      IF(D(I,NC-1).EQ.IL(N)) THEN
         D(I,NC-1)=IR(N)
         L=L+1
         IC(L)=I
         JC(L)=NC-1
         DN(N,K)=DN(N,K)+1
      ENDIF

      GO TO 24

   ENDIF

*  STEP 8
```

```
 24 IF(L.GE.1) THEN
      I=IC(L)
      J=JC(L)
      L=L-1
      GO TO 20
    ENDIF

    WRITE(*,305) IS,JS,K,DN(N,K)
305 FORMAT(2I4,2X,2I4)

      J=JS
      I=IS

    ENDIF

      GO TO 5
    ENDIF

*   STEP 9

 30 IF(N.EQ.1) THEN
      NCL=NCL+K
      GO TO 1
     ELSE
       NCL=NCL+K
       GO TO 40
    ENDIF

 40 PRINT*,'Number of clusters NCL = ',NCL
    PRINT*,'    '

    WRITE(*,102) (J,J=1,NC)
102 FORMAT(5X,13I3)
    PRINT*,'    '
    DO I=1,NR
      WRITE(*,300) I,(D(I,J),J=1,NC)
300 FORMAT(I4,X,13I3)
    ENDDO

    STOP
    END
```